CZECH UNIVERSITY OF LIFE SCIENCES PRAGUE

FACULTY OF ENVIRONMENTAL SCIENCES

DEPARTMENT OF WATER RESOURCES AND ENVIRONMENTAL MODELING

Experimental Methods for Investigating Rainwater Behavior in the Snowpack

DIPLOMA THESIS

Supervisor: Ing. Roman Juras, Ph.D.

Advisor: Ing. Johanna Blöcher

Author: Bc. Kryštof Dytrt

CZECH UNIVERSITY OF LIFE SCIENCES PRAGUE

Faculty of Environmental Sciences

DIPLOMA THESIS ASSIGNMENT

Bc. Kryštof Dytrt

Landscape Engineering
Water in the Landscape

Thesis title

Experimental methods for investigating rainwater behaviour in the snowpack

---

Objectives of thesis

The main goal of the thesis is to evaluate data from the sprinkling experiments.
The thesis will especially focus on 3 main objectives

- Analyse the changes of snow properties affected by rain
- Estimate the uncertainties of used investigation methods
- Calibrate the device for snowpack runoff monitoring

Methodology

Student will analyse data from the previous sprinkling experiments. The changes in the rain affected snowpack will evaluated from the photographs of the snow profile and snow properties data prior and post the sprinkling experiments. Student will determine the uncertainties of the data and suggest improvements for future experiments. The runoff monitoring device will be calibrated in the laboratory.

The proposed extent of the thesis

50 pages

Keywords

Rain-on-snow, experiments, rainfall simulator

Recommended information sources

Juras, R., Würzer, S., Pavlásek, J., Vitvar, T. and Jonas, T.: Rainwater propagation through snow pack during rain-on-snow events under different snow condition, Hydrol. Earth Syst. Sci., 21, 4973–4987, doi:10.5194/hess-2016-612, 2017.

Würzer, S., Wever, N., Juras, R., Lehning, M. and Jonas, T.: Modeling liquid water transport in snow under rain-on-snow conditions – considering preferential flow, Hydrol. Earth Syst. Sci. Discuss., 0, 1–29, doi:10.5194/hess-2016-351, 2016.

Expected date of thesis defence

2019/20 SS – FES

The Diploma Thesis Supervisor

Ing. Roman Juras, Ph.D.

Supervising department

Department of Water Resources and Environmental Modeling

Advisor of thesis

Johanna Ruth Blöcher

Electronic approval: 10. 3. 2020

doc. Ing. Martin Hanel, Ph.D.

Head of department

Electronic approval: 11. 3. 2020

prof. RNDr. Vladimír Bejček, CSc.

Dean

Prague on 30. 06. 2020

Declaration

I declare that I have written my master thesis by myself and I have used only the sources mentioned at the end. As the author, I declare that the thesis does not break copyrights of any their person.

In Prague on 30. 6. 2020   …..………………………...........

                                                                    Kryštof Dytrt

Acknowledgement

I would like to thank my supervisor Ing. Roman Juras, Ph.D for his patience and support and to my advisor Ing. Johanna Blöcher for the encouragement and her advice. I appreciate being involved in the experimental team and the attitude throughout the entirety of this project.

Abstract

This thesis focuses on methods of investigation rain on snow events and validation of water behavior in snow at three locations in the Czech Republic. Experiments were carried out in winter 2019 where rain simulator was used to get a vision what kind of flow paths can rain on snow event caused in snowpack. Three approaches of analyses have been created in this work to analyze water behavior in snow from photos taken during experiments. The first "Localization analysis" classifies data from photos and provides a fundamental view on water regimes induced after experiments in coordinate system. Next analysis determines photos reliability by created indexes where comparison of heights of all photos, distortion and lysimeter desk determination have been composed together to point out on weak points in the photographing technique and to suggest new methods of conducting rain on snow experiments. The third analysis uses R interface and tests new developed package "bluesnow" as a tool for visualizing snow after dye tracer experiments. Approaches of bluesnow and localization analyses have been put together to validate water flow paths in snow with combination of altered snow properties after experiments at each experimental site. At Luisino Údolí site horizontal formation of flow patterns was recorded with heterogeneous properties of snow. Luisino Údolí was typical with preferential flow paths and lateral flow regime. Kubova Huť 1 site was evaluated with heterogenous properties of snow as well as Luisino Údolí, with prevailing of flow patterns in horizontal direction mainly with lateral flow. The third Kubova Huť 2 site was studied during spring and more homogenous properties were recorded. Uniform character of snowpack could not retain water and prevailing of vertical flow caused release of water with matrix flow regime. New suggested methods of rain on snow investigations implements newly designed tipping buckets which are evaluated in this thesis as well.

Keywords: Rain-on-snow, experiments, rainfall simulator

Abstrakt

Tato práce se zabývá metodami a vyhodnocením dešťových experimentů s dopadem na pohyb vody ve sněhové pokrývce ve třech lokalitách v České republice. Experimenty probíhaly v zimě roku 2019, kde se využíval simulátor deště, který poskytl pohled na rozliv vody po dešti. V této práci jsou vytvořeny tři přístupy analýzy fotek po experimentech. První přístup klasifikuje data a poskytuje fundamentální pohled na utvoření režimu proudění ve sněhu v koordinačním

systému. Další typ analýzy porovnával spolehlivost fotek, na základě indexů, kde probíhalo porovnání zkreslení, variace výšky sněhu v profilu a lokalizace lysimetru. Zjištěné nedostatky daly za základ vzniku nové metodě probíhání experimentů. Třetí pohled analýzy byl proveden v prostředí R, který testoval nový balík „Bluesnow", vyvinut pro analýzu fotek po experimentech. Přístupy lokalizace a bluesnow byly použity pro vyhodnocení chování vody ve sněhové pokrývce, na každé lokalitě v kombinaci se studiem stavu sněhu před a po vykonání experimentů. Lokalita Luisino Údolí, byla typická s dominancí horizontální formací pohybu vody po experimentech, které se vyznačovalo laterálním režimem s preferenčními cestami, díky heterogenním vlastnostem sněhu. Lokalita Kubova Huť 1, měla také heterogenní charakter typický se změnami vlastností sněhu ve stádiu před experimenty a po experimentech. Tyto změny vlastností daly vzniknout převážně horizontální orientaci pohybu vody s již zmíněnými preferenčními cesty a laterálním prouděním. Třetí lokalita Kubova Huť 2, měřena v jarních podmínkách, vykazovala homogenní vlastnosti sněhu ve všech ohledech. Dominantní byl na rozdíl od všech experimentů, vertikální vliv tvoření pohybu vody ve sněhu, kde pohyb vody určovala gravitace po zaplnění veškerých pórů částic tvořící pokrývku. Tyto faktory vedou k nízké schopnosti akumulace vody. Nově navržená metodika rovněž počítá s implementací nového designu měrného překlopného systému, který byl v této práci navržen ve třech fází kalibrace.

Klíčová slova: Déšť na sníh, experiment, simulátor deště

Table of content

List of tables

List of figures

List of abbreviations

ROS   Rain on snow

SWE   Snow water equivalent [mm]

LWC   Liquid water content [%]

PF   Preferential flow paths

LF   Lateral flow

FF   Finger flow

MF   Matrix flow

CHMI   Czech Hydrometeorological Institute

SNOTEL   Snow Telemetry

LU   Luisino Údolí (Experimental site)

KH1   Kubova Huť 1 (Experimental site)

KH2   Kubova Huť 2 (Experimental site)

TB   Tipping bucket

1 <u>Introduction</u>

Water behavior in snow is being investigated from many points of view (Würzer et al., 2017) to predict its abilities and examine its positive impacts and beneficial functions as well as negative ones, such as the potential to cause floods, landslides or avalanches. Snow with its properties is one of the main elements of water conservation in the mild climate. It influences water distribution and contributes to water supplies for the summer season where drier summer caused by climate change affects water capacities. Water distribution in the central Europe is dependent on the rain fall events that are being influenced by the climate change (Jacob et al., 2014). Different principles of rainfall distribution are recorded and being examined from many sides to predict hydrological impacts. SINGH ET AL. (1997) stated that rain on snow (ROS) events have larger potential to cause floods than the regular spring snowmelt. Presence of liquid water impacts the mechanical strength of the snow cover and can increase risks related to triggering avalanches, faster melting and slush flow. However, ROS events tend to occur more often than the snowfall during the winter season, influencing the snow cover stability as well as hydrological behavior for the other seasons (Pan et al., 2018). The middle Europe's dependency on precipitation is crucial and ROS events research could help understand water distribution for drier seasons to prevent the lack of water. Snow knowledge is therefore impactful for water scarcity prevention and has not yet been fully explored.

In this thesis rain on snow effects are studied to describe water flow induced by the ROS events. ROS events were simulated on experimental sites during winter 2019. Snow properties in all experimental sites were compared in pre and post experimental conditions to specify the changes being driven by the ROS event and water movement in snow was validated. However, main goal of this thesis is to examine the methods of sprinkling experiments to provide more reliable data which are used for hydrological model predictions. The potential to increase the input data precision is expected to enhance further modeling of water behavior in snow as well as improve the hydrological understanding. Improvement of experimental ROS simulation methods should lead to other potential ways of advancement in this field of study to provide better and more cohesive methods for rain on snow research.

2 <u>Goals</u>

The main goal is to evaluate data from the sprinkling experiments on snow performed during winter 2019 and to propose new methods improving precision of data for further modeling. This is categorized as follows:

- Analysis of the changes of snow properties affected by rain
- Analysis of flow paths in snow
- Validation of water regimes in snow
- Definition of photo uncertainties
- Enhancement of methods of snow experiments
- Designment of tailored made tipping buckets for snowpack runoff

This thesis should cover all the categories for the further examination of ROS experiments to provide understanding of water behavior in snow.

3 <u>Literature review</u>

3.1 Snowstorm

According to NATIONAL SNOW AND ICE DATA CENTER (2019), snowstorm can occur under specific conditions in the atmosphere where each storm can produce a different type of snowfall and snow does not fall everywhere equally. Even during the same storm, contribution of snow is not the same as in other neighborhoods where depth of snow varies. This unequal distribution of snow is caused primarily by wind during the snowfall event and by melting afterwards. Snow on ground is then defined as a snowpack where other properties of snow are examined.

3.2 Snowpack

Snowpack is made of individual snowfall events which produce a stratified deposit, where each layer has its own properties that affect the liquid water movement in the snow afterwards. Layers are distinct in texture and hydraulic properties, which means that a snowpack can store various volumes of liquid water (Singh et al., 1997). Snowpack is a complex penetrable medium with properties being changed in time by the influence of climate conditions, such as pressure, temperature, wind, and precipitation during a period of the year (De Michele et al., 2013).

Within a snowpack, transfer of heat is caused by number of different processes. Predominantly, conduction through the structure of snowpack by interconnected snow crystals, but also by pressure pumping, conduction through the interstitial air space, and vapor transport driven by temperature gradients. The low thermal conductivity of air makes snow an excellent insulator for the underlying soil, where temperature is usually 0°C or close to 0°C (Burns et al., 2014). This is possible because the soil is generally not frozen when the first snow covers the ground. Wintertime snowpack also plays its own role, providing a cover for hibernating animals and vegetation (Seibert et al., 2014). During the snowmelt period, which is ordinary in spring, most snowmelt water infiltrates into the soil. A perceptible redistribution of the infiltrated water is observed. Water transfers into soil moisture, recharges groundwater storage, contributes to evapotranspiration or produces streamflow (Webb et al., 2018). The depth of accumulated snow usually increases with increasing elevation and the accompanying increase in the numbers of snowfall deposition events and decrease in melt and evaporation. This happens when vegetation, relief, wind and other factors are omitted (Pomeroy and Gray, 1995). It is related to the snow elevation line which

represents snow season occurrence (the snow cover due to elevation as a boundary between accumulation and ablation zone of snow) (Kormos et al., 2014). However, this distribution is not permanent and shifting of this line due to the climate change has been reported (Hammond et al., 2018).

3.2.1 Metamorphism

Whenever snow layers reach 0 °C, additional energy flux to the snow surface imparts to rising water content. Snowmelt will continue to occur whenever the cold content of the snowpack exceeds 0 °C or until the snow has fully melted (Pan et al., 2018).

In dry snowpack grains are rounded when temperature is just below melting point due to vapor sublimation on the surface. Molecules of water in vapor settle on empty sites of grains. Small temperature gradient generates slow growth rates of grains that lead to coupling of grain particles that are bonded and create stable snow. Large temperature gradient is associated with large growth and rounded particles reform the shape and recrystallize in faceted forms because vapor transfer is faster than snowpack with the smaller temperature gradient. When large temperature gradient comes, grains grow into faceted forms and bonds are weakened among particles. Metamorphism within wet snow significantly depends on liquid water content (LWC). Low water content around 0 – 3% causes grain clusters that are characterized by strong bonds because of a surface energy is lowered from the liquid to the solid form. Because cluster grain has weak bonds, snowpack is becoming less stable. No temperature gradient is found in the wet snowpack along the profile, but it can be found among particles. Smaller grains are typical with lower temperature which causes heat flow between larger and smaller grains. The process of the heat flow through the snowpack is responsible for balancing temperatures between different grain sizes and causes melting of smaller grains that are consumed by bigger grains. With large LWC close to 15%, particle bonds significantly decrease and stable snowpack turns into slush (Colbeck, 1986).

The melting phase period depends on the energy equation (1) that can be expressed with three forms by DINGMAN (2015).

Warming phase: The absorbed energy raises the average snowpack temperature to isothermal at 0 ℃.

5

Ripening phase: The absorbed energy causes the melting of snow, but the meltwater is retained in the pores by surface tension forces. At the end of this phase, retained water maximum can be seen in the snowpack and the snowpack is "ripe".

Output phase: Water output occurs, which then appears as runoff, infiltration or evaporation.

Ripening is a process where snowpack reaches a state where it yields meltwater, including heating snow to 0°C. When the snow is ripe and air temperature is higher than 0°C, snowmelt occurs, otherwise positive energy first brings down snow to the freezing point (Singh et al., 2011).

3.2.2 Energy balance

Energy balance equation is one of the determining approaches of the snowmelt. In fact, snowmelt is the last phase of the metamorphism process.

The snowmelt depends on the amount of energy provided to the snowpack for melting. The energy balance describes the fundamental approach for understanding all the fluxes between atmosphere, soil and snow and puts them in relation together (Seibert et al., 2014). In other words, the snow energy balance indicates the amount of energy needed to contribute towards melting (Mazurkiewicz et al., 2008). It is described by DEWALLE AND RANGO (2008) as

$$Q_i = Q_{ns} + Q_{nl} + Q_h + Q_e + Q_r + Q_g + Q_m \qquad (1)$$

where:

- Q_i = Internal sensible and latent heat storage change in snowpack. (±)
- Q_{ns} = Net shortwave radiant energy exchange (≥0)
- Q_{nl} = Net longwave radiant energy exchange (±)
- Q_h = Convective exchange of sensible heat with the atmosphere (±)
- Q_e = Convective exchange of latent heat of vaporization and sublimation with the atmosphere (±)
- Q_r = Rainfall sensible and latent heat (≥0)
- Q_g = Ground heat conduction (±)
- Q_m = Loss of latent heat due to meltwater creating the runoff from the snowpack (≤0)

All these exchange energy expressions are understood as energy fluxes density expressed as energy exchange per unit surface area per unit time [W m^{-2}] (Seibert et al., 2014).

3.3 Snowpack properties

Properties of snowpack being constantly changed have strong influence on storage and release capacities of the snowpack (Kinar and Pomeroy, 2015).

Snowpack properties (grain properties, ice layers or capillary barriers) are influencing ingredients of liquid water propagation through the snow. Liquid water in the snowpack is usually used as the key factor of further predictions for snow melting and avalanche release. Wet snow tends to appear when liquid water arrives at the snow base (Katsushima et al., 2013). To quantify water stored in a snowpack, bulk density combined with snow depth is used. In snowpack, the bulk density is defined by strongly non-linear behavior due to the occurrence of both dry and wet conditions of the snow (De Michele et al., 2013). Snowpack properties influence the liquid water storage and release.

3.3.1 Grain size and shape

Snow texture, grain shape and size are important parameters where all components influencing water movement in snowpack (Techel et al., 2008).

Grain size of the snow influences the permeability depending on the pore size parameter. The grain (particle) size parameter is constantly shaped or influenced by metamorphism driven by temperature, LWC, ROS, wind, topography and settling of the snowpack. Grain size parameter at the wet snow stadium is described as (grain clusters, melt-freeze particles, slush (Figure 1)) and for dry snow as (faceted or rounded (Figure 1)). Particle growth rate decreases for dry snow when snow density increases. However, the particle growth rate increases with a temperature gradient, which is an element composed of air and ground temperature (Colbeck, 1986).
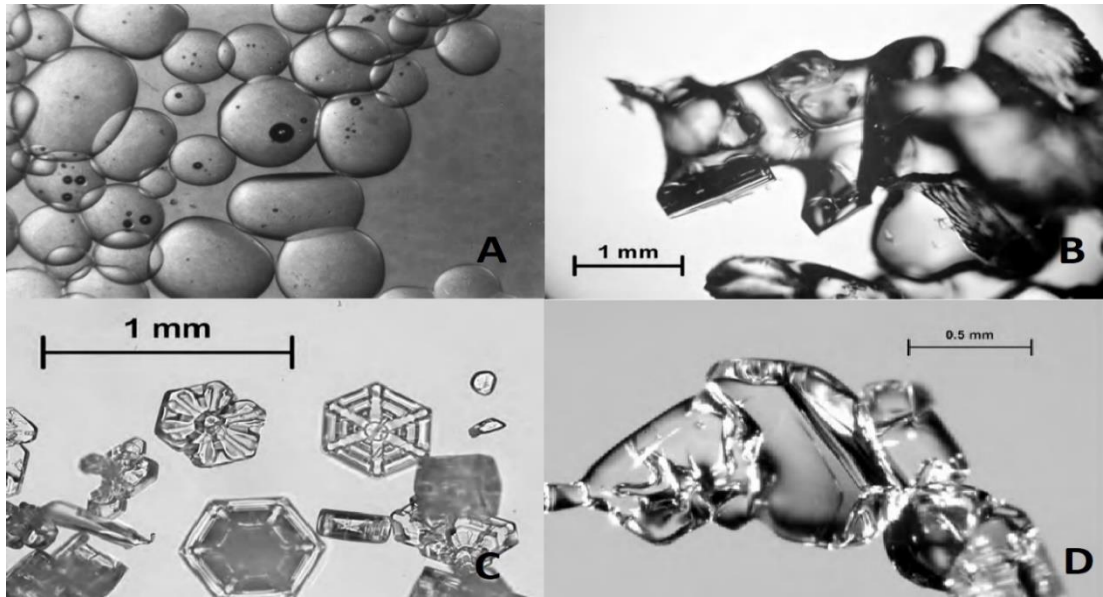
Figure 1: Examples of grain types. A) Slush, B) Melt freeze crust, C) Plates, D) Faceted rounded particles. Adapted from FIERZ ET AL. (2009)

Due to natural disruptive forces and conditions named before influencing the grain size and shape, an international classification was created. (Fierz et al., 2009)

Table 1: Main morphological grain shape classes, adapted from FIERZ ET AL. (2009)

Class	Symbol	Code
Precipitation Particles	+	PP
Machine Made snow	◎	MM
Decomposing and Fragmented precipitation particles	╱	DF
Rounded Grains	●	RG
Faceted Crystals	□	FC
Depth Hoar	∧	DH
Surface Hoar	∨	SH
Melt Forms	○	MF
Ice Formations	▬	IF

3.3.2 Snow Water Equivalent (SWE)

The snow water equivalent (SWE) is defined as the water stored in snow that can potentially contribute to the runoff, if the mass of snow melted completely (Fierz et al., 2009). In other words, SWE is the depth of the water in the snowpack that needs to be melted instantaneously (Perez et al., 2017).

Relation of SWE and the bulk density is as follows:

$$SWE = h_s \frac{\rho_b}{\rho_w} \qquad (2)$$

where:

Snow depth [h], ρ_b bulk snow density and ρ_w is density of water. The SWE equation is then a nonlinear function of h_s (Sturm et al., 2010).

3.3.3 Liquid water content (LWC)

LWC in snow originates from melt, rain or combination of both. LWC of the snowpack describes the wetness of the snow expressed as the liquid water accumulated in the snow pores. The snow wetness can be an indicator of melting and snow stability. An increase of the liquid water content in the snowpack can lead to beginning of snowpack runoff in a catchment. The higher is the wetness found in snow, the more important of a factor faster melting is. In combination with ROS and temperatures above the freezing point, LWC plays an important role in predictions of floods and other related events (Perez et al., 2017). Measurements of LWC are described as either a volume or mass fraction. Liquid water moves if residual water content is exceeded. It is the water that can be held by surface forces against the capillarity. Depending on the type of snow, residual water content corresponds commonly to a volume fraction of about 3 – 6 % (Fierz et al., 2009).

LWC is calculated as follows.

$$\theta_v = \theta_m * \frac{\rho_s}{\rho_w} \tag{3}$$

where:

- θ_v = volumetric liquid-water content in m^3 of liquid water per m^3 of snow.
- θ_m = LWC based on mass, kg of liquid water per kg of snow.
- ρ_s = snowpack bulk density, kg m^{-3}.
- ρ_w = liquid-water density = 10^3 kg m^{-3}.

Wetness categories are determined by FIERZ ET AL. (2009)

Table 2: LWC classification, adapted from FIERZ ET AL. (2009)

Term	Wetness index	Code	Description	Approximate range of $\theta_{w,V}$ (volume fraction in %)[1]		Graphic symbol
				range	mean	
dry	1	D	Usually T_s is below 0°C, but dry snow can occur at any temperature up to 0°C. Disaggregated snow grains have little tendency to adhere to each other when pressed together, as in making a snowball.	0	0	
moist	2	M	T_s = 0°C. The water is not visible even at 10× magnification. When lightly crushed, the snow has a distinct tendency to stick together.	0–3	1.5	|
wet	3	W	T_s = 0°C. The water can be recognised at 10× magnification by its meniscus between adjacent snow grains, but water cannot be pressed out by moderately squeezing the snow in the hands (pendular regime).	3–8	5.5	||
very wet	4	V	T_s = 0°C. The water can be pressed out by moderately squeezing the snow in the hands, but an appreciable amount of air is confined within the pores (funicular regime).	8–15	11.5	|||
soaked	5	S	T_s = 0°C. The snow is soaked with water and contains a volume fraction of air from 20 to 40% (funicular regime).	>15	>15	||||

3.4 Liquid water propagation through the snowpack

3.4.1 Rain on snow (ROS)

Rain on snow (ROS) events can accelerate snowmelt and have the potential to generate floods. They are also a very important factor for water movement in the snow. ROS as a crucial point of the flooding potential has been reported for many catchments during the high water level events in the US, Europe, and around the globe in the past (Würzer et al., 2017).

ROS events from the past have shown that the snowpack under ROS conditions can either release runoff directly or delay it considerably. The delay is described as the result of refreezing of liquid water and water transport which is influenced by snow structure (grain properties, ice layers or capillary barriers) (Würzer et al., 2017).

ROS in open areas has higher potential to cause runoff than in forested fields. It has been found that snowmelt in forested areas during ROS events was much lower than in open areas. Absence of vegetation is therefore very important for further predictions

of the ROS events impacts the snowpack stability as well as other known components like slope temperature etc. (Mazurkiewicz et al., 2008).

Raising temperature due to the climate change has the potential to increase the frequency of ROS, especially in high elevation areas (Würzer et al., 2017). Higher temperatures have impact on the presence of snow during the season and liquid form of precipitation is observed in winter. This climate impact results at the precipitation distribution. Recent studies have revealed that liquid precipitation will occur more often during winter. The changes in precipitation distribution depend on the location. In Northern Europe, higher intensities of rain are predicted, whereas the South is predicted to have fewer precipitation events (Jacob et al., 2014). However, the distribution of ROS events and their response to climatic changes are uncertain and not properly studied (Pan et al., 2018).

3.4.2 Water movement in snowpack

Hydrological predictions of water movement are interpreted by mathematical models that have been widely used (Hirashima et al., 2014). Models vary in a need of the hydrological impact as well as in use for other predictions. For instance, SNOWPACK is a physical one-dimensional model to provide avalanche warning predictions. Model calculates partial differential equations governing the mass, energy and momentum conservation within the snowpack. Input data to SNOWPACK are obtained from fully automated weather stations (Bartelt and Lehning, 2002). SNOWPACK requires air temperature, relative humidity and the wind speed as an input parameter. Valid results can be modeled when accurate input parameters are measured (Lehning et al., 2002). Many studies have implemented SNOWPACK model to their research (Wever et al., 2016), (Avanzi et al., 2016) as well as (Hirashima et al., 2010). Other models for the purpose of this work are omitted.

Models have rarely been validated for natural snowpacks and their accuracy and impact in liquid water processes remain unknown yet not highly studied (Hirashima et al., 2019). The accuracy of models is the crucial element of modeling and the input data play an important role. Experiments WÜRZER ET AL. (2017), KATSUSHIMA ET Al. (2013) better help to understand the water storage and release in the snowpack but more experiments are needed to provide reliable data for models.

For understanding liquid water movement in snow, various field studies have been conducted by spreading water-soluble dye on the snow surface and studying the end

conditions by excavating pits in the snow after rain and creating the snow profile analysis. Experiments have shown that irregularity in infiltration during ROS occurs with high variations. As mentioned before, presence of liquid water in snow weakens the bond among grains and alters the snow texture. This results in lower mechanical strength of the snowpack (Singh et al., 1997). The dye tracer experiments have demonstrated water regimes in the snowpack as well as existence of PF (preferential flow paths) paths in snow (Waldner et al., 2004).

Flow regimes

Even though more regimes might be determined in literature, most referred regimes are described in this work.

Matrix flow (MF)

Matrix flow (MF) is an even liquid water movement reaching very slow velocities and solutes through the medium while occupying most of the pore spaces in snowpack (Figure 2). Snowpack with MF has more uniform and homogeneous texture than the snowpack where another flow regime is observed (Avanzi et al., 2016). MF tends to dominate in ripe, isothermal snow. Unlike PF, MF does not concentrate runoff quickly with intense peaks. (Hirashima et al., 2019).
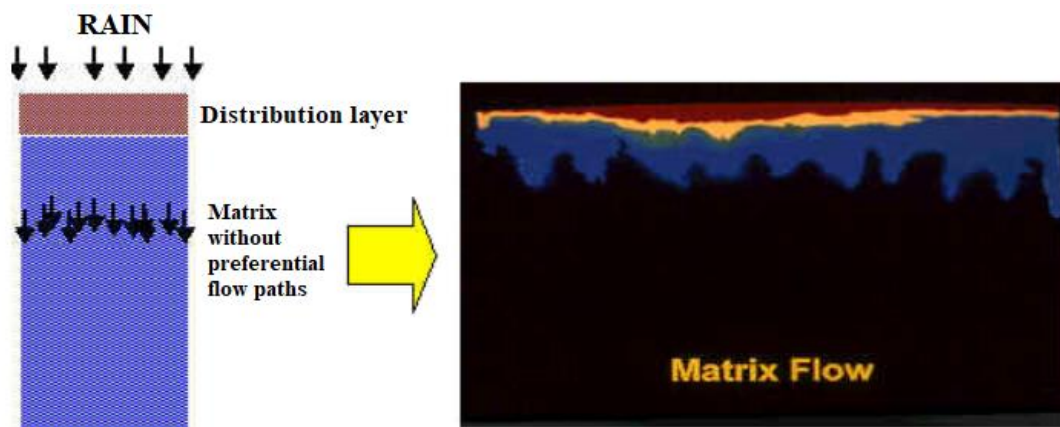
Figure 2: MF regime, adapted online from CORNELL UNIVERSITY DEPARTMENT OF BIOLOGICAL & ENVIRONMENTAL ENGINEERING (2020)

Preferential flow (PF)

PF occurs when small variations in seemingly homogenous snow lead to small dissimilarity in hydraulic conductivity. In vertical flow profile, water penetrates through

the snow deeper and faster resulting in isothermal conditions at greater depth than during homogenous wetting (Figure 3). The infiltration velocity ranges from 0.01 to 0.1 m s^{-1} (Techel et al., 2008). The snowpack runoff and speed of the PF is defined by distribution and size of preferential flow paths, which are dependent on the snow structure. (Würzer et al., 2017).

Four general types of PF have been classified: burrow flow, crack flow, finger flow (FF) and Lateral flow (LF) (Wang et al., 2018). LF and FF are the selected flow regimes described for the purpose of this thesis.
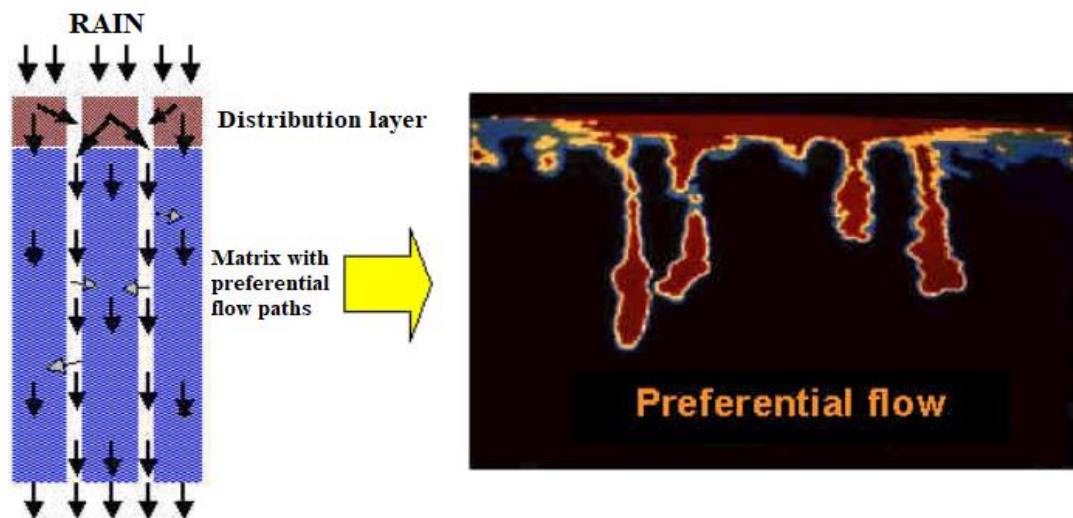
Figure 3: PF regime, adapted online from CORNELL UNIVERSITY DEPARTMENT OF BIOLOGICAL & ENVIRONMENTAL ENGINEERING (2020)

Finger flow (FF)

PF refers to the heterogeneity of the porous media where FF is a type of PF vertically driven by the gravity develop owing to the infiltration of snow meltwater or rain into a dry snow (Katsushima et al., 2020). When FF develops, the water breaks into the porous media through fingers rather than uniformly through the entire layer (Wang et al., 2018).

Lateral flow (LF)

LF works on the base of capillary barriers impeding vertical water flux to form. It occurs at the layer interface between two types of different snow when pressure differences exist. Once pressure equilibrium across the borderline is established, water flow may pass this barrier and (most likely) preferential flow is formed (Techel et al., 2008).

Transformation of the flow regimes

COLBECK (1973) claimed that the flow paths are persistent because liquid water can accelerate grain growth and the unsaturated hydraulic conductivity is locally increased within PF paths. On the other hand, WALDNER ET AL. (2004) stated that COLBECK (1973) did not consider refreezing, which predominantly occurs in dry snow when temperature is close to the freezing point. Due to the accelerated grain growth and the reduction of small pore sizes, the presence of liquid water increases the probability of the matrix flow regime occurrence. The remaining pore spaces in combination with the transfer of water from the preferential paths into the surrounding matrix cause a gradual translocation of the preferential paths. PF regime is likely to be persistent and tends to be used for further melting. However, PF is also influenced by freezing processes that might lead to MF, lesser pore spaces and reduced permeability among subsequent melt phases leading to favorable conditions for new preferential paths at different locations in the snowpack (Waldner et al., 2004).

Preferential flow paths form when the pressure in the MF exceeds the water entry (ROS, condensation, melt) pressure of the layer below (Wever et al., 2016)

Layering is formed as a microstructural transition inside the snowpack. The small vertical extend of layers can impact processes in the snowpack significantly on the large scale. Layers can reduce the storage capacity of the snowpack in deeper parts of the snow along the profile and water can refreeze, form or flow along the layer. This movement of water can be addressed to the LF, where percolation through the snowpack is more typical for PF regime. Layers tend to be formed in both regimes (Wever et al., 2016).

3.5 Catchment reaction to ROS events

The potential to generate floods during ROS depends not only on the magnitude of rainfall but also on the areal extent of the earlier snow cover with its properties and the spatial - temporal interaction between these snowpack properties and meteorological aspects (Würzer and Jonas, 2018). Due to findings of WÜRZER AND JONAS (2018) study, factors like large snow - covered fraction, spatially homogeneous snowpack properties, prolonged rainfall events, and a strong rise in air temperature produce a higher probability of snowpack runoff occurring synchronously within the catchment, which in turn favors higher overall runoff rates.

In spring and autumn tendency of floods generated by ROS is likely to rise due to the snowpack's homogeneous conditions on a local scale.

ROS events can result in different scales variously. Based on the WÜRZER ET AL., (2016) study conducted on the point scale, correlation between high initial LWC values and runoff excess for point scale can vary in comparison with the catchment scale. This means that locations at the point scale may not necessarily transfer into catchment level findings. In this example, spatially heterogeneous snowpack properties add additional complexity to the problem and may dilute, or even reverse effects that hold true for individual locations due to partial snow cover and asynchronous timing of runoff from different parts of a catchment (Würzer and Jonas, 2018).

3.5.1 Future scenarios of the watershed reactions on the ROS events

On the large scale, ROS events can cause different patterns in the hydrological distribution due to the climate change. As the seasonality changes, magnitude and frequency of ROS floods in the future can vary. This has been studied by SEZEN ET AL. (2020). In their research the CemaNeige GR6J lumped conceptual model was applied for the simulation of ROS floods in combination with the results of five GCM/RCM models for the RCP4.5 climate scenario. For catchments located at higher elevations with mountain climate characteristics, the strength of seasonality of ROS events could decrease in the future. This means that ROS floods may occur more frequently in the periods of the year. A shift in the time of occurrence of ROS floods could be expected as well as more ROS floods can be witnessed in the future. Moreover, the magnitudes of the most severe ROS floods could increase.

3.6 Dye tracer experiments

Water movement in the snowpack, and especially preferential flow of liquid water through snow can have a distinct impact on timing and amount of snowpack runoff (Würzer and Jonas, 2018). These aspects have been examined using dye tracers many times, where brilliant blue dye is sprinkled on snow and excavation is done to observe water movement formation in the snowpack (Schneebeli, 1995; Würzer et al., 2017). From these experiments it can be concluded that penetration during an infiltration event in snow is the prevalent pattern in melting snow covers (Schneebeli, 1995). Through the application of a brilliant blue dye to the surface of a snowpack and later snow pit excavation as conducted in STÄHLI ET AL., (2004) study, dye

tracers allow visualization of flow paths and formation of structurally different layers (Waldner et al., 2004; Williams et al., 2010). Many approaches have been examined to visualize the water movement in the snowpack after sprinkling experiments and the subsequent visualization of images after dye application leads to conclusions of understanding the nature of water flow in the snowpack (Schneebeli, 1995). An innovative approach of visualizing the water behavior in snowpack after sprinkling experiments was conducted by WILLIAMS ET AL., (2010). In their study a snow guillotine was used. This instrument consists of a metal and PVC framework with a blade that slices uniform cross-sections (about 1 m ð 1 m) at 1 cm intervals. Digital images are taken of each cross-section after the blade has removed a uniform section from the snowpack. Application of image processing techniques allows collection of three-dimensional (3D) data on dye presence that provides information on meltwater flow through a snowpack.

3.7 Snow monitoring techniques

In general, two approaches exist, ground and distance techniques. To measure the snow on ground, many manual techniques are available, such as a widely used snow probe for determining the depth of the snow. During the snowfall event, weather stations are used to get information of the falling fresh snow, which are usually equipped with a snow stake that can be read by an observer without entering the surrounding area of the station and not affecting the snowpack. (Doesken and Judson, 1997). On the other hand, distance techniques are techniques that measure snow usually from the orbit, but can also measure from different, farther locations.

Depending on what data we need to obtain, we choose the measuring technique. In this chapter some important techniques will be mentioned and many of them will be omitted for the purpose of the thesis.

3.7.1 Ground base measurements

Permanent monitoring

Snow pillow

Snow pillows are envelopes of stainless steel usually shaped as and rectangle or a square, containing an antifreeze solution. The principle of the snow pillow is that the loaded snow is sensed either by a pressure transducer or by the fluid level in a standpipe. These apparatuses transform the weight of the snow to an electrical

reading of the SWE. The precipitation gauge measures all precipitations events in any form, while temperature is obtained by the sensor (DeWalle and Rango, 2008).

Network monitoring

In the Czech Republic, Czech Hydrometeorological Institute (CHMI) maintains and collects data from the network of the automatic snow pillow stations. Stations are equipped by the snow pillow and are able to measure snow depth (Figure 4) and SWE (Figure 5) (both examples are from the same station). Sites are technically constructed with laser and ultrasonic sensors. Data are stored on-line <http://portal.chmi.cz/files/portal/docs/poboc/PR/grafy/snih-lnk.html> and uploaded on the webpage of the institute (CHMI©, 2017)
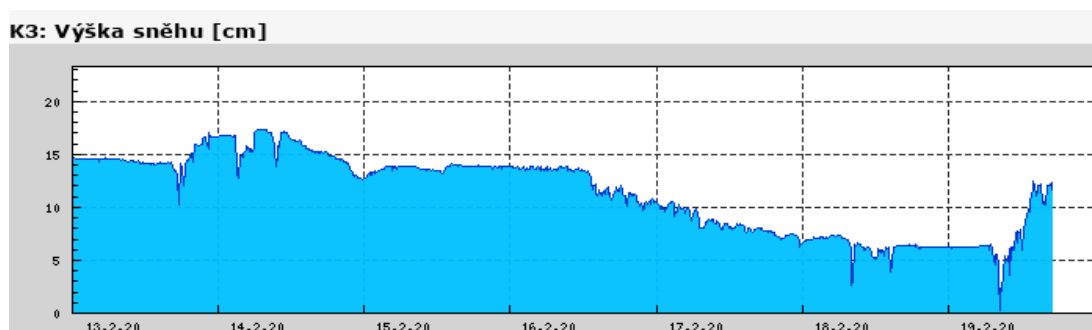
Figure 4: Snow depth collected from the CHMI snow pillow network station. Derived from CHMI© (2020)
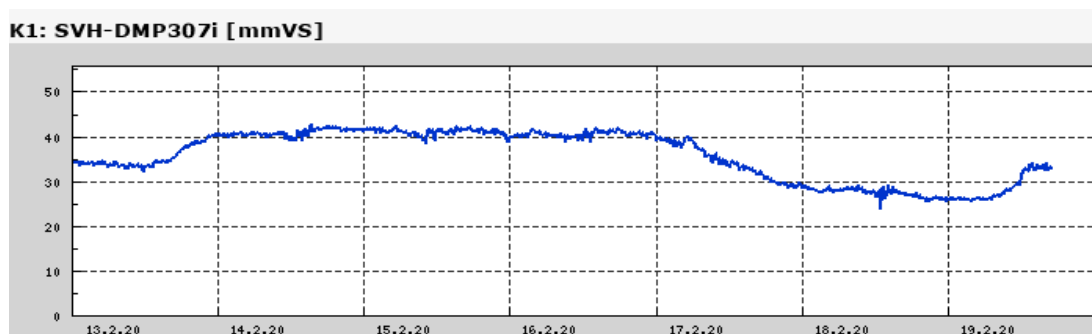
Figure 5: Calculated SWE from the snow pillow network station. Taken from CHMI© (2020)

In the United States, SNOTEL is used to collect snowpack and climate data in remote regions, predominantly in the western parts of USA (Burns et al., 2014). Data from the SNOTEL are collected and relayed using the meteor burst communications technology to National Weather and Climate center in Portland, where data are stored. SNOTEL sites are equipped with a pressure-sensing snow pillow, a sonic depth sensor, an air-temperature sensor and storage precipitation gauge. The

SNOTEL can hold additional sensors that could be used for other environmental problems (DeWalle and Rango, 2008).

3.7.2 Remote sensing/scanning of the snowpack

Visual satellite images

Images of the planet Earth are continuously transmitted from the satellites that collect data from the terrain of the surface. Because snow is an excellent reflector of sunlight in the absence of clouds, images enable us to see snow covered areas. This technology is problematic in many aspects of measuring specific properties of snow. Forested regions and mainly coniferous forests complicate this method to obtain ground floor data with snow on it (Doesken and Judson, 1997).

Gamma radiation

The use of gamma radiation to measure SWE is based on the natural terrestrial radiation by the mass of water in the overlying snow. The radiation is emitted from (K, U, Th) elements. The intensity of radiation is recorded using a gamma radiation spectrometer, which is installed on an airplane (DeWalle and Rango, 2008). The greater the SWE the less the emission of radiation into the atmosphere. This technology has been used to estimate potential flood risk from the snowmelt in the northern parts of the US (Doesken and Judson, 1997).

Visible and near infrared imagery

In this way a multispectral scanner subsystem on satellite is used for mapping the snow areas. Snow extent mapping used to be performed manually using photointerpretive devices. More recently, digital mapping of the snow cover has been the preferred way using the red band at 0.63–0.69 µm. This method is problematic because of the poor observational frequency (DeWalle and Rango, 2008).

Mapping data of the snow on surface can be obtained from satellites (Landsat, Terra and others) with sensors like MODIS, or AMSR. The geospatial information of terrain and snow cover can provide space for investigating the ROS patterns and underlying physiography driven by the climate change. For instance, frequency and distribution of ROS events by remote sensing was examined by PAN ET AL. (2018).

4　Methods

4.1　ROS experiments description

Experimental sites descriptions

ROS experiments took place in the Czech Republic with data from the 2019 season. There were 4 established experimental sites in 2018 but only 3 sites were loaded enough of snow to be able to conduct sprinkling experiments on. The experiments were carrying out in 2019 winter season at three sites. The involved sites of experiments were Luisino Údolí and two more sites close to each other in Kubova Huť village (Figure 6). Horní Němčice site was not involved in the experiments though. Luisino Údolí was examined on 2nd of January, first of Kubova Huť site $14^{th} - 15^{th}$ January and the second experimental site of Kubova Huť lately on $15^{th} - 16^{th}$ March. All sites where experiments were carried out have been abbreviated in this work as follows: Luisino Údolí – LU, Kubova Huť (January) – KH1 and Kubova Huť (March) – KH2.

For investigation, sites are variously equipped. For example, LU was with meteorological station to measure snowfalls and temperature in soil and in the air in two meters above the surface. All the sites of experiments have a lysimeter board installed where water infiltration to the soil is prevented and information of snowmelt recorded. Hence, flow is drained by channel and from the known area of the lysimeter desk a discharge is gauged by the tipping bucket at the end of the system.
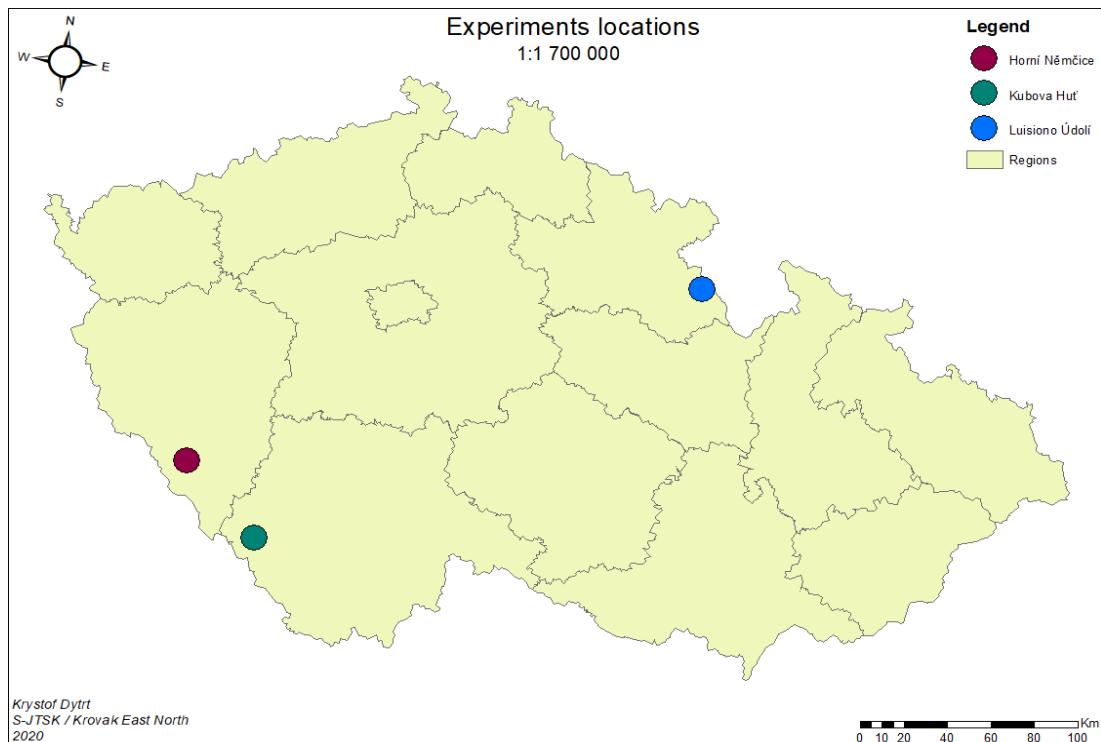
Figure 6: Locations of the experimental sites

At the experimental sites a ROS event simulator was used (explained later) where stations had been prepared before the winter season. When a station got prepared a precision localization method was used to determine spatial distribution of all the objects on site. This method consists of marking every object of the station into layout (Figure 7) that is used in the winter season for the placement of the ROS simulator. It is essential the simulator is placed right above the lysimeter desk as well as operating on site without affecting the snow. Only undisturbed snow can provide solid data of the water behavior in the snowpack.
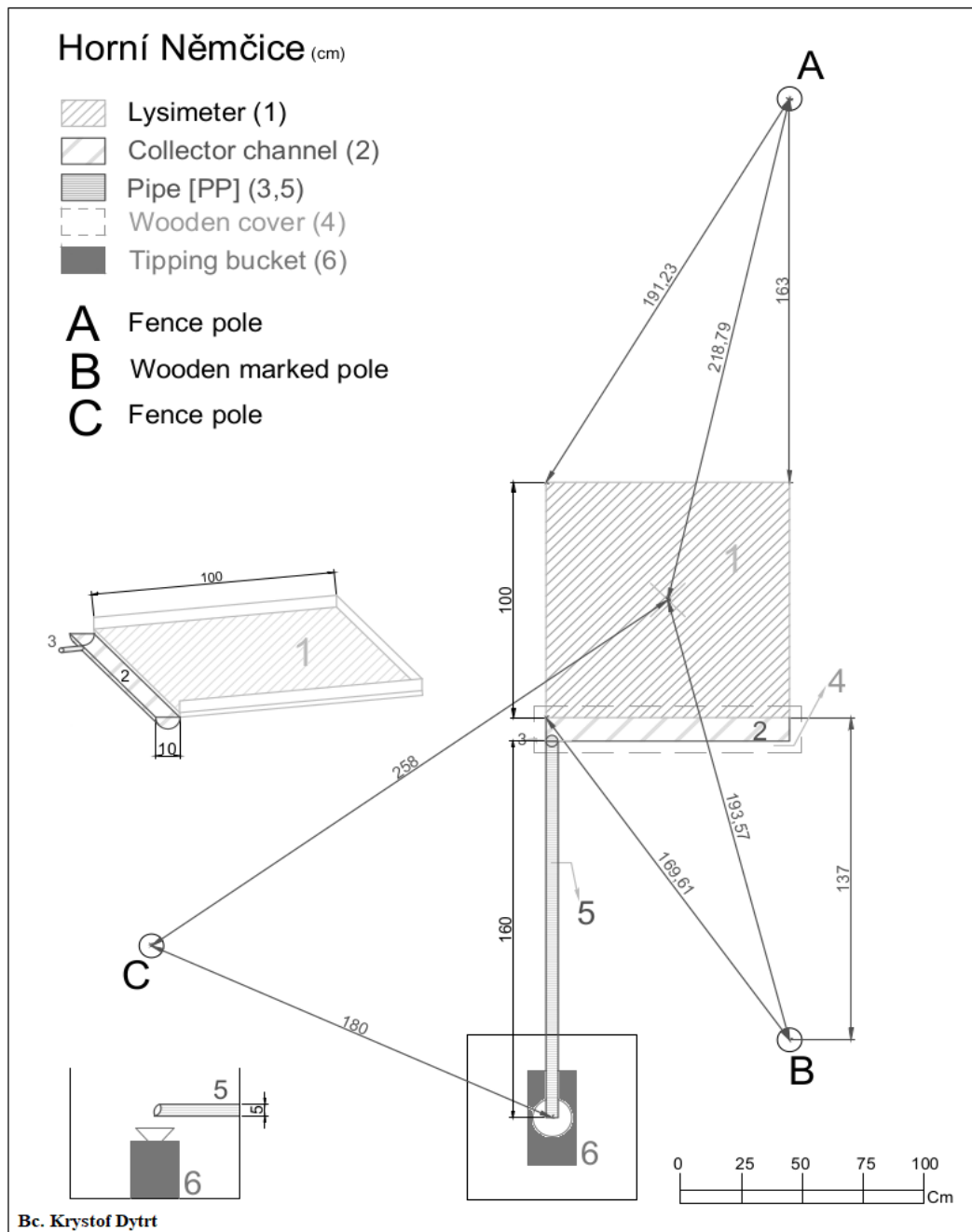
Figure 7: An example of the localization method used at the Horní Němčice site.

ROS simulations

ROS simulation data were obtained by the ROS experimental team and processing them has been done in this thesis without author's presence on the experiments in terrain.

The experiments consist of simulating the rainfall-runoff mechanisms where physical processes are investigated. For the snowpack examination purposes, a ROS event

simulator was used to imitate rainfall. Similar device yet refined as in WÜRZER ET AL. (2017) was applied to the experiments. Adjustable variations of intensities of rainfalls lasting certain time are generated by this device. Simulator's construction has a solid frame with nozzles hang up on the ceiling. Via nozzles a rain is simulated and then infiltrated into the snowpack below. Water going through the snow cover continues via the desk of the lysimeter to the channel. Water is seized and outflowing to the tipping bucket that collects data of water released from the snowpack. The tipping bucket is connected to the logger that can count automatically every minute operated. During the simulations, temperature of snow, water and air are measured.

After simulation process

Snow affected by the simulated rain is examined by excavating pits in snow. This provides information how much water has been accumulated, water regimes in the snowpack or release. Usually 5 slices were cut out of the snowpack after simulations where each slice showed water accumulation or water fluid paths. However, it is necessary to point out that the profile analysis was not done in this segment nor for each slice of the snowpack. Procedure of the profile analysis was conducted always twice for each site (before and after experiments).

4.2 Pre and post experimental properties investigation

Altered properties of snow are detailly investigated for the purpose of the water regime determination through the snowpack. Data of changed properties can help to understand the water storage of the snow or can point out to the estimations of water release. To model properties of the snowpack, snow profiles are visualized before and after the ROS experiments. Properties under investigation are

- Temperature
- Stratigraphy / structure
- LWC / Denoth density
- Density

Because ROS simulations are man - made simulations. Surrounding environment of the examined snowpack and experimental site is affected and properties of the snow could be as well. It is necessary to take this factor into account. Energy exchange fluxes were minimized or influenced by the ROS experiments with an impact to the energy balance equation. Energy fluxes were minimized such as turbulent heat

exchange due to the tarpaulin cover of the simulator, ground heat flux due to the lysimeter board and shortwave radiation was reduced by the tent walls. The simulation process also provided energy to the snowpack by different temperature of the dye tracer.

To proceed to the properties investigation the profile analysis had to be done on site first as the main source of information for this purpose.

4.2.1 Snow profile analysis

The snow profile analysis is suitable method to obtain data for the snowpack modeling, especially the modeling water movement in snow. The most widespread way that is used for snow profile analysis is when a pit is dug in the snow and then every layer is observed. After the pit has been dug and flattened the data are collected from the top to the ground. The profile is measured by a ruler or measuring scales and the area of the profile is established. Layers are observed and recorded in the profile. Temperature data are measured every 5 - 10 cm (density measurement depends on what situation is modeled) to obtain a temperature gradient along the profile. This procedure continues with grain size analysis where we take samples from every specific layer or we collect grain size in specific interval usually every 5 cm along the excavated profile. Size of the particles are observed on the crystal card equipped with a grid scale. To be more exact we use magnificent glass to determine on the crystal card the class of the grain. The determination of the grain size parameter is very subjective, depending on the observer (Fierz et al., 2009). Other properties are measured in the profile as well. LWC is measured by Denoth meter that works on the base of permittivity of snow using snow density. In this way the undisturbed snow is measured (Denoth, 1994).

Sampling method in the profile analysis can result in unexpected changes. For instance, as the water flow induced by the ROS experiment penetrates through the snow the flow can divert by layering as well as can refreeze (there are also other possibilities of water behavior). The sampling method does not have to match to the reaction of ROS precisely because it does not cover the examined profile entirely. For example, profile analysis could not have taken in account all diverted flow paths that were possibly formed, because a sample could have been taken from part of the profile where not desired data were situated. Thus, samplings can influence the overall impression of the studied property under investigation. Nevertheless,

investigation of properties was focused on precise sampling method, but it is necessary to mention that this method can lead to inaccuracies.

Figure 8: The SLF Snow Sensor based on the Denoth Meter capable of measuring density of snow and liquid water content. Adapted online from FPGA COMPANY © (2020)

The SLF Snow Sensor measures the density or the liquid water content (LWC) of snow by a sensor that generates an electrical field permeating the snow. (FPGA COMPANY, © 2020)

The profile analysis could be done in different approach to obtain data effectively depending what is needed to be examined and what data are modeled afterwards. Nevertheless, this is the common approach that has also been used to collect data from the experimental sites.

Visualization itself was partially carried out by the online interface (https://niviz.org/).

Kubova Huť sites obtained post-experimental data the second day of the experiments.

4.3 Photo analyses

Photo analyses are supposed to give some detailed information of the water behavior through the snowpack after the ROS simulations to determine what kind of flow paths and how much water was released from the snowpack. Photo analysis in this work is segregated into three related explorations. The first one "The reliability analysis" the second "Water movement localization" and "Bluesnow analysis". All types of analyses

are used to validate the photo inputs from the ROS experiments. All photos processed by all the approaches were taken by supervisor of this thesis.

4.3.1 Water movement localization analysis

The water movement localization analysis (in this work sometimes referred as only "localization analysis") was performed in the way of classifying each picture and of assigning pictures into a group where the picture was originated from. Photos had to be horizontally leveled for the purpose of the side scales to be readable correctly and leveled photos were studied one by one where water outflow spots were noted.

Because distortion on the top of the snowpack was caused by the position of the camera and by wide angle lens, another approach has been done. This approach recounts the distortion for the purpose of locating the snowpack into a representable system where water regimes in the snowpack after ROS could be examined. Thus, distortion is found when both rules indicate different values even though pictures have been horizontally leveled. To count with distortion, first differences at the bottom had to be flatten (wrong placement of scales). The difference at the bottom is then compared with the top values of the snowpack. If different values have been found (different bottom and top values after flattening), a recalculation was implemented into the flow paths localization after ROS. This recalculation takes the difference between bottom and top (if there is any) and proportionally gives new values towards the top distortion. However, this distortion recalculation is oriented only on the right scale so the values on the left scale stay the same even if the distortion was found. All localized records of water behavior induced by the ROS after experiments is compressed into tables of coordinates per each site.

It is clear now that the values of the snow depth have less reliability due to many aspects making it very difficult to cope data from photos into a comprehensive format. And if the left scale was placed wrong the recalculation could not have been sufficient.

4.3.2 Bluesnow analysis

The bluesnow analysis as the water movement localization analysis processes the pictures from the ROS experiments. The main difference is that the Bluesnow analysis uses a package developed in the R interface written by Ing. Johanna Bloecher for identifying water movement in the snowpack, caused by the dye tracer during ROS experiments. Bluesnow package is located online at

<https://rdrr.io/github/Jorub/bluesnow/>. The input to the package is an image to be processed by every pixel.

Blue – snow package is composed of four main functions.

- *BB_filter:* This function uses RGB thresholds to allocate one of four colors to each pixel (white, dark blue, medium blue or light blue). Grey shadows are assigned white.
- *BB_fraction:* A function that takes the BB_filter outputs and calculates the proportion of total blue pixels, dark blue, medium blue and light blue pixels.
- *BB_hor_distribution:* Takes the result of BB_filter and returns a vector with fractions over the length of an image. This shows the horizontal distribution of the blue accumulations of water in the snowpack.
- *BB_vert_distribution:* A function that processes the outputs of BB_filter and returns a vector with fractions over the depth of an image. BB_vert_distribution is than a visualization of the vertical flow pattern in the snowpack.

Prevailing formation of flow paths after the Bluesnow analysis is calculated as vertical and horizontal distribution of blue fraction processed by every excavation of the snowpack as an input. Where mean of (H / V) distribution of blue fraction per each excavation is calculated with conditional function where values higher than the mean are represented by "TRUES". Number of "TRUES" is then divided by number of all blue fraction values times by one hundred. This shows the percentual prevailing formation as domination in horizontal or vertical formation of fluid paths after ROS. This method compares values of certain excavation and does not compare all excavations together.

4.3.3 Photos reliability analysis

Information from photos were prone to lack of certainty according to the side scales. Because of the uncertainties discovered during the analyses, uncertainty classes had to be made. Uncertainties were not caused by only different values of the side scales, but also by distortion found in the photos and by difficulties of finding the lysimeter desk. The validation of reliability of photos is very subjective and depending on author because it is on author to distinguish uncertainty of the photos.

- First category of the uncertainty class is the lysimeter desk determination. Locating the lysimeter desk is necessary for the purpose of the ROS experiments. Any other procedure without knowing the location of the lysimeter desk is valuated as erroneous. Lysimeter desk was sometimes difficult to distinguish from the snow and sometimes obstructing by the bottom meter. Scale of uncertainty (from 1 to 3, where 3 represents high uncertainty and 1 high certainty) had to be used to interpret certainty of the lysimeter desk determination.

- The second category of uncertainty was created to represent height uncertainties. This class of height uncertainty computed average snow depth and differences in height of snow excavation in photos from the same site. For instance, an average value of snow height (that was measured while ROS experiments were carrying out) and height of snow for each profile were compared for every photo. Because height of snow varied unexpectedly in every picture. Differences between average height and height of each excavated pit were evaluated as the bigger the difference in height for each snowpack, in comparison with the average depth of snow, the bigger the unsureness of the height. In the other words, the bigger the dispersion between average height and profile excavation height, the bigger the unsureness. This level of uncertainty was represented in a scale from 1 to 5, where 5 interprets high uncertainty in height of snow and 1 high certainty.

These classes of certainty show reliability of each photo evaluated in the reliability analysis. Photos with high uncertainty index (validation of the uncertainty by both methods) are less representable than the pictures where the aspect of the lysimeter desk and height dispersion play lower role. Each excavation of snowpack indicates uncertainty of the further localization of layering, leaking water or water movement in the snowpack after the ROS experiments.

4.4 Tipping buckets calibration

An old tipping bucket (TB) device was used in all the examined cases of the experiments where snow melt was drained from the lysimeter desk to the TB. TB that was used for the ROS experiments followed standard mechanisms of measuring the outflow. However, TB was evaluated as a weak point of the experiments and implementation of a new design was decided. New design of the tipping buckets is different in the parameters of the construction, but the common principle remained same as it was before. The principle of the TB is to measure the outflow where two buckets overturn when the volume is filled. The volume of buckets is controlled by the bolts and number of tips is recorded. Thus, outflow is measured by the known volume of the bucket by knowing number of overturns (Figure 9) (Molini et al., 2005).
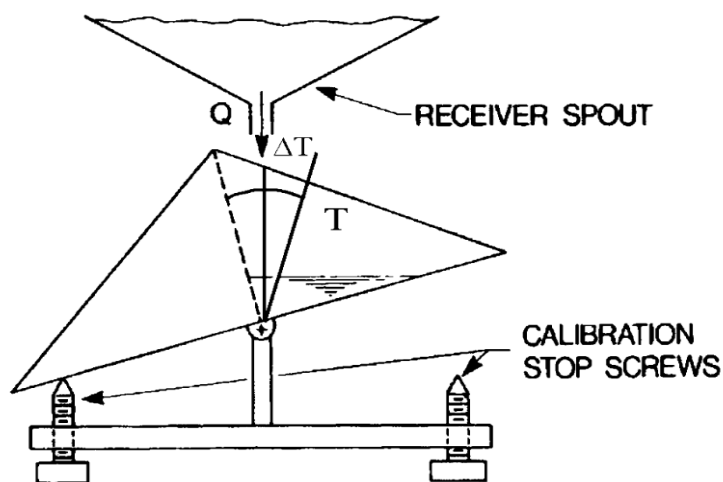
Figure 9: Tipping bucket scheme, adapted from MOLINI ET AL. (2005)

The calibration was focused on improving and implementing new TBs where validation of their measurement error was established. Parameters of tipping buckets were tested with their influence on the measuring precision.

The laboratory calibration was done in three tests to determine what design is the best for implementing. All the calibration sets were tested with static and dynamic approach. As both calibration methods are commonly used (Calder and Kidd, 1978).

Dynamic calibration method

Dynamic method is a technique where 1 liter per minute was executed through the TB system and errors were reported. The dynamic approach consists of counting

number of tips and measuring the rest of the 1 liter seized in the bucket. The rest of the water represents how precise the tipping bucket is.

Static calibration method

The static method checked overturning of the TB where each overturn was studied, and errors reported. In static calibration each bucket was filled slowly by a burette, checking for defects in design. Hence static calibration represents the filling ability of the bucket and bucket's capacity. Dynamic calibration is a simulation of the process when both buckets are working. Secondly, signs of a bad design have been noted and new proposals of innovations implemented into calibration process as a result of an improvement.

5 Results and discussion

5.1 Snowpack properties changes in profile

At the KH1 and LU site, no evidence of water outflow from the snowpack was reported.

5.1.1 LU site profile visualization
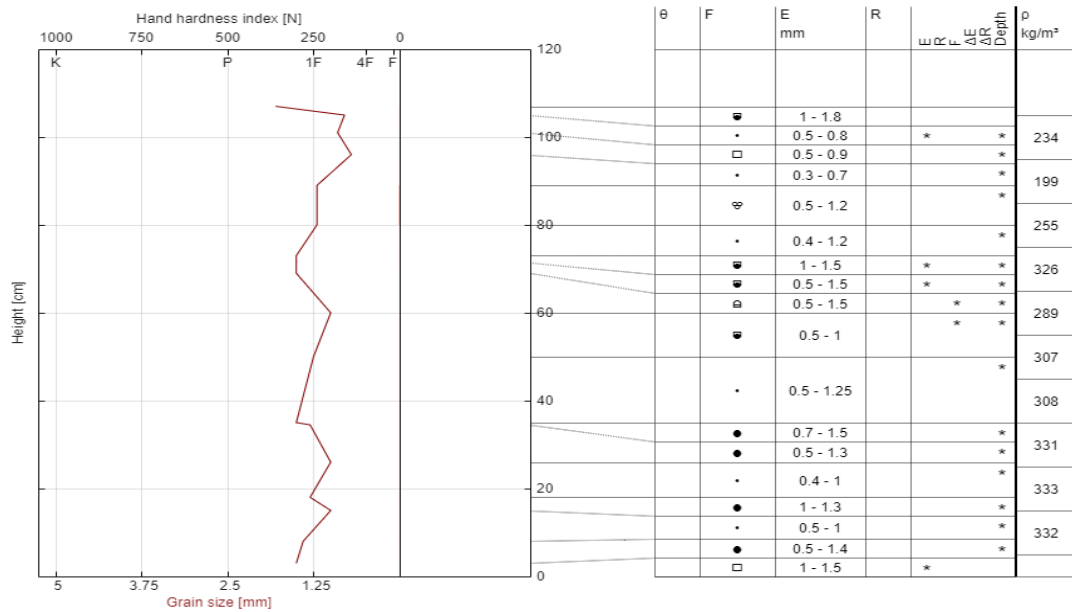
Structure profile

Figure 10: Structure profiles at Luisino údolí site, A) pre – experimental structure profile, B) Post – experimental structure profile. (Grain size [E] - plot, F - grain shape, ρ - density)

The biggest change in structure occurs in the very upper layer where much larger particles were observed (Figure 10). Particles were refrozen after the experiments coupling into much larger parameters. Grain size did not vary dramatically but the particle shape was slightly different after experiments.

Altered properties of pre and post experimental conditions

Figure 11: Altered properties at the Luisino údolí site, A) Temperature profile in pre and post – experimental stadium, B) Density profile in pre and post – experimental stadium, C) LWC only for the post experimental condition due to no measured data in pre – experimental condition.

Temperature

Pre – experimental temperature examination provided colder temperature along the snowpack profile where post – experimental profile indicates changes in the energy balance expressed by warmer temperatures. Rainfall sensible and latent heat are dominant fluxes to have impact on the deflection in the post experimental conditions. This is mainly seen at the top of the profile. Temperatures intersect in both cases along the profile around 60 cm of depth of the snow cover (Figure 11, A).

31

Density

Density comparison shows variations on the top of the snowpack where snow tends to be distinctive denser. Central depths of snow are typical with decent changes in snow that are overlapping and getting closer to each other in both density conditions. Snow in post – experimental condition indicates to be denser except in two cases at around 40 cm and at 10 cm snow depth (Figure 11, B).

Denoth density / LWC

LWC profile is displayed just for the post – experimental profile with no comparison to the pre – experimental profiles. It is so because of the 0% of LWC measured in profile in the pre – experimental stadium.

LWC of the examined profiles is calculated from the air snow emissivity, where pre and post – experimental emissivity was measured as the part of the ROS experiments. LWC is a product of subtraction of post – experimental air emissivity with pre – experimental values of the emissivity in condition function where post-experimental emissivity is higher than the pre-experimental data.

LWC of the post – experimental profile is higher at the top of the snowpack as quite similar, to the deflection in the density comparison (Figure 11, B) where values consolidate in the middle of the snowpack after top variations. LWC refers to some new liquid water added to the snowpack after ROS experiments where rain was simulated. LWC is therefore higher at the top because rain has higher potential to cause higher concentration in the top layers of the snowpack before it penetrates deeper (Figure 11, C).

5.1.2 KH1 profile visualization
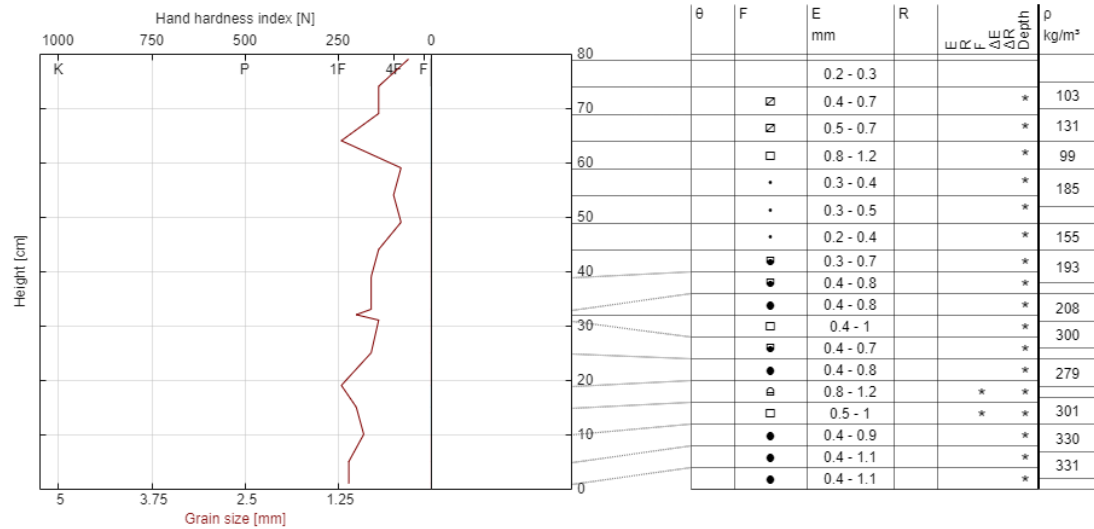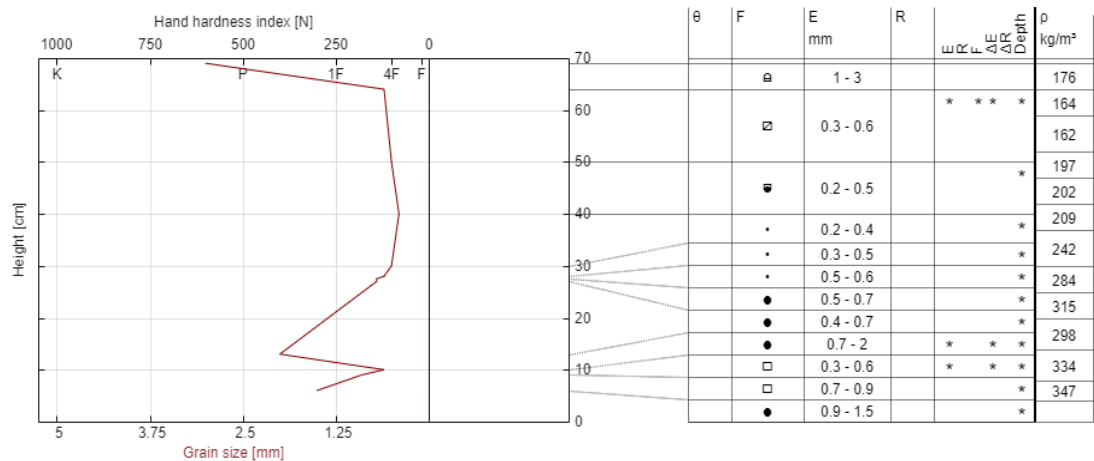
Structure profile

Figure 12: Structure profiles at Kubova Huť 1 site, A) pre – experimental structure profile, B) Post – experimental structure profile. (Grain size [E] - plot, F - grain shape, ρ - density)

Post – experimental structure profile indicates more fluctuations in grain size where the top of the snowpack evidences larger grain parameters. Most of the grain shapes remained the same after experiments or tended to be similar to the pre – experimental condition. Post – experimental profile close to the bottom shows fluctuations in the grain size as the pre – experimental profile was typical with smaller particle sizes (Figure 12). Larger grain size can lead to the capillary barrier effect. Although, the capillary barrier also depends on snow condition.

Profile changes by individual properties
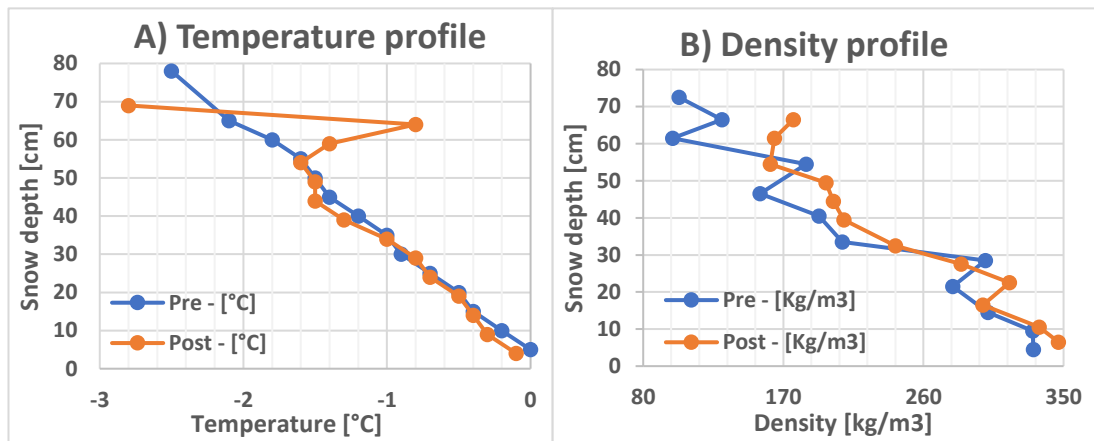
*Figure 13: Altered properties at the Kubova Huť 1 site, A) Temperature profile in pre and post –
experimental stadium, B) Density profile in pre and post – experimental stadium.*

Temperature

Temperature changed through the snowpack towards 0 °C in both cases similarly with
no significant changes except in the upper layers where at first glance clear warmer
temperature was captured around 55 – 65 cm due to the changes in energy balance
(Figure 13, A). Rain on snow caused a reaction in the energy balance of the snowpack
where rainfall sensible and latent heat influenced the upper part of the snowpack
profile.

Density

The upper part of the post – experimental snowpack was denser than the pre-
experimental. Both experimental density profiles meet around 55 cm depth of snow.
Middle part of the density profile provided similar values for both samples but the snow
after experiment tends to be denser. The lower part of the density profile showed
some changes where denser snow for the post – experimental profile can be seen
with no significant variations (Figure 13, B).

LWC

In January at the KH1 site 0% of LWC was recorded in both pre and post –
experimental cases.

5.1.3 KH2 profile visualization

Structure profiles

A) Structure profile in pre - experimental condition   **KH2 site**

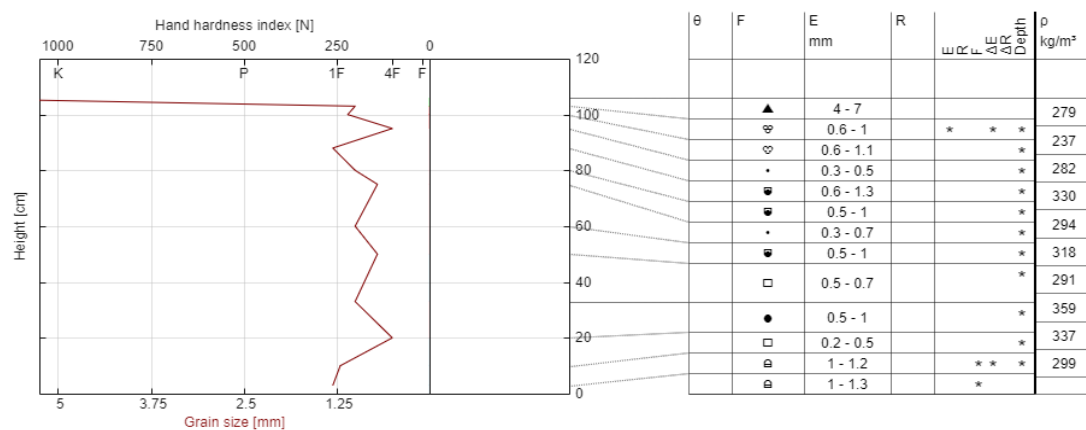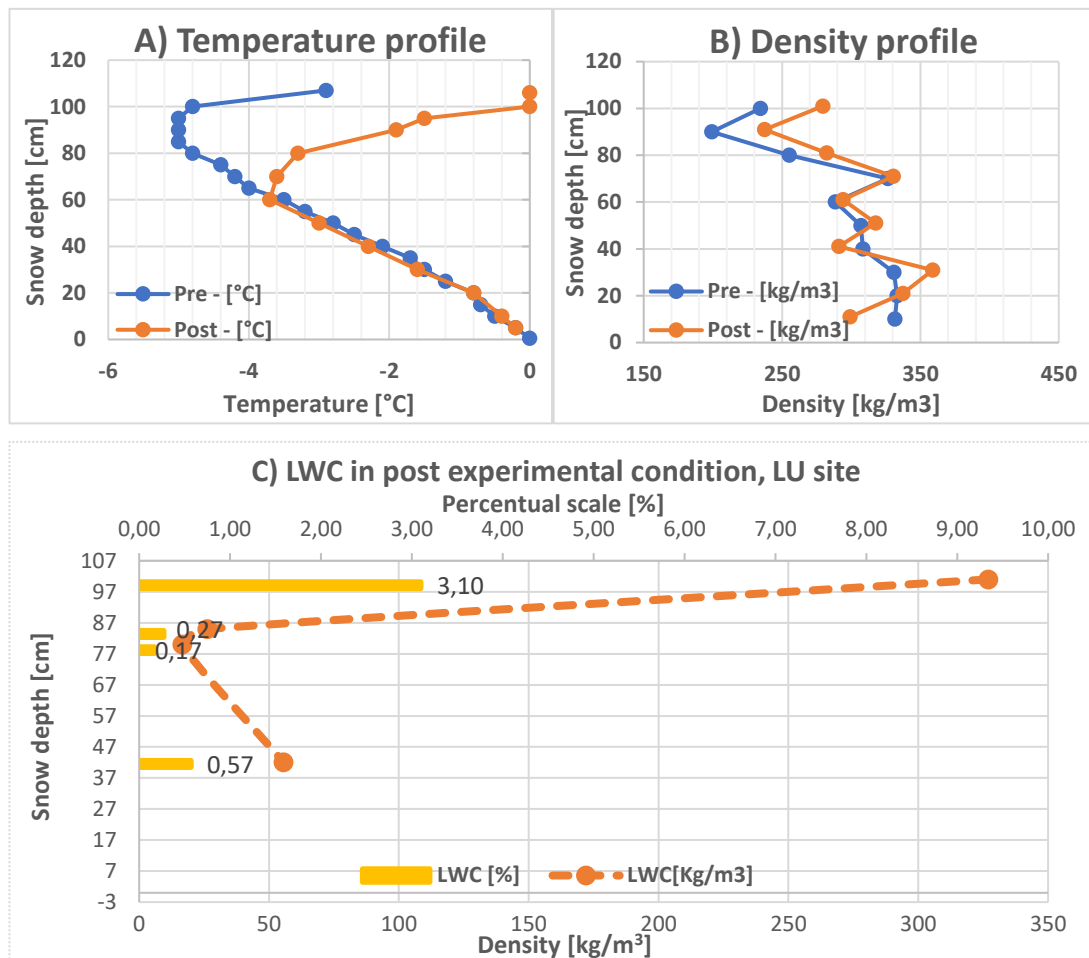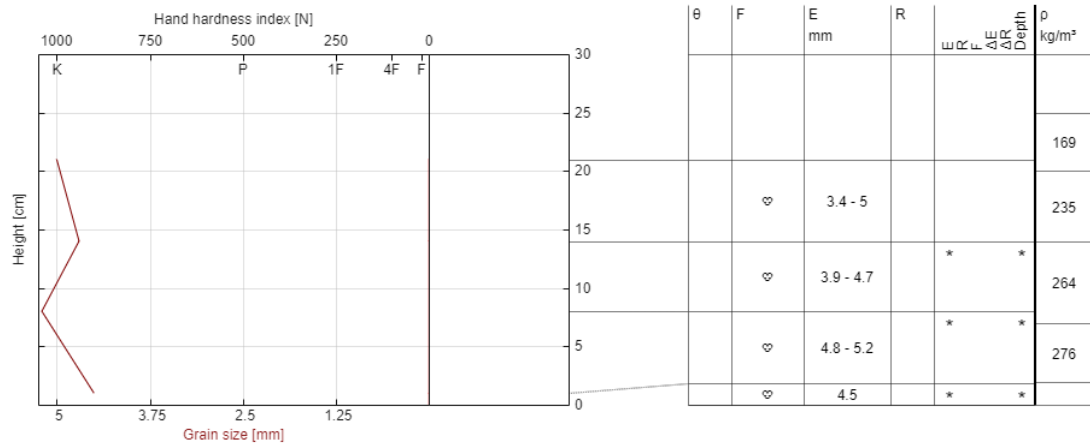**B) Structure profile in post - experimental condition**   **KH2 site**
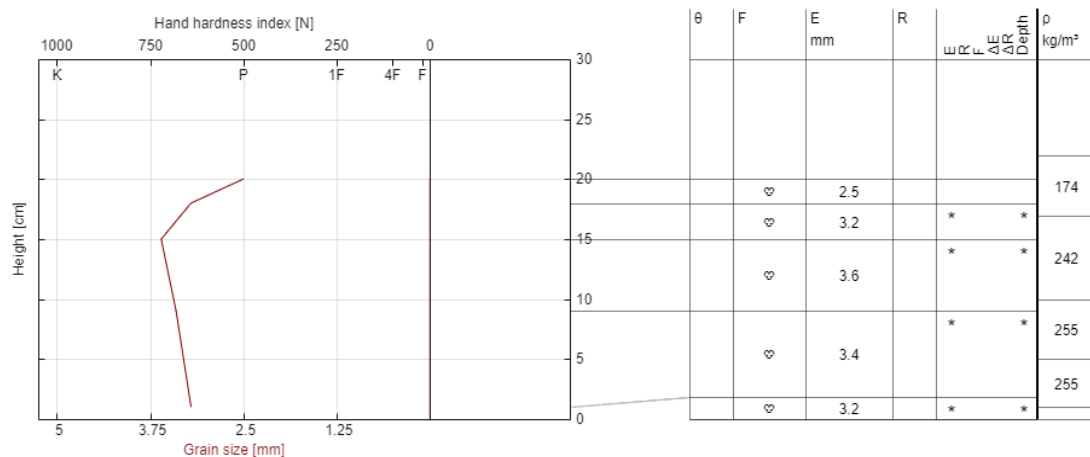
Figure 14: Structure profiles at Kubova Huť 2 site A) pre – experimental structure profile, B) Post-experimental structure profile. (Grain size [E] - plot, F - grain shape, ρ - density)

Grain size varied after experiments towards smaller dimensions. Grain shape did not change and was the same for every layer of sampling during the profile analysis. Therefore, snowpack with homogenous structure was registered in both conditions (Figure 14). Smaller grain size could be explained as the already melting phase influenced the diameter of the grain towards smaller values.

Profile changes by individual properties
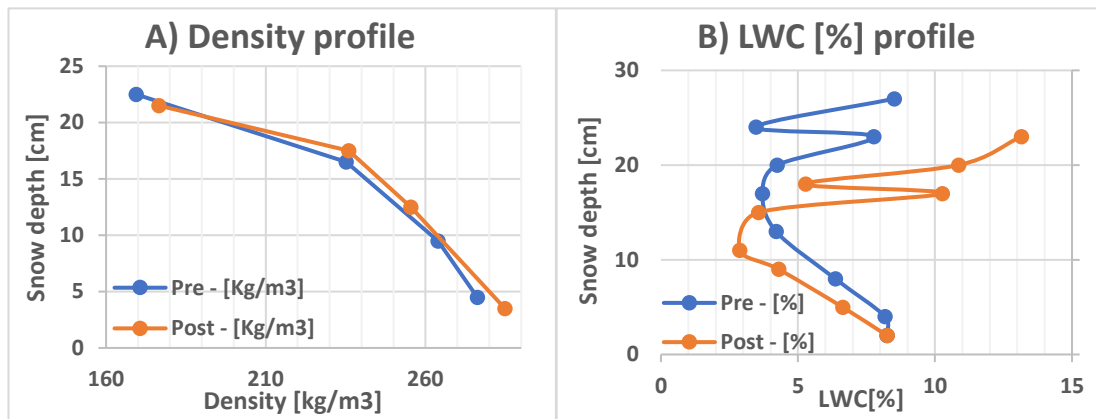
Figure 15: Altered properties at the Kubova Huť 2 site, A) Density profile in pre and post – experimental stadium, B) LWC profile in pre and post – experimental condition.

Temperature

Due to the lack of data of the profile analysis for the temperature profile, no visualization has been carried out.

Density

Density comparison is quite similar for both pre and post – experimental phases (Figure 15, A). Snowpack is more uniform and post-experimental profile has more less the same values along the profile as the pre-experimental. Post- experimental profile is slightly denser and does not have any fluctuations.

LWC

LWC of the KH2 experimental site is varying through the snowpack with some changes in both conditions, where LWC tends to be higher in the upper part of the snowpack. After crossing at 15 cm height in profile, post-experimental profile had lower LWC than the pre – experimental. On the other hand, higher LWC is seen in the upper part of the snowpack in the post – experimental condition. ROS experiments contributed to more liquid water in the snowpack especially on the top of the snowpack after experiments (Figure 15, B). LWC of the KH2 site corresponds to the ripening phase of the snowpack

5.2   Water behavior in snowpack after experiments

Water movement localization analysis

Photo analysis composes data into tables from the pictures taken during the experiments where tables describe water propagation through the snowpack. This description of the propagation represents the water accumulation after the ROS experiments per each site.

Bluesnow analysis

Blue snow visualization provides more complex data of the images. Each photo of the excavation is processed and water movement in the snowpack determined as it has been done with the localization analysis. The bluesnow analysis calculates the pixels of "brilliant blue", this source of information is then used to determine horizontal and vertical distribution of blue in photos.

Photos of LU, KH1, KH2

All photos as an input for further analysis per each site
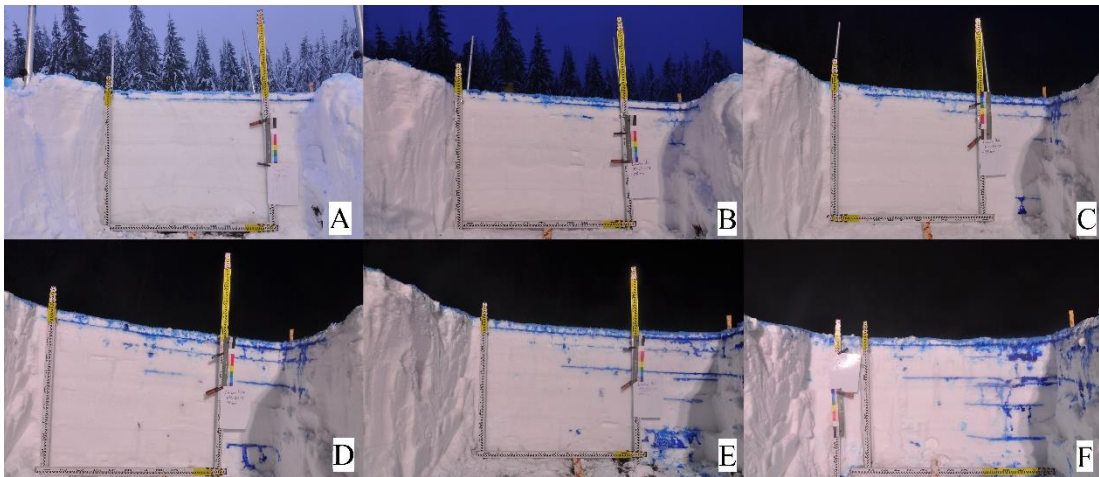
Figure 16: Bulk photo of the Luisino Údolí site. A) Snow pit excavation in 3-4 cm from the lysimeter desk, B) 20 cm, C) 35 cm, D) 60 cm, E) 75 cm from the lysimeter desk, F) Diverted flow paths out of the lysimeter desk.
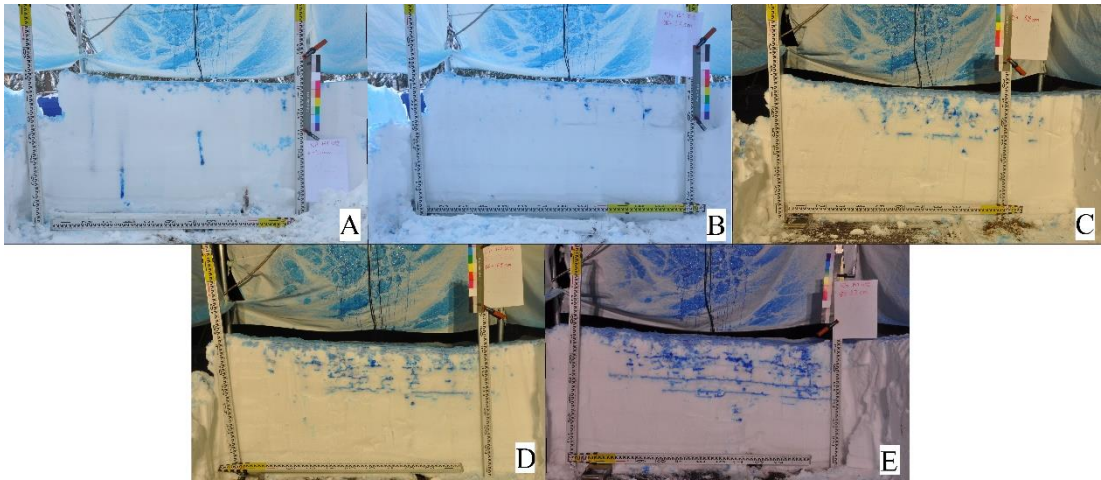
Figure 17: Bulk photo of the Kubova Huť 1. A) Snow pit excavation in 6-9,5 cm from the lysimeter desk, B) 16-17 cm, C) 51-53 cm, D) 66-69 cm, E) 80-83 cm from the lysimeter desk.
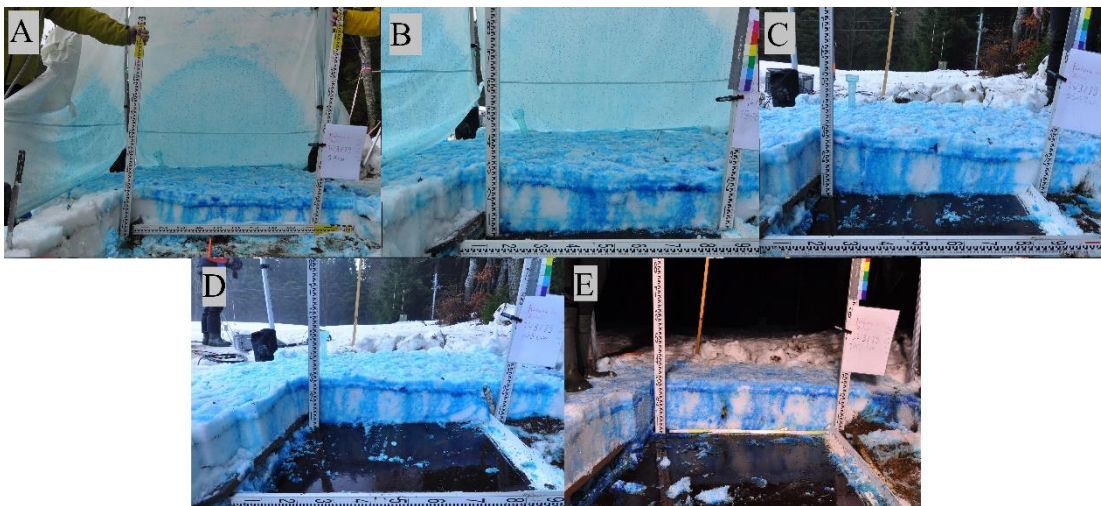
Figure 18: Bulk photo of Kubova Huť 2. 1) Snow pit excavation in 0-5 cm from the lysimeter edge, 2) 15-10 cm, 3) 45-48 cm, 4) 65 cm, 5) 100 cm from the lysimeter edge.

Table 3: Dimensions of all photos in pixels over length of the photo and depth. A) photos from Luisino Údolí, B) photos from Kubova Huť 1, C) photos from Kubova huť 2

LU Photos	Pixels over length	Pixels over depth	KH1 Photos	Pixels over length	Pixels over depth	KH2 Photos	Pixels over length	Pixels over depth
A)	1336	1136	A)	2229	1288	A)	1912	413
B)	1368	1192	B)	2288	1145	B)	1694	533
C)	1276	1200	C)	1912	1150	C)	1586	465
D)	1397	1295	D)	2217	1145	D)	1375	389
E)	1259	1190	E)	2262	1162	E)	1302	383

Horizontal presence of fluid paths in snowpack expressed by blue fraction

Horizontal blue fraction distribution composes dimensions of pixels over the length.
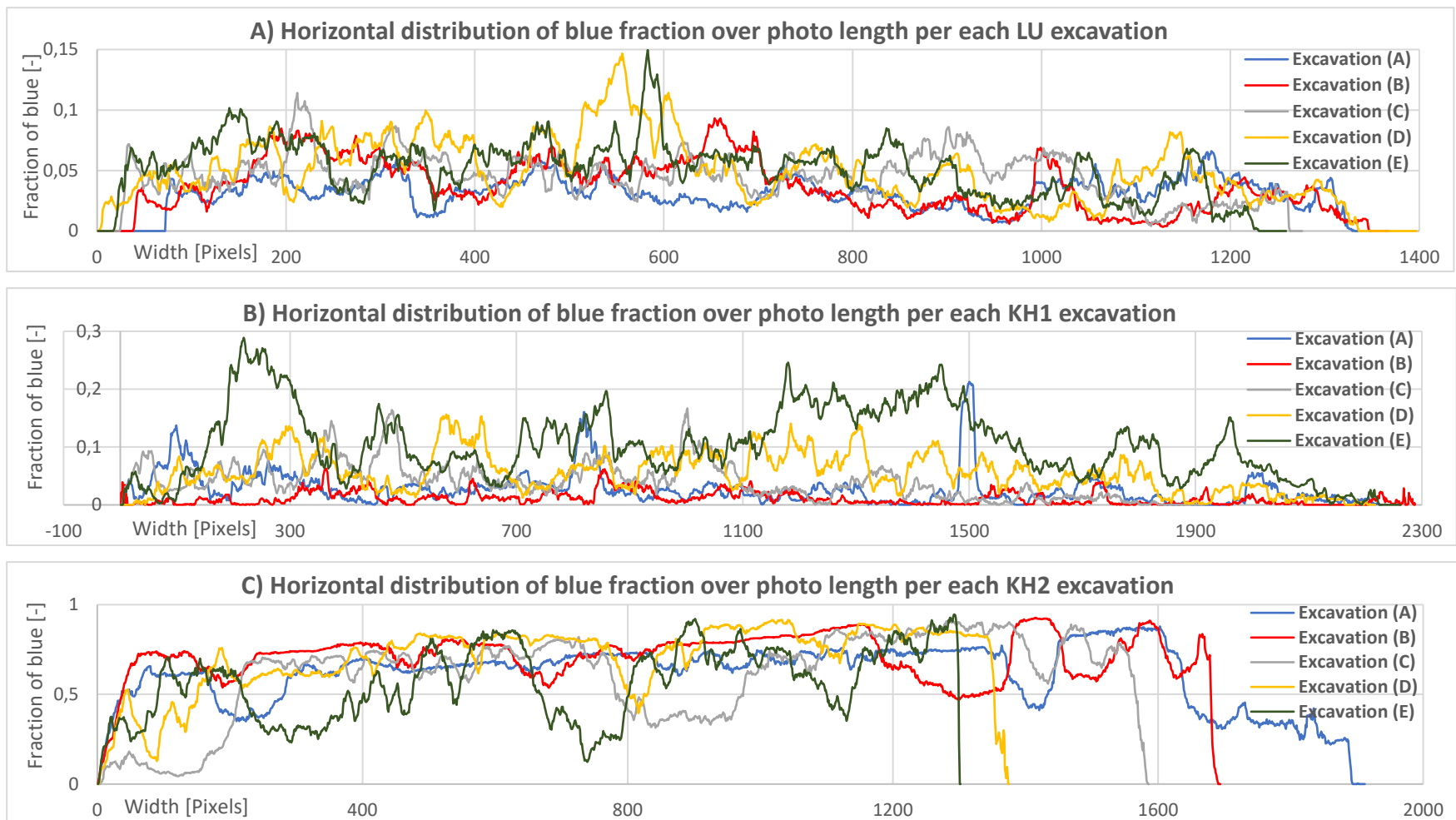
Figure 19: Horizontal distribution of fraction of brilliant blue calculated from filtered photos per each excavation. A) Luisino Údolí, B) Kubova Huť1, C) Kubova Huť 2

Vertical presence of fluid paths in snowpack expressed by blue fraction
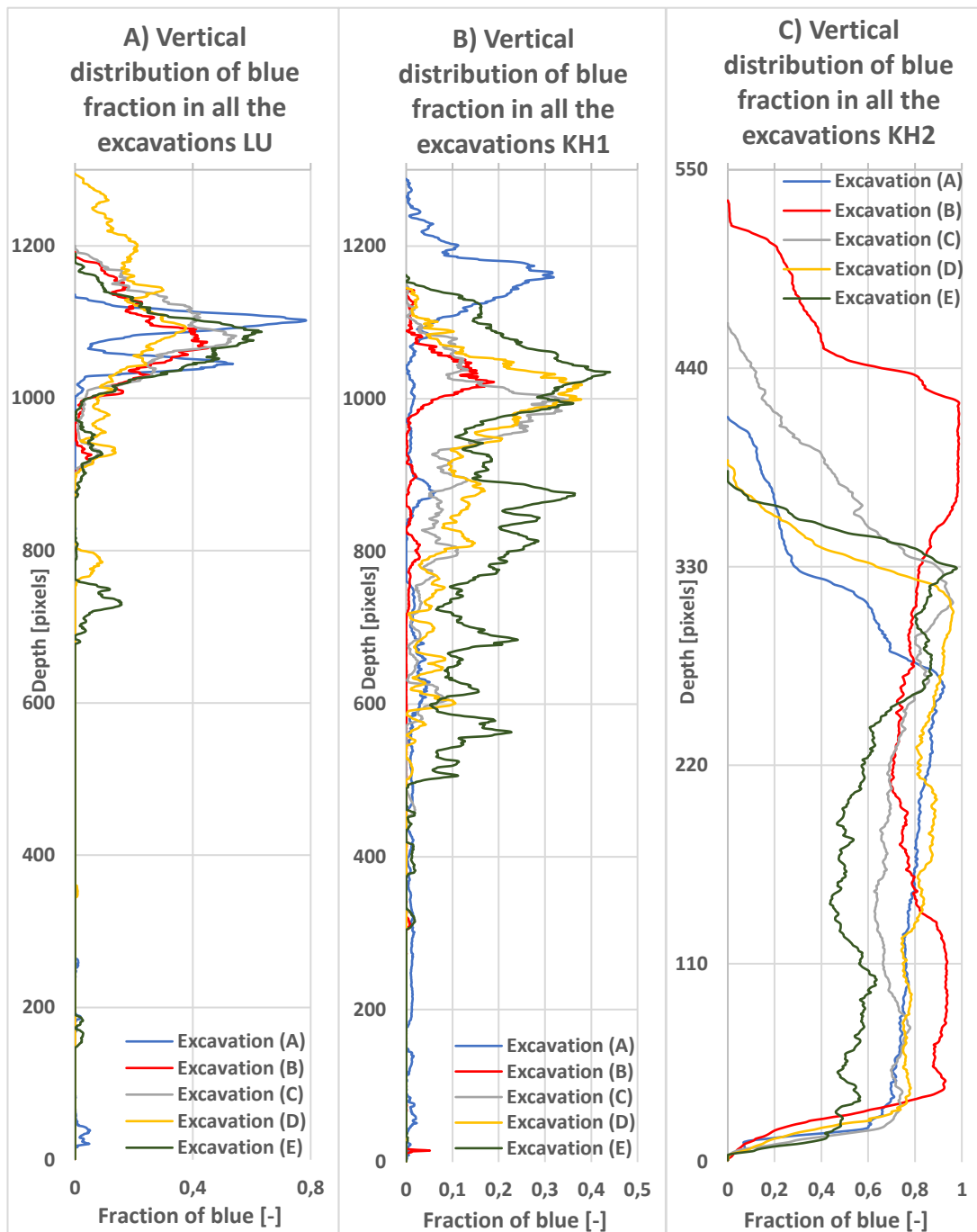
Figure 20: Vertical distribution of brilliant blue over the depth of all photos per each excavation. A) Luisino Údol, B) Kubova Huť 1, C) Kubova Huť 2.

In (Table 3) all photos dimensions are presented, both horizontal (Figure 19) and vertical (Figure 20) distributions of blue fraction correspond to the length and depth values of photos. Moreover, this influences further calculations with bluesnow as the number of pixels affects the proportion of pixels with blue fraction. Each photo has different number of pixels due to fact of analyzing crop photos. Dimensions in pixels

could seem to be indefinite but they are used despite this fact, because all photos were cut. Thus, each photo has different number of pixels in depth and length dimensions caused by the shape of the profile. The shape of the profile is not a square or a rectangle so automatically white color filled these gaps in cropped photos and adjusted the number of pixels in the cropped photos to create rectangular shaped photo. This can be demonstrated in (Figure 45), where dimensions of the cropped profile are [108 cm length and 110 cm snow depth], it seems that the snowpack is more vertically oriented than horizontally, in spite the (Table 3), where numbers of length and depth [1397, 1295] referring to more horizontal orientation than the vertical. This is caused by the fact, that the shape of the snowpack is shifted towards the right side and length values increased to form the cropped photo. Cropped photos fill blind spots (caused by the shifting) with white pixels influencing the bluesnow calculations and distribution. For this purpose, no relative scale was used to interpret pixels because it would be hard and not precise to determine what is 100% in the length and depths distribution of pixels or addressing the actual coordinates of the snowpack because of the shifting of the profile.

Prevailing formation of paths induced by the ROS
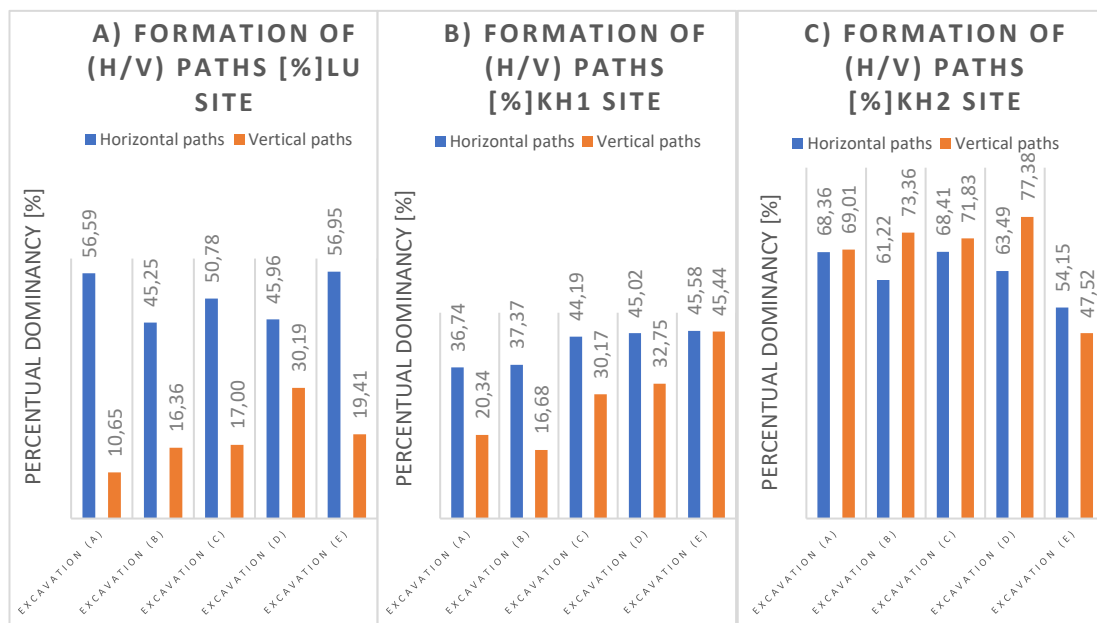
Figure 21: Calculated prevailing formation of flow paths in the snowpack per each excavation in percent. A) at Luisino Údolí site, B) at Kubova Huť 1 site, C) Kubova Huť 2 site

Calculated prevailing of formation of flow paths in the snowpack refers to the number of pixels with blue fraction higher than the mean of the blue fraction per

each excavation in percent. This calculation is used for horizontal and vertical blue fraction pixels where one formation predominates in comparison. Basically, if denser blue fraction is found in horizontal formation horizontal formation will have higher values in the prevailing formation of flow paths because it has more values above the mean of blue fraction over the length of photo than over the depth. The formation of flow paths is calculated in percent not creating per each excavation 100% but only describing preference of formation over length or depth of photo above mean values(Figure 21). This is influenced by the pixels dimension of photos (Table 3). For instance, different number of pixels in length can help to dense the filtered blue fraction in horizontal direction or to cause the opposite. Nonetheless, photos tend to have similar format of pixels per each photo and the prevailing formation and all the bluesnow calculations are only influenced by small variations in pixels.

5.2.1 Flow patterns at the LU site [1]

Localization of water movement

Table 4: Detection of accumulated water per each excavation A – E, at the Luisino Údolí site

Photo	Detected layer	Height range [y axis] L. 1		Height range [y axis] L. 2		Height range [y axis] L. 3		Horizontal range [x axis] L. 1		Horizontal range [x axis] L. 2		Horizontal range [x axis] L. 3		Layer width L. 1	Layer width L. 2	Layer width L. 3	Thickness L. 1	Thickness L. 2	Thickness L. 3
A	L. 1	105	103.5					12	116.5					92.5			1		
B	L. 2	96.5	90	83	81.5			13	114.5	71	91			86.5	20		1	1.2	
C	L. 2	97	92	85	84			20.5	106.5	83	106.5			86	23.5		1	0.5	
D	L. 3	102	95	86	78	69	67	0	108	47	108	61	85	108	56	25	1	0.3	0.4
E	L. 3	103	96	91	87	73.5	71	0	109	51	109	56	109	109	45	54	1	0.25	0.5

LU site

Snow pit excavations after the experiments are composed together to coherently provide a look where the water accumulated most and how was the snowpack influenced after experiments.

Table 4 for LU site shows the response of the ROS experiments. This table focuses on the localization of water accumulated in snowpack induced by the ROS. Layers represent type of water movement that was typical for this site. Each layer is recorded and monitored for the further investigation. Localization of the infiltrated water is expressed by two numbers (examples: 105 – 103.5 = height range in profile, 12 – 116.5 = horizontal location range in profile) first number shows height of the layer in

---

[1] Graphical representations of all the excavated profiles are listed one by one in the appendix section.

snowpack from the left side in the excavated profile and the second one represents the final height of the reported layer. The same approach is used at the horizontal localization (first number indicates the beginning of the layer horizontally where the second number stands for the end of the layer). For better understanding of the main layers (water accumulation recorded in the table), snow pit photos are graphically represented.

Filter of blue fraction

The blue fraction distribution refers to the range of blue created by the filter of the bluesnow. Fraction of blue in each pixel represents water accumulation in the snowpack, the darker the color got the higher concentration of water after the experiments is assumed.

Most water after ROS experiments was stored in the profile excavation (E) as it refers 5.11% of all blue fraction mainly represented by medium blue color range. The most soaked example is the excavation (B) with its 0.55 % of dark blue fraction (Figure 41, LU site).

Formation of horizontal flow paths

Horizontal formation of flow paths induced by the ROS experiments depicted in (Figure 19, A) shows all the excavated profiles of the LU site. Horizontal formation of fluid paths gets more intense at every excavated profile as the horizontal distribution of blue fraction refers to the fraction of blue pixels in the whole image over the length of image. In this example cases with more accumulated water represent higher values of the horizontal distribution. Only the (D) and (E) illustrations have deviations in the horizontal water behavior in the middle parts of the chart depicted with values reaching 0.14 - 0.15 of blue fraction. This means more water accumulated in this part of the image. For better understanding of horizontal flow paths in the snowpack (Figure 22) depicts horizontal distribution of blue fraction and the filtered image together. Notice that the x axis values of had to be reversed as opposed to the (Figure 19, A). This is caused by the bluesnow package and horizontal calculations. Same approach can be done with vertical distribution of blue fraction and image together.
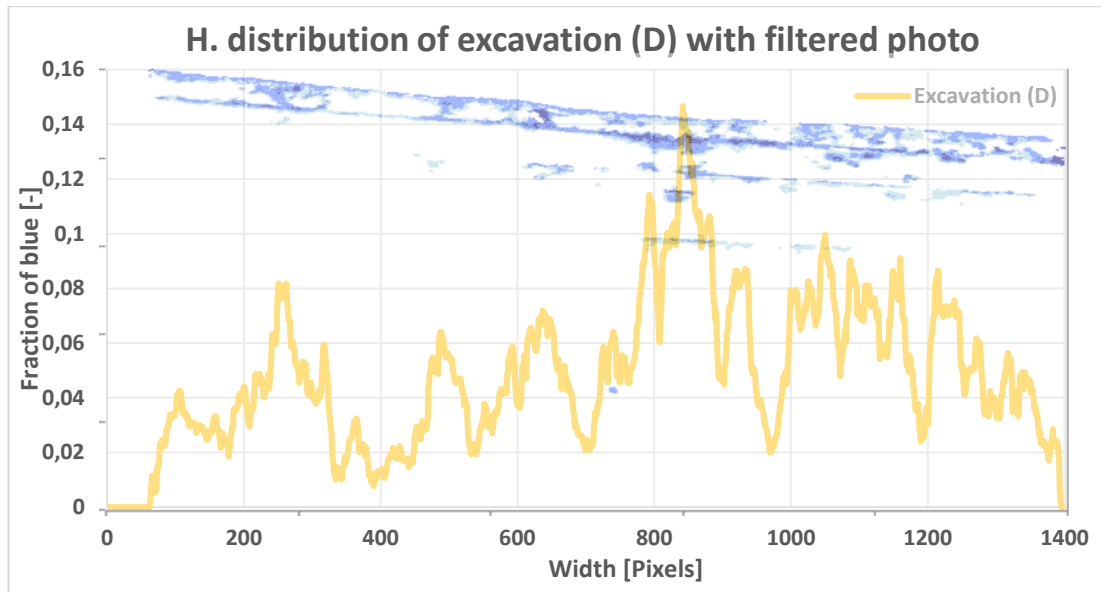
Figure 22: Example of Horizontal distribution of the excavation (D) with comparison of filtered photo from the same (D) excavation at the Luisino Údolí site, referring to most of the accumulation horizontally

Horizontal distribution of water induced by the ROS experiments predominates the vertical formation of flow at the LU site as shown in the (Figure 21, A) in all excavations.

Formation of vertical flow paths

Vertical flow formation of all the LU site excavations is depicted in (Figure 20, A). Most of the water was stored in the upper layers of snowpack after the ROS experiments. The accumulation of water is shifted by each excavation deeper as the first excavation (A) tends to store water in the top few layers and the last excavations (D) and (E) form the accumulation deeper over the profile, approx. at about one third of the upper profile.

5.2.2 Flow patterns at the KH1 site

Localization of water movement

Table 5: Detection of accumulated water per each excavation A – E, at the Kubova Huť 1 site

Photo	Accumulation	Height range [y axis]				Horizontal range [x axis]				Layer width [cm]				Thickness [cm]			
		PP.1/D.1/L.1	PP.2/D.2/L.2	D.3/L.3	L.4	PP.1/D.1/L.1	PP.2/D.2/L.2	D.3/L.3	L.4	L.1	L.2	L.3	L.4	L.1	L.2	L.3	L.4
A	PP. 2	49.5 32	32 17			73.5 76	37.5 38			1	1			1	1		
B	D. 3	60	57	57		79.5	94.5	109.5		1.5	1	3		0.5	1	1	
C	L. 3	62 61	60 58.5	47 44		56 65	80 97.5	55 99.5		9	17.5	36.5		1	1.5	0.7	
D	L. 4	60 59	53 51	48 47	46.5 45	30 123	47 92	58 93	46.5 123	93	45	35	76.5	0.5	0.3	0.3	0.3
E	L. 4	61 57	55 48	49 42	41.5 37	21 110	23 125	16 129	42.5 129	80.5	43	109	82.5	1.1	0.8	0.5	0.3

KH1 site

According to the photos of snow pit excavations after experiments snowpack shows in the upper part an influence of the ROS experiments. Most of the water was stored in the last excavation.

Preferential paths are represented in (*Localization of water movement*

Table 5) by (PP) abbreviation. Dots are expressed by one localization number and (D) abbreviation. Propagation through the snowpack formed 4 main layers (L) where some layers are not solid but fragmented into few smaller layers as a dashed line. Width of these layers is shortened by the blind spots where no flowing occurred. Fragmenting can escalate at understanding the table where the beginning and the end of the layer has bigger extension than the width of the layer itself.

Graphical representation of layers that are fragmented in profile is represented by slash lines. The more the layer is fragmented, the more is the representation line shattered. See appendix chapters (8.2 and 8.3).

Filter of blue fraction

Distribution of blue fraction shows that the excavated profile (B) is slightly less water soaked than the previous excavated profile. With exception of this case, snowpack of the KH1 site tends to accumulate more water at each excavation. Dark blue has the highest values for the last excavation as well as the excavation (E) accumulated the most water at all (10.33%) (Figure 41, B).

Formation of horizontal flow paths

Horizontal distribution of all the blue fraction pixels is spread along all the entire length of pictures (Figure 19, B). As the Excavation (E) shows the highest depiction

of blue fraction. Excavation (B) has most of the fluctuations in the horizontal distribution of blue fraction. This is caused by irregular distribution of water accumulation along the profile and different type of water movement that helped water penetrate much deeper and form vertical flow patterns in lower part of the excavated profile as depicted in (Figure 57). Different pattern of flow tended to store darker fraction of blue in the vertical perspective.

Horizontal distribution of water induced by the ROS experiments predominates the vertical formation of flow paths in all KH1 cases (Figure 21). Excavated profile (E) tends to have prevailing horizontal formation of flow paths and vertical flow paths similar, however this is caused by values higher than the mean of the blue fraction over the depth than over the length of the photo and pixels dimension of photo. It is necessary to point out that the vertical formation prevalence of fluid paths is the highest from all the excavations in the profile excavation (E) but only the horizontal distribution has smaller values in all pixels over the length than in the previous examples (medium blue = 9.33% in (Figure 41, A)). This explains the importance of the dark blue distribution (Figure 61) when the irregularity of dark blue distribution influences the formation of accumulation (the flow paths). It is so because dark blue has more likely higher values than the measured mean of blue fraction.

Formation of vertical flow paths

Vertical formation of flow paths (Figure 20, B) in the KH1 snowpack is conditioned by the stratigraphy of snow. The presence of flow paths grew in every excavation and so did the vertical distribution of blue fraction, as the accumulation of water tends to be denser, the water penetrates deeper. In all the cases, the higher the accumulation of water was after ROS, the deeper the water penetrated along the profile. This is one of the reasons why the vertical flow pattern in the snowpack is shifted by every excavation down along the profile. Vertical influence of fluid paths is in the excavation (A) and (B) represented on the top of the snowpack whereas, excavation (E) stored water from the top towards deeper parts of the profile, approx. to the middle of the profile. Excavation (A) refers oscillations more than the excavations (B) and (C), this is caused by the alteration of flow regime. This could be explained in (Figure 21, B) where the vertical formation of flow paths drops from the excavation (A) to (B).

5.2.3 Flow patterns at the KH2 site

Localization of water movement

Table 6: Detection of accumulated water per each excavation A – E, at the Kubova Huť 2 site

Photo	Detected layers	Height range [y axis] L. 1		Height range [y axis] L. 2		Horizontal range [x axis] L. 1		Horizontal range [x axis] L. 2		Width [cm] L. 1	Width [cm] L. 2	Thickness [cm] L. 1	Thickness [cm] L. 2
A	L. 2	25	17.5	22	16.5	10	85	5.5	100	69	94.5	1	1.4
B	L. 2	25	17.5	23	15.5	15	62	5	85	45	75	0.8	1.6
C	L. 1	23	16.5			0	90			90		1.3	
D	L. 2	22	14	7	9	0	90	38	90	90	52	1.1	0.2
E	L. 2	23	21	10	0	0	90	0	90	90	90	1.3	0.4

KH2 site

All snow pit excavations indicate two main layers in the snowpack except excavation C and gradual discharge of water beneath the main layer (L.2) in (Figure 18) and (Table 6). Graphical representation of snow pit excavation after experiments has not been done due to the snowpack conditions that help water penetrating not creating specific accumulation.

Filter of blue fraction

Distribution of blue fraction at the KH2 site represents high rates of pixels that refer to the water in the snowpack after the ROS experiments. High values highlight high factor of water release and penetration ability of the snowpack. Water induced by the ROS spills over the length and depth of image. Excavations do not vary gradually in contrast to the previous examples, they seem to have a more unified character with high distribution of released water.

Formation of horizontal flow paths

Horizontal flow pattern accommodates water in the profile along the length of images as the blue fraction reaches higher values than in the previous examples (LU, KH1). Horizontal distribution represented by the blue fraction of pixels spreads horizontally above the lysimeter desk and does not form any specific layering in the snowpack. In fact, stratigraphy of snow did not deflect flow paths after the ROS, but gravitational force caused higher vertical distribution (Figure 19, C).

Formation of vertical flow paths

Vertical flow pattern tends to be more unified in all the excavated profiles, reaching very high values. The vertical distribution has higher values than the horizontal and is found permanently along the excavated profiles. Vertical prevalence formation of fluid paths predominates but is the lowest in the last excavation (E), where horizontal flow tends to overtake the dominancy of the flow paths formation (Figure 21, C).

5.3 Evaluation of the post – experimental snowpack condition per each site
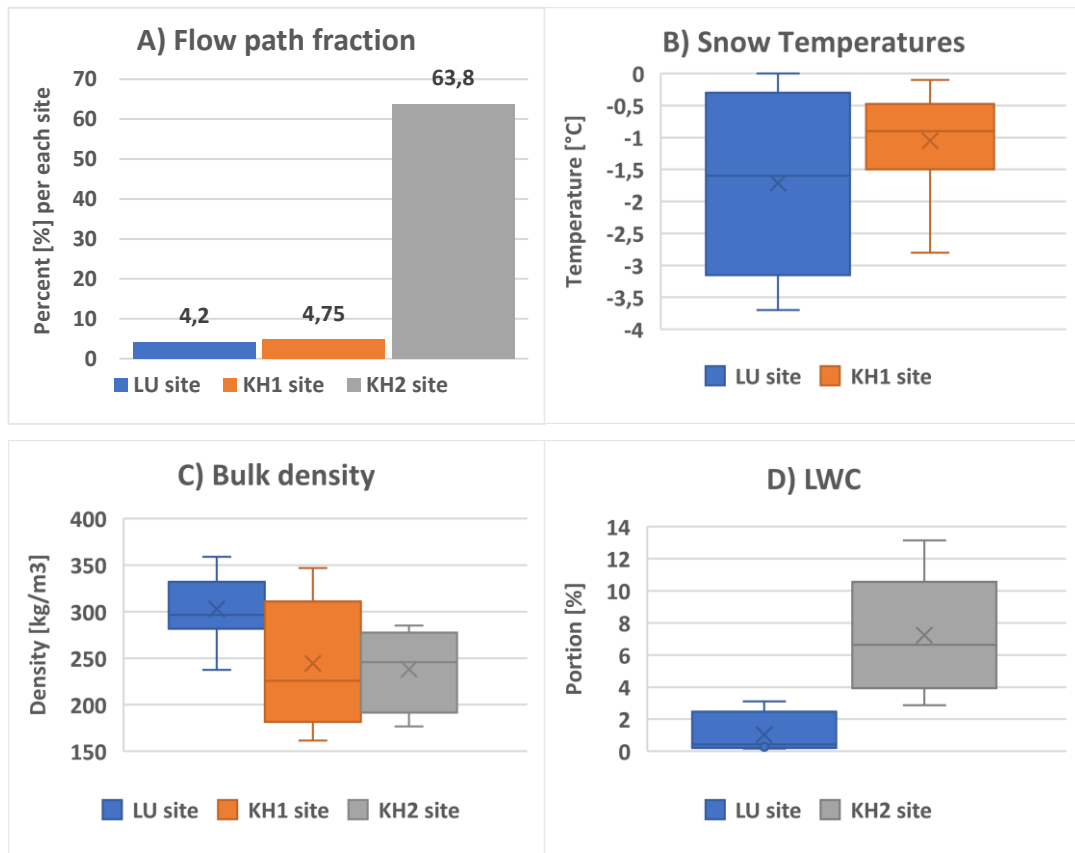
Figure 23: A) Percentage fraction of blue area from entire snow profile, B) Temperatures per sites (only Luisino Údolí and Kubova Huť 1 site depicted due to no data for Kubova Huť 2), C) Bulk density per sites, D) LWC portion in profile per sites (Kubova Huť 1 has not been recorded with LWC in the profile). Box plots description: x = mean, line = median, lower and upper whisker = range of measured values [min, max], box bottom = 1st quartile, box top = 3rd quartile

5.3.1 LU site snowpack

PF paths were formed in the snowpack as can be mainly seen in the snow pit photo (E) of the photo set depicted in (Figure 16) and all photo visualizations. By the localization analysis layers indicate LF in all cases. As the LF is caused by the capillary barrier once the pressure equilibrium across the borderline is established, water flow passes this barrier and FF is formed. In the case of LU snowpack FF has not been determined in the examined coordinate system but thanks to Blue – snow analysis FF regime has occurred, but dominancy of horizontal flow pattern was significant. However, high influence of FF is depicted in photo F in (Figure 16) but this photo has not been examined. Snow depths is highest in the photo A and despite some changes it gets lower in the last photo. Three main layers have been

identified: L1, L2, L3 (Figure 45). The first layer preserves where other layers are getting distinctive by each profile excavated in the water movement localization. First layer is the first response of the experiments where a strong influence of sprinkling is observed. For instance, the first layer is thicker than the others and is the longest in every profile (layer width in Table 4). The thickness of the layer interprets higher water accumulation and a borderline of a different type of snow structure in the snowpack as the layers in profile are induced after ROS on the interface between structure differences.

Snowpack properties investigation match to some of the layers in the snow pit excavation. Main layering is observed in the upper part of the snowpack above the 60 cm height of snow. This corelates with the temperature investigation where most of the changes in profile occurred above 60 cm height in snowpack (Figure 11). Highest LWC is concentrated on the top of the snowpack (100 cm) (Figure 11, C) as well as the most saturated layer (100 – 107 cm) (L.1 in Figure 42) from the snow pit excavation examination.

The prevalence of horizontal flow formation is evident with a LF regime. This is because meltwater flow is found to be strongly controlled by stratigraphic layering. Strong stratigraphy is related to density of the profile where LU site has the highest measured density (Figure 23, C) of all the experimental sites. High heterogeneity and stratigraphy incline to lateral flow occurring along many of the layer interfaces, they can be even subtle and not identified in snow pit sampling according to findings in WILLIAMS ET AL., (2010) study.

5.3.2 KH1 site snowpack

KH1 site indicates PF paths in the snowpack. Mainly FF paths with combination of LF paths were formed along the profile. LF is caused by the capillary barrier and FF connect layers. Dots of accumulated water are explained as local changes in snowpack's texture. Most of the water stayed in the upper layers of the snowpack with the first layer (L. 1) that is validated as the most saturated by the ROS due to its dark color and thickness.

Changes in the profile properties correspond to the layering depicted in the snow pit photos. Density profiles intersect at around 55 cm snow depth (Figure 13, B) where crossing of temperature profiles is observed in the same height (Figure 13, A). KH1 site is typical in comparison with the other sites with its different flow regime in the

snowpack where FF is observed playing important role in the tendency of formation of the water movement in snowpack and changing the flow pattern through the snowpack to more LF regime afterwards. Snowpack of the KH1 site has more of the blue fraction than the LU site (Figure 23, A).

5.3.3 KH2 site snowpack

KH2 site shows an inclination to the MF regime according to photos and to changed properties before and after experimental conditions. Decent layers are seen along the profile, but snowpack tends to be saturated with higher LWC with a tendency to the MF flow regime than preferential flow paths. Storage capacities of the KH2 snowpack are low and most of the water is, after occupying all the pore spaces in the snowpack, released. Water does not have any tendency to deflections as the structure (Figure 14) is uniform and water flows through the soaked snowpack by gravity forces. Properties of snow do not change dramatically (Figure 15) indicating water release rather than accumulation. Higher LWC can contribute to lower snowpack stability. High LWC results in lower water accumulation potential and faster water release and it justifies the ripening phase of the snowpack. In all the cases LWC was recorded as the highest (Figure 23, D).

As the snowpack tended to be mainly vertically flow influenced (Figure 21, B), vertical meltwater flow paths within layers can be found to be most prominent near the surface, with MF apparently becoming more important at depth (Williams et al., 2010). KATTELMANN AND DOZIER, (1999) used a capacitance probe to measure liquid water content in the snowpack. The LWC was found to generally increase over time with older snowpacks and their study found that LWC can potentially destroy layer interfaces helping the MF to occur. This correlates with the snowpack's spring condition that for the KH2 site had the character as remaining snow after the winter season. Snowpack did not have layering composed of new fallen snow with its structure properties, such as grain size, profile properties, such as higher LWC, along the profile rather fitting with the character of snow near the surface with MF water movement.

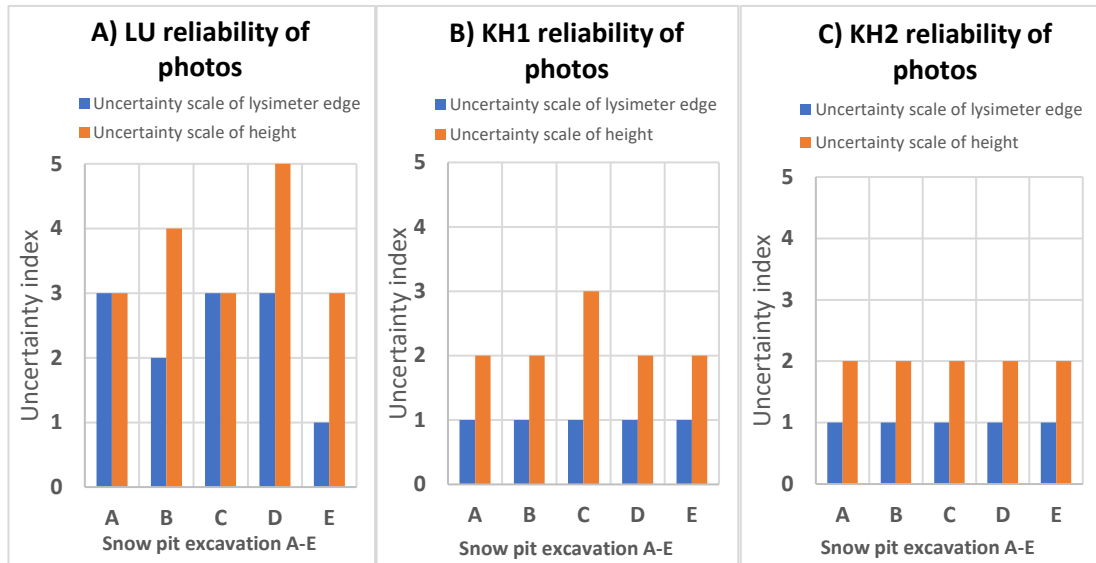## 5.4   Photos reliability of snow excavations after ROS experiments

Figure 24: Reliability of photos per each excavation, expressed by both lysimeter determination uncertainty [1 – 3] and height uncertainty [1 – 5] indexes per each site. A) Photo reliability at Luisino Údolí site, B) Photo reliability at Kubova Huť 1 site, C) Photo reliability at Kubova Huť 2 site.

Photos from LU

The lower the accuracy of localization the coordinate system of the profile the higher the uncertainty index number. Snow pit excavation D is the lowest accurate and E is the most accurate from the whole photo set for LU (Figure 24, A). Under high uncertainties, LU photos could be considered as inaccurate. Localization of the water movement is therefore very dependent on the reliability of photos. Localized water accumulation can vary throughout the whole snowpack and does not have to have corresponding values to the originated coordinates. Height uncertainty is mainly caused in this example by the top distortion, and scale placement.

The uncertainty index can be demonstrated for example, in (Figure 45) and (Figure 46) where the layers are under influence of shifting. Snow pit excavation E is validated as the most reliable in the set of photos of LU site and the excavation D where high uncertainty index has been determined as the lowest reliable. In both examples shifting of layers in all directions (L.1 – L.3) is noticeable. Shifting could be assigned to the snowpack properties, structure and stratigraphy, but also to the inaccuracy of the photos which should play some role in this case due to the high indexes values.

Photos from KH1

As the snow cover got thinner the reliability has increased from the previous photo set of the LU site. The uncertainty index is the same for all photos except excavation C of the snow pit KH1 where higher distortion has been noted (Figure 24, B). Photos could be considered as mildly accurate. The height uncertainty still plays an important role in the reliability where mainly disconnected scales and crooked placement of the scales caused higher index values in the height uncertainty for KH1 photo reliability. The lysimeter desk is located at every photo with high certainty but photos are still under some height uncertainties with consequences to the snowpack's after experimental water accumulation location. Due to lower uncertainty indexes we see lower rate of snow height changing in the photos. The coordinate system is then more accurate than the one at the LU site.

Photos from KH2

Reliability of pictures has steadied as well as height uncertainty except in one photo. Every photo is reliable with the same rate. Uncertainty index indicates height certainty 2 of all the excavations of KH2 snow pit where photos are not still accurate (Figure 24, C). The height uncertainty is given by the placing method of measures where the procedure is insufficient. Height of the snowpack varied inadequately in every image. Even though the certainty of this site has increased and shows the highest sureness. If a proper method of using scales had been used the height uncertainty would have decreased. In all cases it is noticeable that the depth of snow influences the height uncertainness.
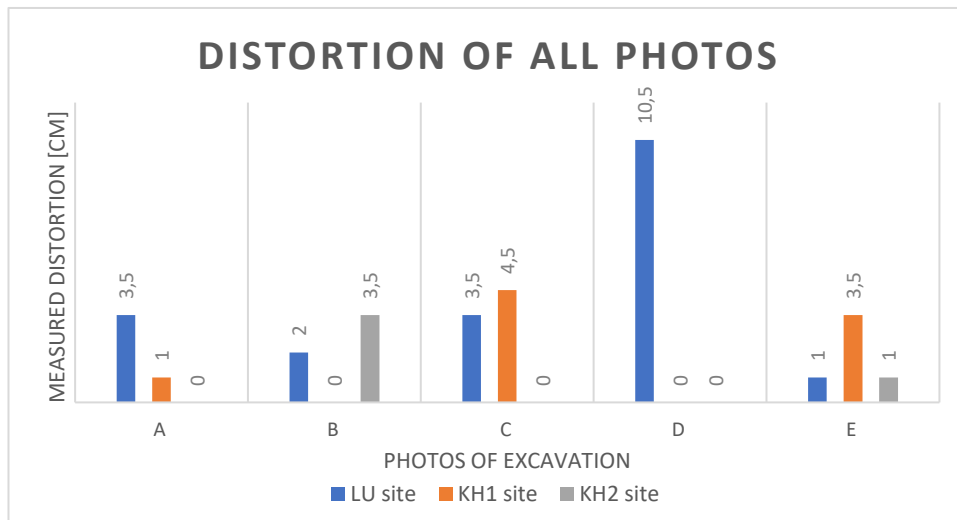
5.4.1 Top distortion

Figure 25: Top distortion of all photos per each excavation from all sites

Indexes help categorize photos but there is also another factor that plays a role - the top distortion. When the top distortion was found the coordinates of photo had to be recalculated and new values with distortion were assigned. This results in the graphical representation where localization of fluid movement is then recalculated toward the values of the distortion. It seems that the distortion is a more reliable factor for validating photos than the indexes. This is not actually right because when recalculation of the distortion was needed, the recalculation was always focused on left scale. Distortion found during the reliability analysis is therefore highly influenced on the left side. It is obvious that the left scale could have been positioned wrong as well as the right one was many times. The measured distortion is then just the difference between scales on the top accordingly to the bottom values of the scales. This aspect is not the part of the reliability evaluation because indexes can more complexly determine if the photo is reliable based on other factors even though indexes are influenced by the subjective author's opinion. Nevertheless, distortion is important for graphical visualization of the water movement localization where the top distortion was the part of the localization as the recalculated values were implemented into tables of coordinates. Old values (less representable) were adjusted with the values of the distortion accordingly to the vertical location in the snowpack.

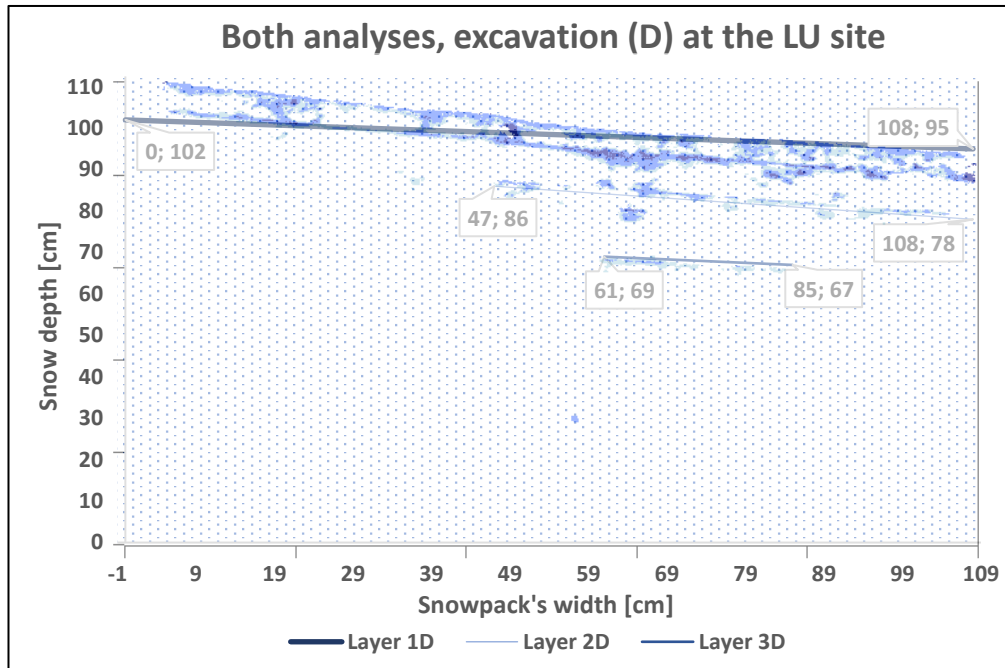## 5.5 "Localization" and "Bluesnow" analyses comparison

Figure 26: Both analysis comparison. An overlapping of the graphical visualization (Localization analysis) and filtered image (Blue - snow analysis)

Graphical representation (Figure 50) and the filtered photo (Figure 60) as the outputs from both analyses comparing both approaches from the same profile excavation in the (Figure 26). Comparison of both approaches shows that the localization analysis is less accurate especially at the top of the snowpack. where the L1 layer tends to be anchored inaccurately when both approaches overlap. This is mainly related to the top distortion of the snowpack or to wrong localization of the layer. Both photos are compared because photo excavation (D) has been evaluated in chapter (5.3) as the lowest reliable and with the highest top distortion (by the reliability analysis). Localization of the first layer is not precise due to higher uncertainty index (finding the height was laborious and uncertain with high dispersion in height in comparison with other photos (reliability analysis)). It is also important to note that the top distortion found on the top of the snowpack (10.5 cm) in (Figure 25) plays significant role. If the distortion recalculation had not been added to the water movement localization, values would have had lesser representable localization values in other layers found in the snowpack (L.2, L.3) in (Table 4). Location of these layers could have been different in height in snowpack in dispersion of 10.5 cm which is not the case of this example because distortion was recalculated proportionally per each value of the right scale. Overlapping both analyses demonstrate recalculation of the distortion.

The "Water movement localization" analysis provides data of localization of the water movement in the coordinate system. Having known the spatial distribution of water behavior in the profile after ROS is very important as well as knowing the snowpack coordinates. This shows potential distortions accordingly to the coordinate system.

The "bluesnow analysis" does not provide data of the coordinate system of the profile. If we wanted to obtain coordinate data of the profile, values would be influenced by the distortion that would not be recalculated accordingly as it has been done with the localization analysis. It is obvious that if we wanted to obtain coordinate data of the snowpack with bluesnow analysis values would not be representable and they would be varying, in this case in 10.5 cm dispersion of height in profile.

5.6 Suggested profile measuring and photographing procedure

5.6.1 Defects found by the "Photo reliability" analysis

Processing the photos has revealed some incorrectness that should be fixed for the next experiments. Due to the photo reliability analysis errors have been found. These errors can be represented by the reliability index of photos. When the snowpack was deeper the probability of distortion got higher thus, the certainty of coordinates of the pictures collapsed. For instance, low reliability is depicted in (Figure 24) where pictures from the LU site refer the deepest snow cover reported from the all sites. For other locations, as the snowpack gets thinner, the reliability tends increase.

Defects causing distortion and inaccuracies comprise mainly the following:

- Top distortion caused by the camera angle and camera position, while taking pictures
- Crooked scales defecting data accuracy
- Certainty of the lysimeter desk position

These issues had some influence on the whole distortion of the pictures and all of them are connected. But the top distortion is perhaps the defecting element that plays the largest role at the defection. Distortion at the top of the snowpack was caused by the angle of the camera and perhaps by the angle of the vertical scales with the bottom scale. When the camera was not positioned during the shooting right in the middle in front of the excavated profile and the snowpack had higher snow depth, it caused some distortion visible on the top where a small difference on the surface caused a bigger distortion on the scale on the top of the snowpack. Left scale of the profile sometimes showed about 10 cm differences in values compared to the right one due to the top distortion. The top distortion was typical when a small difference on the surface caused unevenness between the scales escalating on the top especially when the angle with the bottom scale was unknown. It is also possible that the top distortion was caused by the factor of different angles between bottom and vertical scales. But any huge gaps of values have not been found during the analysis by the deflection of the vertical scales. All that was found with certainty is that the distortion went higher when the snowpack had higher snow depth. For instance, unevenness on the surface of about 3.5 cm (8 – 11.5 cm) where these 3.5 cm was the difference between both scales on the surface caused distortion of 14.5 cm (108.5 – 122.5 cm) on the top of the snowpack. Right scale does not refer to the left side (Figure 18).
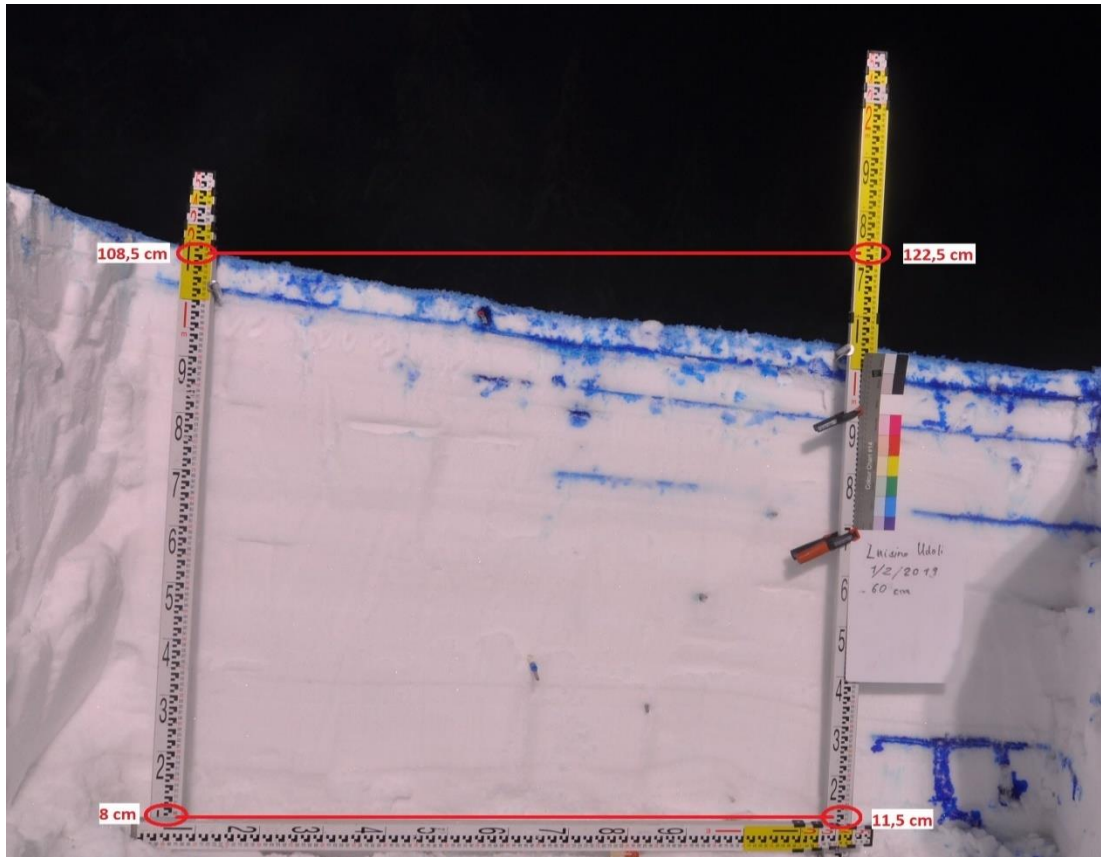
Figure 27: A top distortion example. Both scales do not refer to the same horizontal level values in a certain point. Photo by supervisor of this thesis.

The position of scales was therefore a defecting factor. Scales were standing on the frozen surface and sometimes on snow. They were neither on the same level horizontally nor vertically anchored to the surface and to the bottom scale. Hence, side scales did not report same values.
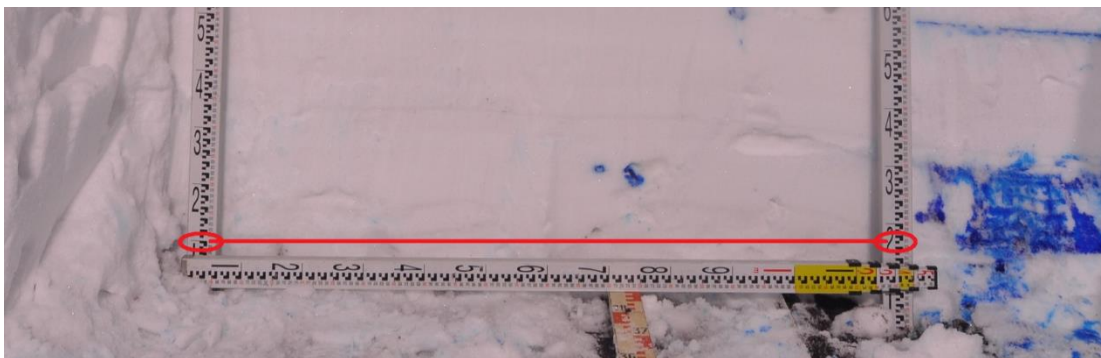

Figure 28: Unevenness on the surface where scales do not follow horizontal values. Photo by supervisor of this thesis

The uncertainty of the lysimeter position happened to be also important. The lysimeter desk was sometimes covered by snow and indicating the desk from the previous

photos had to be done which leads to inaccuracies (this is also the case of lysimeter desk uncertainty index in Figure 24).

Measuring scales sometimes made the reliability analysis more difficult due to the time pressure during taking the pictures in terrain. Because of the rush, some scales were not placed properly and reading them afterwards made determining real values time consuming. Scales did not follow the same order in every picture. For instance, the bottom scale even obstructing the view of the lysimeter was not connected to the left vertical scale and sometimes values of the bottom scale did not refer to zero value (Figure 30). That means the bottom scale could obstruct the left scale or it could be placed too far to one side. In some photos bottom scale was lying on the ground and facing sky instead of the camera (Figure 29). The changing values on scales for each photo were made by no specified order of placing them.

Figure 29: Bottom scale facing upwards causing laborious consequences at determining the horizontal accumulation of water. Photo by supervisor of this thesis

Figure 30: An example of disconnected scales causing difficulties in horizontal water accumulation determination. Photo by supervisor of this thesis

5.6.2 Profile frame

Based on the identified uncertainties of the photo analysis a frame for the further profile analysis is suggested. This frame should cover all the defects mentioned above and fix them for the next experiments. It also has to fulfill portable requirements as well as dismantle abilities due to fact of operating in terrain.

The frame will be put together every time it is needed and dismantled after using it. The suggested frame is made of wood and withdrawable scales from previous experiments are implemented as well to measure the excavated profiles. Vertical scales are applicable for changes at depth of snow and could be adjusted any time, this aspect is also good for the mobility in terrain with the frame. The frame will measure profiles with inner area of 1.5 x 2 meters. Vertical scales are connected by two 1.7 meters long horizontal wooden sticks under 90° angle (Figure 31). 10 cm space on both sides of the middle part of the frame takes for fastening the vertical scales when a lot of snow frame would be anchored to the profile by hooks on the outer sides (Figure 33). On the other hand, the frame will have to be held by an operator or a crew member. Water level is suggested on both sides to control the frame position.

Instructions of operating with the profile frame

Specific rules need to be followed when using profile frame to prevent defections. At the beginning, snow depth has to be measured to set the camera to the right position. Camera should be placed as to the center of the profile as possible. The middle value of depth of the snow is necessary to obtain to set the camera stand. Camera must stay at the same spot during the shooting to prevent different angles in the pictures afterwards. Distance from the camera to the profile must be the same for every slice cut out of the profile. Once the distance is set, it must be kept during the shooting and has to remain. For example, when 2 meters distance is used for shooting for the first excavated profile the second profile will also be shot from 2 meters. Second person holding the frame is responsible for balancing the water level. The frame must remain equilibrated both vertically and horizontally. The wooden middle part of the frame is moveable vertically. It is necessary to set the middle part above the snowpack to provide data of the horizontal axis and not shielding the lysimeter (Figure 34, where the central part does not cover the bottom of the profile, so the lysimeter is noticeable).

Information table and color scale classes are placed on the outer side of the frame so that nothing disturbs the space inside.
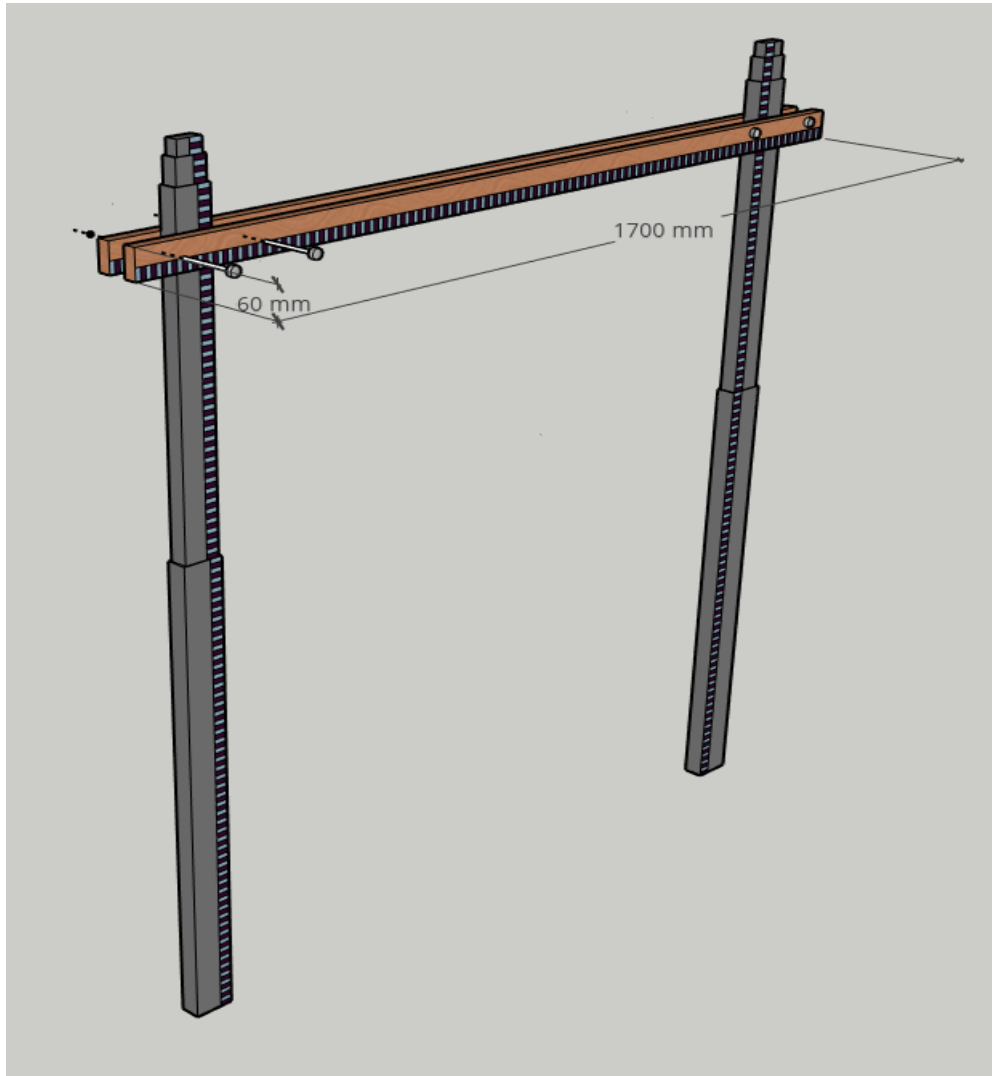
Profile frame exports

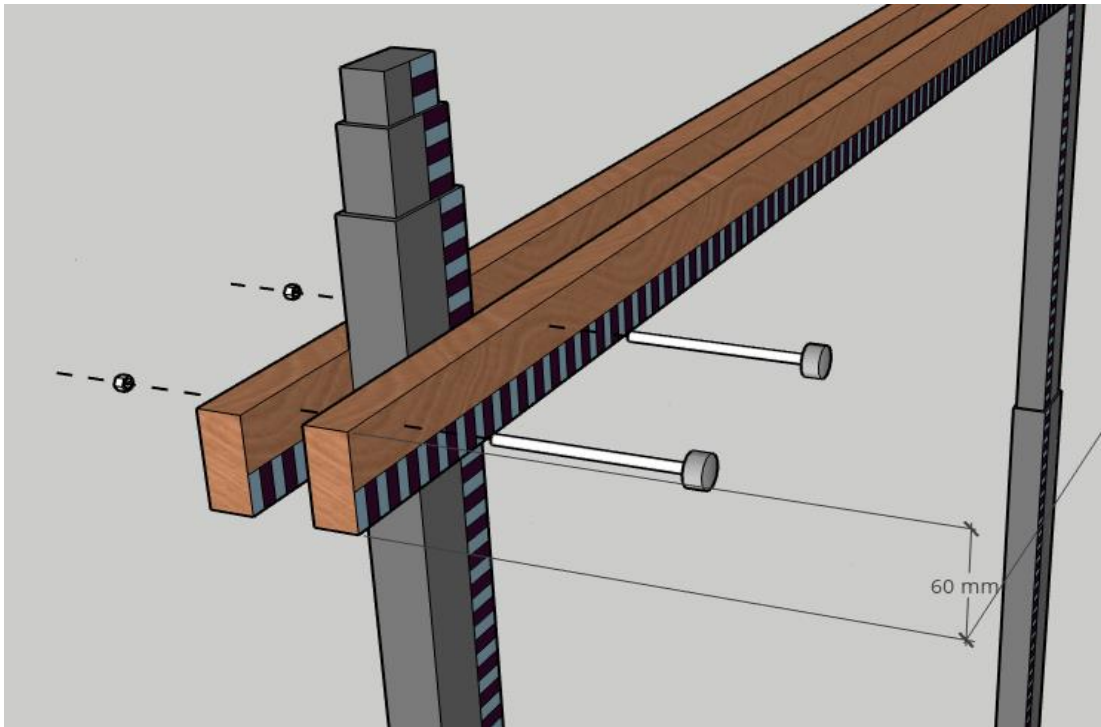*Figure 31: A special tailored made frame for photographing the snow profiles.*

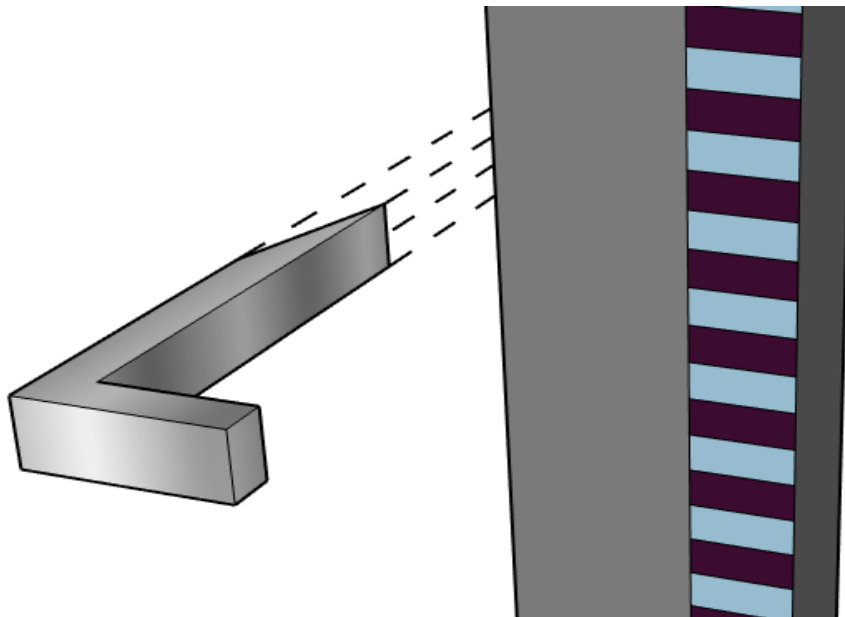*Figure 32: Fastening of the frame when putting together on site*

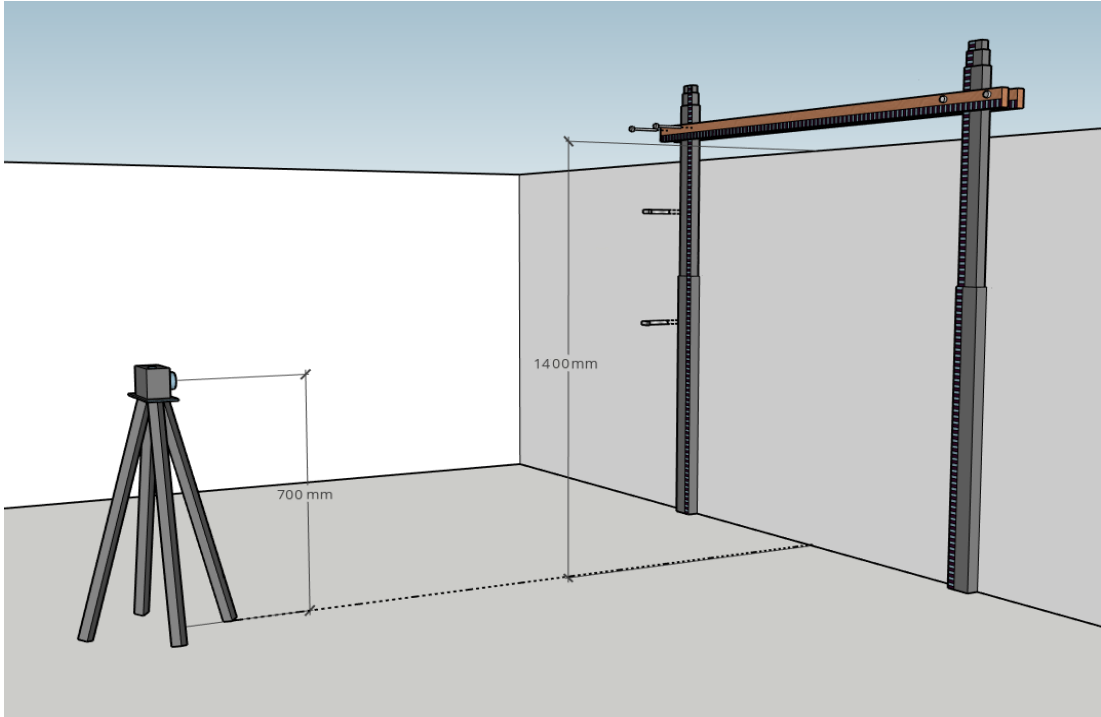*Figure 33: Profile frame anchoring by hooks when deep snow*

1400mm

700 mm

Figure 34: Scene of camera positioning and frame by the profile frame operating instructions

5.7　Tipping buckets implementation

Calibration of new tipping buckets is divided into three phases. First calibration focused on the first design of the tipping bucket (TB) device where defects of design were reported, and volume of the TB was examined. Second calibration implemented knowledge from the first one where design suggestions were carried out, and new parameters were tested. Second calibration is then a design improvements calibration. The third calibration was a process of implementing new tested design on all the TBs.

5.7.1　First calibration

For the first calibration, four different tipping volumes were preset by the adjusting bolts.

Volume range [ml.]

- Max overturn (115 ml / overturn)
- 100 ml / overturn
- 75 ml / overturn
- 50 ml / overturn

Design defects reported by the first calibration

- Bad funnel design
- Water level proportions
- Edge of the bucket barrier
- Distance between funnel and tipping system of the TB device

Funnel design

The funnel did not release the water through the tipping bucket properly. Water from the funnel was dripping around because of the output profile of the funnel. The profile had too large parameters, was not smooth and was contributing to the fact, that the funnel allowed water dripping from the bucket.

Water level proportions

Water level did not show the position of the TB properly and finding the correct position was laborious. First calibration has revealed that inaccurate water level caused different volumes per overturn in the static calibration part (Figure 35). Unleveled TB device was influenced by the gravity that contributed to different volumes of the tipping system. The more crooked one side of the TB device was, the lesser the accuracy was observed.
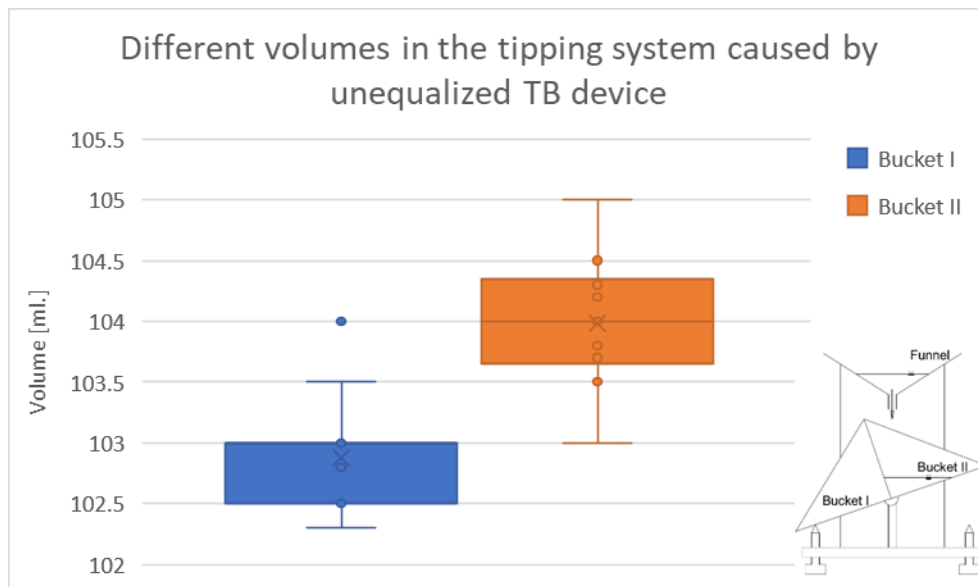

Figure 35: Different volumes of the tipping system caused by uncertainty in position of the TB device. Box plots description: x = mean, line = median, lower and upper whisker = range of measured values [min, max], box bottom = 1st quartile, box top = 3rd quartile, dots out of the range of whiskers = outliers.

Edge of the bucket wall

Edge of the bucket wall influenced flowing of the water through the system. Reported issue of the inadequate thickness of the wall between buckets I and II caused water sprinkling when bucket system outweighed.

Distance between funnel and bucket system

Outflow of the funnel was positioned too high, so the distance between the tipping bucket system and funnel output caused rippling of the water surface when filling up. Ripples and sometimes droplets from the inflowing water to the bucket affected the measuring capabilities of the TB device.

5.7.2 Second calibration

Design improvements

Water level proportions

Thanks to the extended water level, the TB position finding was simple and different volumes per overturns did not influence the filling ability as much as they did previously in the phase one. Both buckets have tendency to have the same volume per each overturn and the gravity force has a lower tendency to cause inaccuracies. The desired state of the TB is when both bucket I and bucket II are even. Nonetheless, even an equilibrated TB will reflect some inaccuracies due to the calibration method and tension forces of water. But the closer the individual buckets are in volume, the higher is the accuracy we can expect. In this example, volumes of bucket I and II are 102.85 ml. and 102.5 ml. respectively, where 0.35 ml. is the difference in the volume in both side buckets. Phase one of the calibration showed difference between both buckets due to the uncertainty in the leveled position 1,1 ml (Figure 35).
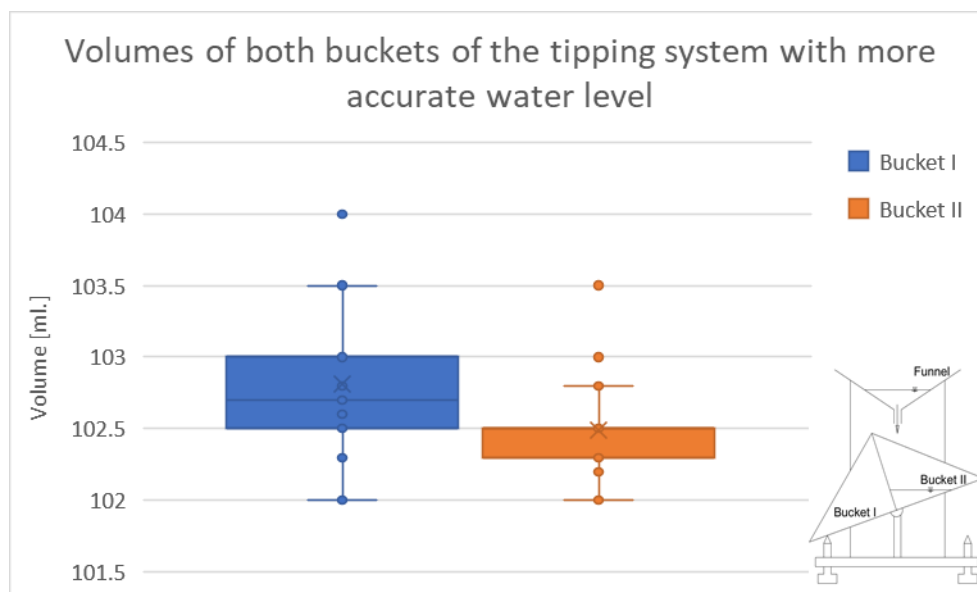

Figure 36: Comparison of buckets of the TB device with redesigned water level. Box plots description: x = mean, line = median, lower and upper whisker = range of measured values [min, max], box bottom = 1st quartile, box top = 3rd quartile, dots out of the range of whiskers = outliers.

Edge of the wall between buckets

The edge between both buckets I and II was sharpened to contribute to smoother design when buckets system overturns. This should prevent splashing of the water

when the edge of the wall gets to the central position of the system where the outflow from the funnel concentrates water.

Funnel design

Funnel calibration, as a reaction to the design improvements, had to be done to compare two different shape parameters of suggested funnels. By the funnel design calibration, two reported issues were solved. Bad design of the funnel and distance between TB system and funnel output. Both tested funnels had been extended (distance between the tipping system and the output was reduced to the minimum) and two different parameters of output were suggested. Funnel A with smaller diameter in profile and funnel B with larger profile. Both were tested with a constant flow of approx. 1 liter per minute. Tables below (Table 7, A, B) show detailed information of the funnel calibrations for both funnels. Tables show information on the number of bucket overturns, last overturned bucket in order and volume of water measured from the last tipped bucket.

Table 7: A) Funnel A calibration records, B) Funnel B calibration records

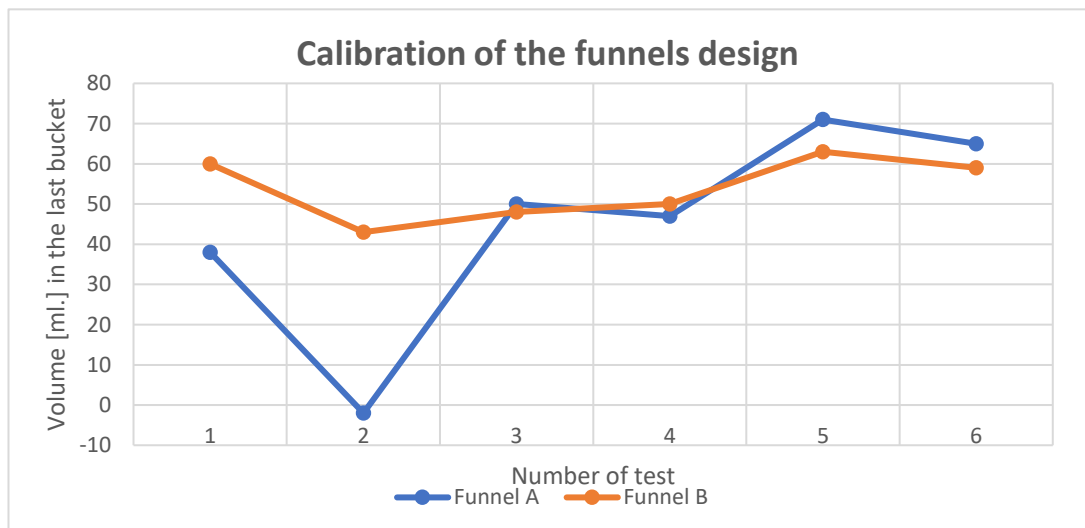| Q	Overturns	Last bucket	Vol. [ml.]	Q	Overturns	Last bucket	Vol. [ml.]
1l/56sec	9	10	38	1020ml/min.	9	10	60
1l/56sec	8	9	98	1020ml/min.	9	10	43
1020ml/min.	9	10	50	1020ml/min.	9	10	48
1020ml/min.	9	10	47	1020ml/min.	9	10	50
1020ml/min.	9	10	71	1020ml/min.	9	10	63
1020ml/min.	9	10	65	1020ml/min.	9	10	59

Figure 37: Funnel design calibration of both (A, B) proposed funnel designs. Calibrated by the dynamic method where rest of the volume in bucket is depicted

A funnel parameter A tends to be less accurate in (Figure 37). However, this could be caused by different inflow to the funnel A (Table 7). When the inflow was the same, the losses of both funnels tended to be alike.

A part of the calibration included also maximum filling abilities of the funnels. Smaller funnel (funnel A) had gotten full by constant flow in 5:33 min. Maximum filling could not be measured due to the larger parameters of the funnel B. Funnel B did not retain the flow and did not provide smooth outflow from the funnel.

Funnel A was transforming flow to the constant outflow where no splashing was evidenced. The filling of the funnel A is limited due to the parameters of the funnel, but it is assumed that a flow higher than 1l/minute will not be observed during experiments. In fact, outflow from the snowpack is expected to be slow that the inflow to the funnel does not have to be the limited factor. On the contrary, slow filling is beneficial to transform outflow into a constant flow which is more convenient for the tipping afterwards. Funnel B provided flow with splashing droplets from the tipping bucket device and the larger parameter of the funnel profile did no concentrate water into a constant flow. Because of the expectations that snow melt will not generate higher flow than the profile of the funnel A can provide, funnel A is suggested to be implemented for the next experiments.

5.7.3 Third calibration

Third calibration was an extended calibration, that applied the design of improvements on all the TB devices (Figure 38). New supposition was applied to the process of static calibration. Approx. 3 ml. of extra volume has been added to the desired volume (100 ml.) of the bucket as a prevention to the expected losses.
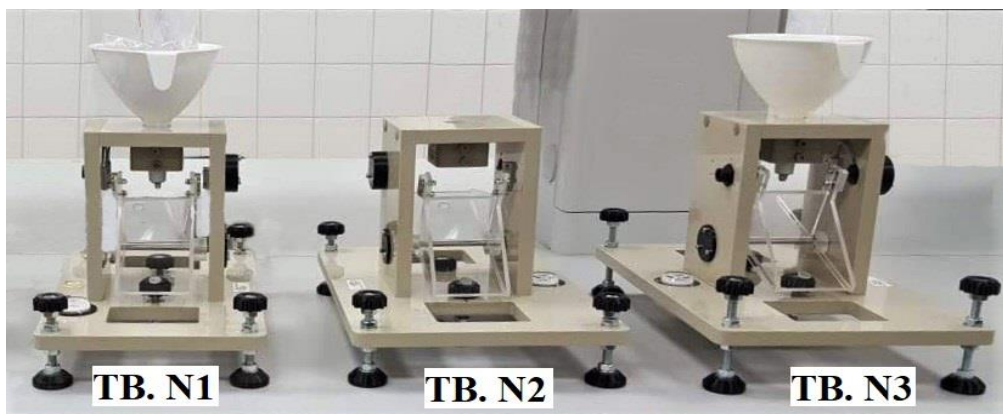

Figure 38: All tipping bucket devices after calibrations. TB.N1 (tipping bucket number 1), TB.N2 (tipping bucket number 2), TB.N3 (tipping bucket number 3)

Dynamic calibration is represented as the last bucket volume after 1liter discharge simulation. In all the cases 10th bucket was evaluated. In graphs only the volumes of the last 10th buckets are seen.
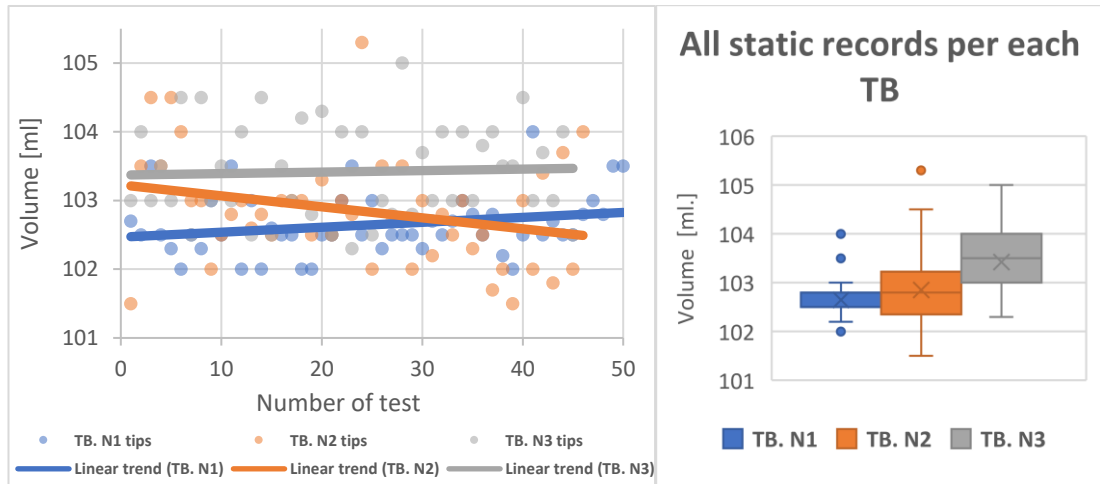

Figure 39: A) Static calibration per each TB per number of runs of tests and measured volume per each tip. Linear trend lines represent volume of calibrated TB during static calibration, B) Representation of volumes of all the tipping buckets from the static calibration (Calibrated volume per each TB) Box plots description: x = mean, line = median, lower and upper whisker = range of measured values [min, max], box bottom = 1st quartile, box top = 3rd quartile, dots out of the range of whiskers = outliers.

The static calibration data show calibrated volume per each tip for each tipping bucket (Figure 39, A). TB. N1 is calibrated for 102.65 ml./tip, TB. N2: 102.85 ml./tip and TB. N3: 103.4 ml./tip (Figure 39, B).
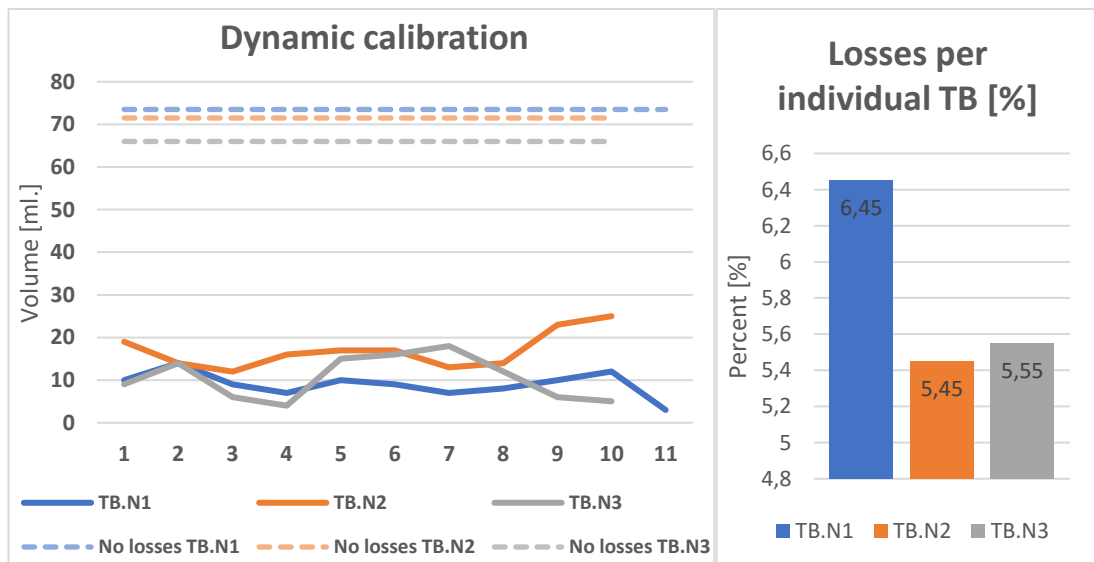
Figure 40: A) Comparison of all dynamic calibrations per each tipping bucket with boundary lines [dashed lines] representing 0% losses, B) Tipping buckets percentual losses after dynamic calibration

Dynamic calibration follows the measured volumes in all the TBs where 10th overturn was recorded (solid lines in Figure 40, A). Zero percentual losses are depicted for the example where the limits of the calibration of all TB devices are. No losses boundaries are lines per each TB that indicate what volume each TB could possibly contain at the dynamic calibration (1000 ml.) without losses.

Tipping bucket number one is the least accurate with the percentual losses of 6.45%. The tipping bucket number two has shown 5.45% losses from the calibration tests and is validated as the most accurate one (Figure 40, B). No losses of the TB device would be obtained if 1 liter of the simulated flow overturned buckets of the system 9th times and the 10th tipped bucket was filled by the extra calibrated volume (volume added as a prevention factor) of each TB times number of tips plus the rest of the calibration inflow. This means that the TB. N1 with volume of 102.65 ml./overturn would leave 73.5 ml. in the last 10th bucket with no losses (as well as depicted in Figure 40, 0% losses lines). It is obvious that the 0% losses would be obtained if volume of buckets were 100 ml and the 11th tips had no water inside. But in our case recalculation is necessary because volume varies with every TB device.

It is expected that all the tipping buckets will, in fact, have higher accuracy when used on site. Laboratory conditions provided a great space for calibrations but the simulations under time restrains could not simulate velocity flow as slow as it is expected during the experiments. It is clear, that more accurate data would be obtained if the water velocity had been lower.

5.7.4 Calibrations summary

Despite some revealed deficits in accuracy, losses will always be manifested due to surface tension of water and the adhesion on the surface of the bucket. It may seem that the tipping buckets are not completely precise (Figure 40,B) but known tipping buckets behavior is better for the ROS investigation than not calibrated tipping bucket that was used during ROS experiments. Known design of tipping buckets, thanks to the calibration, can be enhanced in the future if tipping bucket design improvement is necessary.

The surface tension depends on the temperature of the liquid and it is usually lower for tap water than in case of rain fall. Tap water therefore causes smaller error at calibration (Marsalek, 1981). VASVARI (2005) refers, after his calibrations, that the adhesive retained water in the tipping bucket depending on the bucket material. Metal

tipping buckets could retain more water through corrosion, which raised the specific surface of the TB device. Plastic buckets on the other hand are more water repellent. VASVARI (2005) also found that the larger the tipping buckets are, the more accurate they tend to be. Smaller buckets are characterized by higher potential to losses than larger buckets because the tipping moment is often.

In the case of the tipping buckets in this work, plastic material was used but larger tipping buckets are not desirable because of space limits at examined sites. As the water flow in calibrations was simulated with high velocity, lower intensity of flow is suggested for further calibrations to obtain more precise data. Funnel calibration showed that funnel outflow can eliminate a lot of potential losses as well as the parameters of the water level. Calibrated funnel is not suitable for higher ranges of velocities of the flow as liter per minute thanks to the design and specific designed outflow.

6 <u>Conclusions</u>

This work is mainly focused on methods of investigating ROS events and analyzing formation of flow paths as the main reaction of water behavior in snowpack after experiments. Two main approaches have been applied for the purpose of analyzing water behavior in snowpack "the localization analysis" and "bluesnow analysis". Localization analysis localizes interflow patterns in the snowpack into coordinate system and the bluesnow analysis has been applied for testing a so-called package written in the R programming language as the first use of this method. Bluesnow analysis with snow properties investigation have statistically assessed all the sites. Experimental site Luisino Údolí, has been evaluated with 4.2 % of blue fraction over the entire snow profile, with the highest density [302 kg/m^3] of all sites and coldest temperature profile [-1.7 °C]. Kubova Huť 1 site, with 4.75% of blue fraction and with 244 kg/m^3 density profile. Experimental site Kubova Huť 2, has had 63.8 % fraction of blue distribution and the highest liquid water content profile at all with 7.2 %. A third analysis "the photos reliability analysis" was carried out to validate the methodology of ROS experiments. Methods of improvements consist of suggestions based on the reliability analysis and design calibrations also done in this work for implementing new tipping buckets for measuring the outflow during experiments.

Reliability analysis was conducted by the author of this thesis to find potential renovations in the way ROS experiments are performed. Reliability analysis shows what kind of distortion can we see, and uncertainty of photos divided into two index categories. The first height uncertainty, comparing snow depths of photos (on scale 1 to 5), where 1 indicates high certainty and 5 high uncertainty. The second category is the lysimeter desk determination, where (scale from 1 to 3) is used, as 1, certain localization of lysimeter desk (high certainty) and 3 (high uncertainty), where lysimeter is not observed in photo and an estimation of lysimeter has to be done. Due to high uncertainties new profile frame for measuring is proposed with operating and photographing instructions. Uncertainty index pointed out that the lysimeter desk was sometimes obstructed by the bottom measuring scale (causing high lysimeter desk uncertainty). High index uncertainties were also linked to distortion and wrong placement of scales. Profile frame with right methods of operating instructions is proposed to increase the reliability of photos and to increase precision of collected data from the experiments.

Localization analysis provides classification of water movement in the snowpack and composes data into tables of coordinate. Localization analysis takes findings from the reliability analysis for recalculating the distortion caused be the wide camera angle. This method is good for analyzing each layer in the snowpack induced after the ROS but is very laborious and can lead to inaccuracies because depends on author's precision skills. Nonetheless, this approach justifies the distortion and leads to better understanding of water behavior after ROS with graphical representation of profiles.

Bluesnow analysis is more complex and can be applied on many photos quickly visualizing the water movement with information about the blue fraction in the pixels after dye tracer experiments. This package provides better inputs for calculations that can investigate vertical or horizontal flow pattern formation. In this work prevailing formation of fluid paths was developed. Prevailing formation points out the dominancy of vertical or horizontal distribution of blue fraction in snowpack indicating fluid patterns. This is important with the combination of investigated snowpack's properties data. Horizontal formation tends to be present in more heterogenous snowpack and vertical formation is linked with more uniform and more homogeneous properties of snow. In this thesis, dominancy of vertical flow paths has typical character within higher liquid water content, temperature and causes a trend of formatting matrix flow (Kubova Huť 2 experimental site). On the other hand, snowpack with higher prevailing formation of horizontal flow paths tends to form finger flow and lateral flow with lower values of liquid water content and temperatures along the profile (Luisino Údolí experimental site and Kubova Huť 1 site). Uniform profiles cannot store water and tend to release water after ROS into the soil. The bluesnow package can be used and developed in order to provide other potential analyses.

New tipping buckets are implemented in the methods of improvements with the profile frame, both increasing the precision of measured data. Tipping buckets are more representable due to long term outflow monitoring and tipping bucket design development. Designing of the tipping buckets enhanced their efficiency (6.45%, 5.45%, 5.55% calculated losses per each tipping bucket) and provided space for designing further improvements. New designing can use statistical overviews of the newly calibrated tipping buckets and implement new emendations. Implementation of calibrated tipping buckets is believed to obtain more accurate data from the released water after ROS.

7 <u>References</u>

1) Avanzi, F., Hirashima, H., Yamaguchi, S., Katsushima, T., De Michele, C., 2016. Observations of capillary barriers and preferential flow in layered snow during cold laboratory experiments. Cryosphere 10, 2013–2026. https://doi.org/10.5194/tc-10-2013-2016

2) Bartelt, P., Lehning, M., 2002. A physical SNOWPACK model for the Swiss avalanche warning : Part I : numerical model A physical SNOWPACK model for the Swiss avalanche warning Part I : numerical model. https://doi.org/10.1016/S0165-232X(02)00074-5

3) Burns, S.P., Molotch, N.P., Williams, M.W., Knowles, J.F., Seok, B., Monson, R.K., Turnipseed, A.A., Blanken, P.D., 2014. Snow Temperature Changes within a Seasonal Snowpack and Their Relationship to Turbulent Fluxes of Sensible and Latent Heat. J. Hydrometeorol. 2. https://doi.org/10.1175/JHM-D-13-026.1

4) Calder, I.., Kidd, C.H.R., 1978. A note on the dynamic calibration of tipping-bucket gauges. J. Hydrol. 39, 383–386.

5) CHMI, ©2017: Sborník příspěvků ze semináře XXI. Stretnutie sněhárov (online) [cit.2020.02.19], available from <http://portal.chmi.cz/files/portal/docs/reditel/SIS/publikace/sbornik_Snehari_web.pdf>. [WWW Document], 2017.

6) CHMI, ©2020: Sníh v ČR (online) [cit.2020.02.19], available from <http://portal.chmi.cz/files/portal/docs/poboc/PR/grafy/snih-lnk.html>. [WWW Document], 2020.

7) Colbeck, S., 1986. Classification of seasonal snow cover crystals. Water Resour. Res. 22, 59S-70S. https://doi.org/10.1029/WR022i09Sp0059S

8) Colbeck, S., 1973. Theory of metamorphism of wet snow. Res. Rep. Vol. 311 U.S. Army Corps Eng. Cold Reg. Res. Eng. Lab. 311, 5475–5482. https://doi.org/10.1029/JC088iC09p05475

9) Cornell University Department of Biological & Environmental Engineering, 2020: Why preferential flow is important (online) [cit.2020.03.14], available from <http://soilandwater.bee.cornell.edu/research/pfweb/educators/intro/why.htm>. [WWW Document], n.d.

10) De Michele, C., Avanzi, F., Ghezzi, A., Jommi, C., 2013. Investigating the dynamics of bulk snow density in dry and wet conditions using a one-

dimensional model. Cryosphere 7, 433–444. https://doi.org/10.5194/tc-7-433-2013

11) Denoth, A., 1994. An electronic device for long-terlll snow wetness recording. Ann. Glaciol. 104–106. https://doi.org/10.3189/s0260305500011058

12) DeWalle, D.R., Rango, A., 2008. Principles of Snow Hydrology. Cambridge University Press. https://doi.org/10.1017/CBO9780511535673

13) Dingman, S.L., 2015. PHYSICAL HYDROLOGY Third Edition, Third Edit. ed. Waveland Press, Inc., Long Grove, IL 60047-9580.

14) Doesken, N.J., Judson, A., 1997. The snowbooklet, A. ed. Colorado State University, Fort Collins.

15) Fierz, C., McClung, D.M., Armstrong, R.L., Nishimura, K., Durand, Y., Etchevers, P., Satyawali, P.K., Greene, E., Sokratov, S.A., 2009. The international classification for seasonal snow on the ground (UNESCO , IHP (International Hydrological Programme)– VII , Technical Documents in Hydrology , No 83 ; IACS (International Association of Cryospheric Sciences) contribution No 1). UNESCO/Division of Water Sciences.

16) FPGA Company, © 2020: SLF Snow Sensor (online) [cit.2020.03.28], available from < https://fpga- company.com/slf-snow-sensor/>. [WWW Document], 2020.

17) Hammond, J.C., Saavedra, F.A., Kampf, S.K., 2018. Global snow zone maps and trends in snow persistence 2001 – 2016. Intrnational J. Climatol. 1–15. https://doi.org/10.1002/joc.5674

18) Hirashima, H., Avanzi, F., Wever, N., 2019. Wet-Snow Metamorphism Drives the Transition From Preferential to Matrix Flow in Snow. https://doi.org/10.1029/2019GL084152

19) Hirashima, H., Yamaguchi, S., Katsushima, T., 2014. A multi-dimensional water transport model to reproduce preferential flow in the snowpack. Cold Reg. Sci. Technol. 108, 80–90. https://doi.org/10.1016/j.coldregions.2014.09.004

20) Hirashima, H., Yamaguchi, S., Sato, A., Lehning, M., 2010. Numerical modeling of liquid water movement through layered snow based on new measurements of the water retention curve. Cold Reg. Sci. Technol. 64, 94–103. https://doi.org/10.1016/j.coldregions.2010.09.003

21) Jacob, D., Petersen, J., Eggert, B., Alias, A., Bøssing, O., Bouwer, L.M., Braun, A., Colette, A., Georgopoulou, E., Gobiet, A., Menut, L., Nikulin, G., Haensler, A., Kriegsmann, A., Martin, E., Meijgaard, E. Van, Moseley, C.,

Pfeifer, S., 2014. EURO-CORDEX : new high-resolution climate change projections for European impact research 563–578. https://doi.org/10.1007/s10113-013-0499-2

22) Katsushima, T., Adachi, S., Yamaguchi, S., Ozeki, T., 2020. Nondestructive three-dimensional observations of fl ow fi nger and lateral fl ow development in dry snow using magnetic resonance imaging. Cold Reg. Sci. Technol. 170, 102956. https://doi.org/10.1016/j.coldregions.2019.102956

23) Katsushima, T., Yamaguchi, S., Kumakura, T., Sato, A., 2013. Experimental analysis of preferential flow in dry snowpack. Cold Reg. Sci. Technol. 85, 206–216. https://doi.org/10.1016/j.coldregions.2012.09.012

24) Kattelmann, R., Dozier, J., 1999. Observations of snowpack ripening in the Sierra Nevada , California, U.S.A. J. ofGlaciology 45, 409–416. https://doi.org/https://doi.org/10.3189/S002214300000126X

25) Kinar, N.J., Pomeroy, J.W., 2015. Measurement of the physical properties of the snowpack. Rev. Geophys. 481–544. https://doi.org/10.1002/2015RG000481.Received

26) Kormos, P.R., Marks, D., Williams, C.J., Marshall, H.P., Aishlin, P., Chandler, D.G., Mcnamara, J.P., Watershed, N., Science, C., 2014. Soil, snow, weather, and sub-surface storage data from a mountain catchment in the rain–snow transition zone 165–173. https://doi.org/10.5194/essd-6-165-2014

27) Lehning, M., Bartelt, P., Brown, B., Fierz, C., 2002. A physical SNOWPACK model for the Swiss avalanche warning Part III : meteorological forcing , thin layer formation and evaluation 35, 169–184.

28) Marsalek, J., 1981. Technical Notes [1] Calibration of the tipping-bucket raingage. J. Hydrol. 53, 343–354.

29) Mazurkiewicz, A.B., Callery, D.G., Mcdonnell, J.J., 2008. Assessing the controls of the snow energy balance and water available for runoff in a rain-on-snow environment 1–14. https://doi.org/10.1016/j.jhydrol.2007.12.027

30) Molini, A.T., Lanza, L.G., Barbera, P. La, 2005. Improving the accuracy of tipping-bucket rain records using disaggregation techniques 77, 203–217. https://doi.org/10.1016/j.atmosres.2004.12.013

31) NATIONAL SNOW AND ICE DATA CENTER, ©2019: snow characteristics (online) [cit.2019.11.04], available from <https://nsidc.org/cryosphere/snow/science/characteristics.html>. [WWW Document], n.d.

32) Pan, C.G., Kirchner, P.B., Kimball, J.S., Kim, Y., Du, J., 2018. Rain-on-snow events in Alaska , their frequency and distribution from satellite observations Rain-on-snow events in Alaska , their frequency and distribution from satellite observations. Environ. Res. Lett. 13. https://doi.org/doi.org/10.1088/1748-9326/aac9d3

33) Perez, C., Barreto, J.M., Khanbilvardi, R., Romanov, P., 2017. Proof of Concept : Development of Snow Liquid Water Content Profiler Using CS650 Reflectometers. https://doi.org/10.3390/s17030647

34) Pomeroy, J.W., Gray, D.M., 1995. Snowcover Accumulation, Relocation and Management. Environment Canada, Saskatoon, Canada.

35) Schneebeli, M., 1995. Development and stability of preferential flow paths in a layered snowpack.

36) Seibert, J., Jenicek, M., Huss, M., Ewen, T., 2014. Snow and Ice in the Hydrosphere, Snow and Ice-Related Hazards, Risks, and Disasters. https://doi.org/10.1016/B978-0-12-394849-6.00004-4

37) Sezen, C., Šraj, M., Medved, A., Bezak, N., 2020. applied sciences Investigation of Rain-On-Snow Floods under Climate Change. Appl. Sci.

38) Singh, A.K., Singh, V.P., Singh, P., Haritashya, U.K., 2011. Snow Ripening. Encycl. Snow, Ice Glaciers 1064. https://doi.org/10.1007/978-90-481-2642-2_676

39) Singh, P., Spitzbart, G., Hübl, H., Weinmeister, H.W., 1997. Hydrological response of snowpack under rain-on-snow events: A field study. J. Hydrol. 202, 1–20. https://doi.org/10.1016/S0022-1694(97)00004-8

40) Stähli, M., Bayard, D., Wydler, H., Flühler, H., 2004. Snowmelt Infiltration into Alpine Soils Visualized by Dye Tracer Technique. Arct. Antarct. Alp. Res. 36, 128–135.

41) Sturm, M., Taras, B., Liston, G.E., Derksen, C., Jonas, T., Lea, J., 2010. Estimating Snow Water Equivalent Using Snow Depth Data and Climate Classes. J. Hydrometeorol. 1380–1394. https://doi.org/10.1175/2010JHM1202.1

42) Techel, F., Pielmeier, C., Schneebeli, M., 2008. The first wetting of snow: micro-structural hardness measurements using a snow micro penetrometer. Int. Snow Sci. Work. 1, 1019–1026.

43) Trancón, B., Bogner, C., 2012. Image Analysis for Soil Dye Tracer Infiltration Studies. https://doi.org/10.1109/IPTA.2012.6469517

44) Vasvari, V., 2005. Calibration of tipping bucket rain gauges in the Graz urban

research area 77, 18–28. https://doi.org/10.1016/j.atmosres.2004.12.012

45) Waldner, P.A., Schneebeli, M., Schultze-Zimmermann, U., Flühler, H., 2004. Effect of snow structure on water flow and solute transport. Hydrol. Process. 18, 1271–1290. https://doi.org/10.1002/hyp.1401

46) Wang, Y., Li, Y., Wang, X., Chau, H.W., 2018. Finger Flow Development in Layered Water-Repellent Soils. Vadose Zo. J. https://doi.org/10.2136/vzj2017.09.0171

47) Webb, R.W., Fassnacht, S.R., Gooseff, M.N., 2018. Hydrologic flow path development varies by aspect during spring snowmelt in complex subalpine terrain 287–300.

48) Wever, N., Würzer, S., Fierz, C., Lehning, M., 2016. Simulating ice layer formation under the presence of preferential flow in layered snowpacks. Cryosphere 10, 2731–2744. https://doi.org/10.5194/tc-10-2731-2016

49) Williams, M.W., Erickson, T.A., Petrzelka, J.L., 2010. Visualizing meltwater flow through snow at the centimetre-to-metre scale using a snow guillotine 2110, 2098–2110. https://doi.org/10.1002/hyp.7630

50) Würzer, S., Jonas, T., 2018. Spatio - temporal aspects of snowpack runoff formation during rain on snow 3434–3445. https://doi.org/10.1002/hyp.13240

51) Würzer, S., Jonas, T., Wever, N., Lehning, M., 2016. Influence of Initial Snowpack Properties on Runoff Formation during Rain-on-Snow Events 1801–1815. https://doi.org/10.1175/JHM-D-15-0181.1

52) Würzer, S., Wever, N., Juras, R., Lehning, M., Jonas, T., 2017. Modelling liquid water transport in snow under rain-on-snow conditions - Considering preferential flow. Hydrol. Earth Syst. Sci. 21, 1741–1756. https://doi.org/10.5194/hess-21-1741-2017

8 Appendix

8.1 Brilliant blue distribution per each site
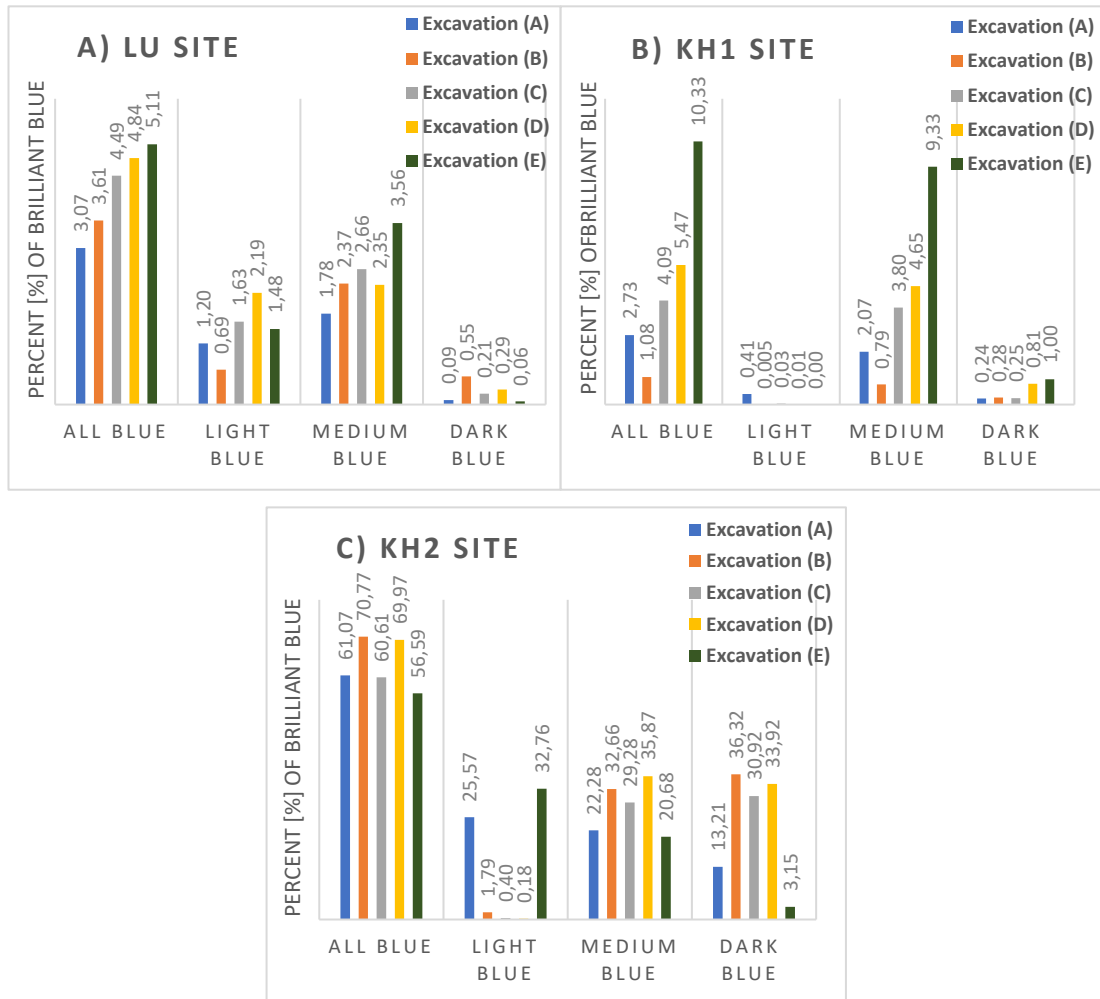
Figure 41: Range of the blue fraction distribution in pixels listed per each site and excavation referring to the categories of fraction of blue (dark blue – light blue) in pixels found by the filter of bluesnow. A) LU site, B) KH1 site, C) KH2 site

8.2 Water movement localization analysis per each excavation at the LU site
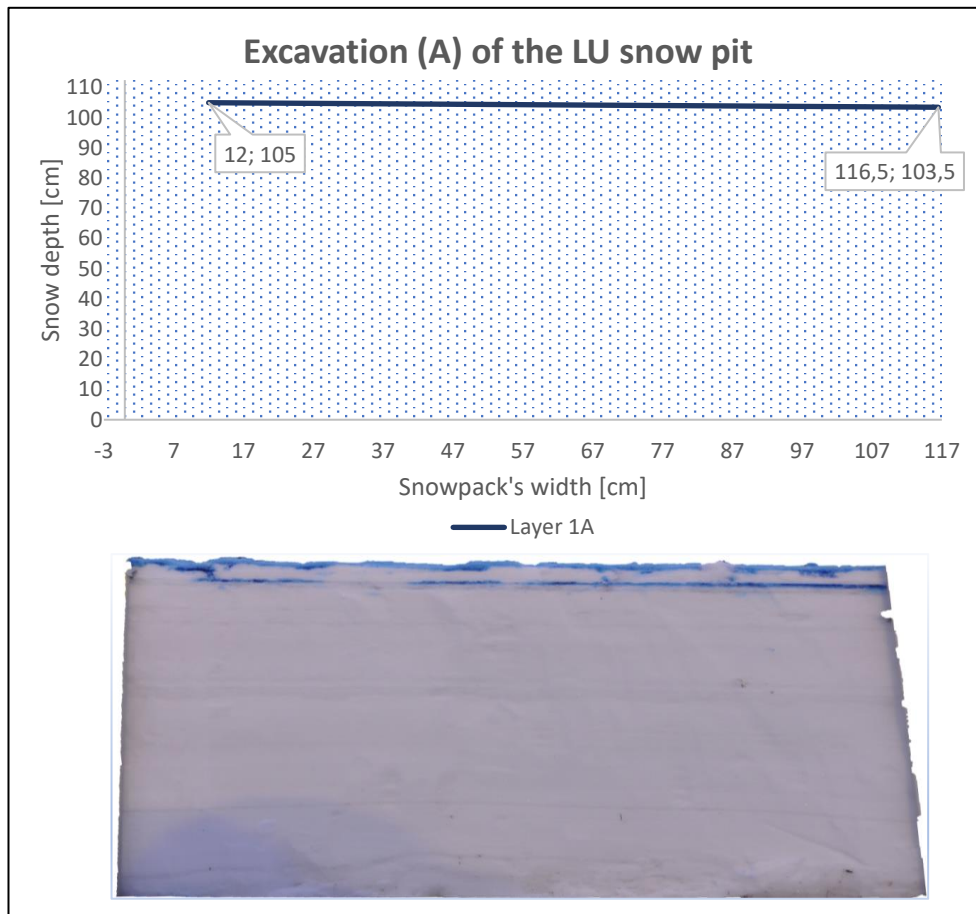
Figure 42: Graphical interpretation of water accumulation compared to the photo of the snow pit excavation (A) at the LU site.
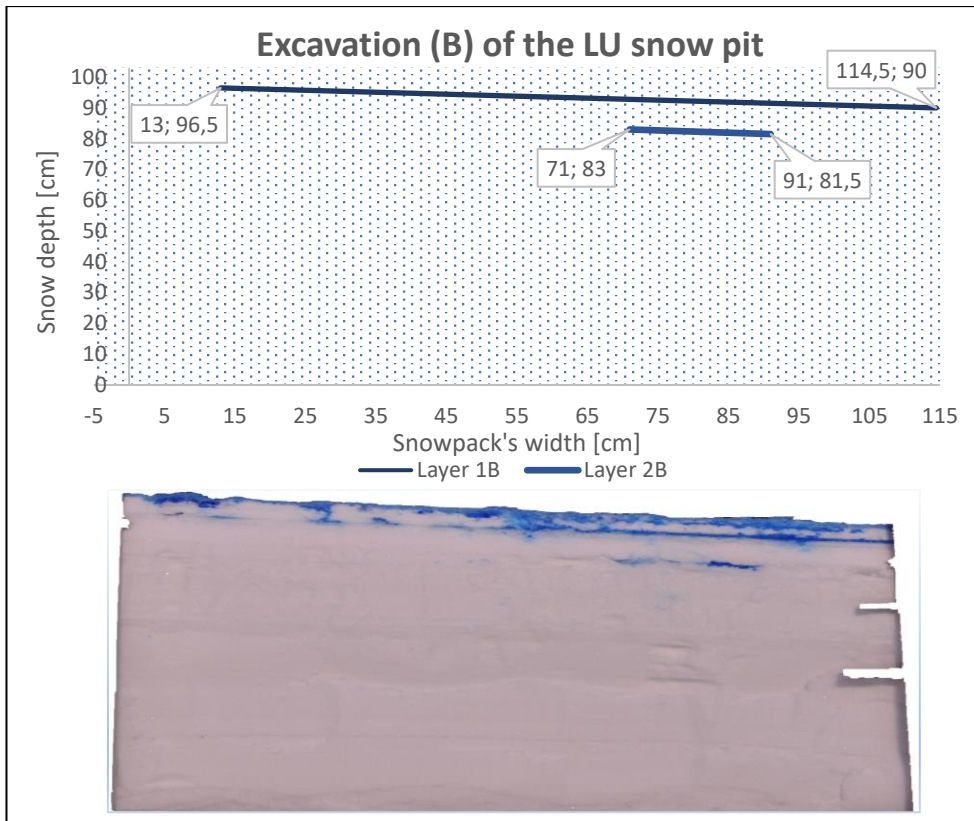
Figure 43: Graphical interpretation of water accumulation compared to the photo of the snow pit excavation (B) at the LU site.
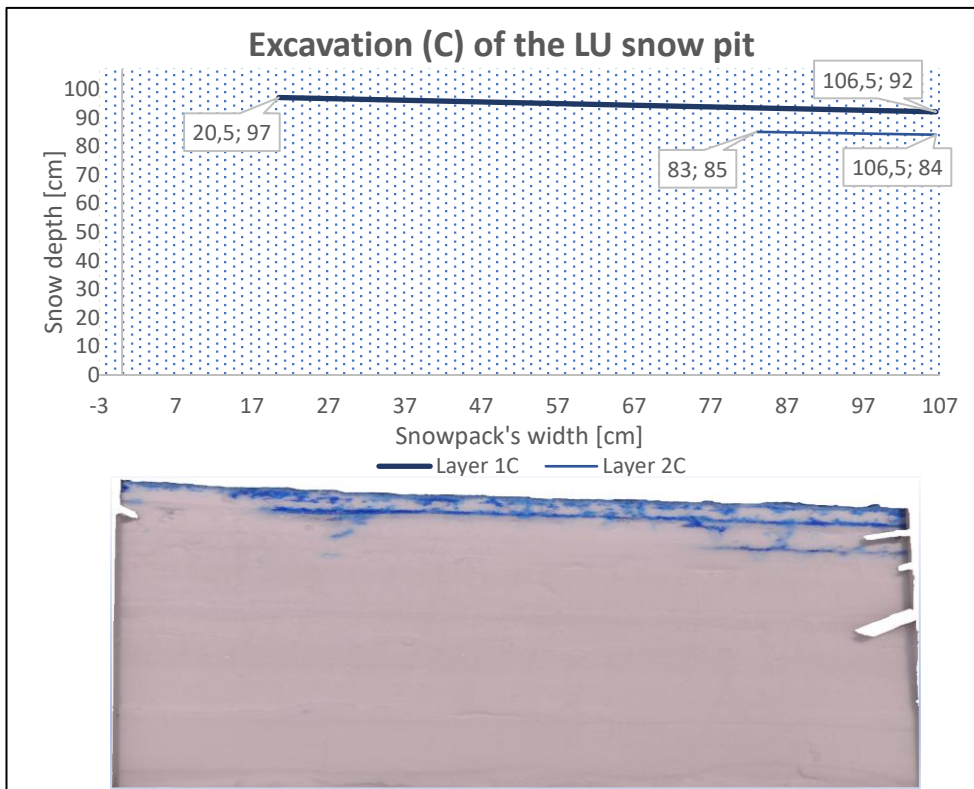
Figure 44: Graphical interpretation of water accumulation compared to the photo of the snow pit excavation (C) at the LU site.
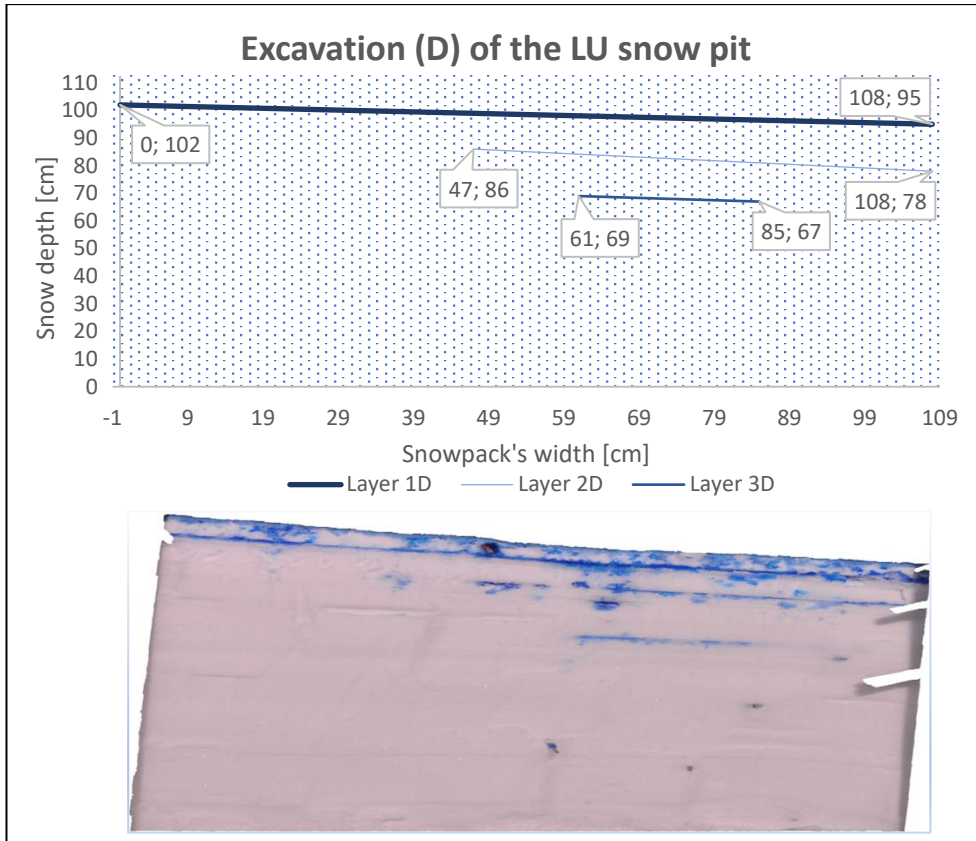
Figure 45: Graphical interpretation of water accumulation compared to the photo of the snow pit excavation (D) at the LU site.
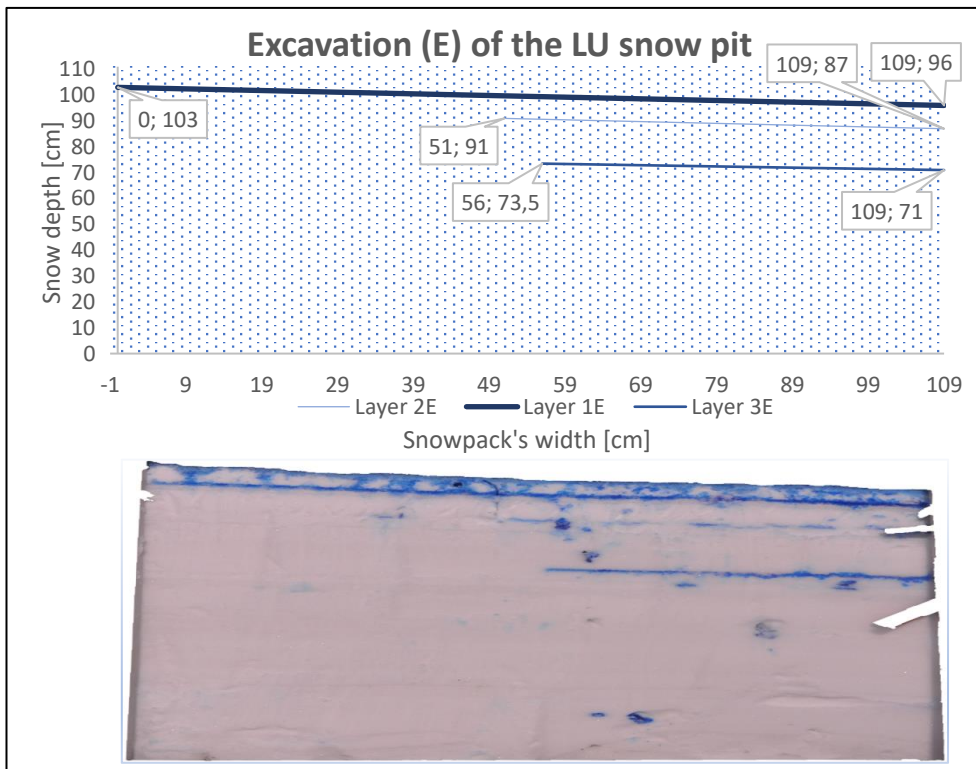
Figure 46: Graphical interpretation of water accumulation compared to the photo of the snow pit excavation (E) at the LU site.

8.3 Water movement localization analysis per each excavation at the KH1 site
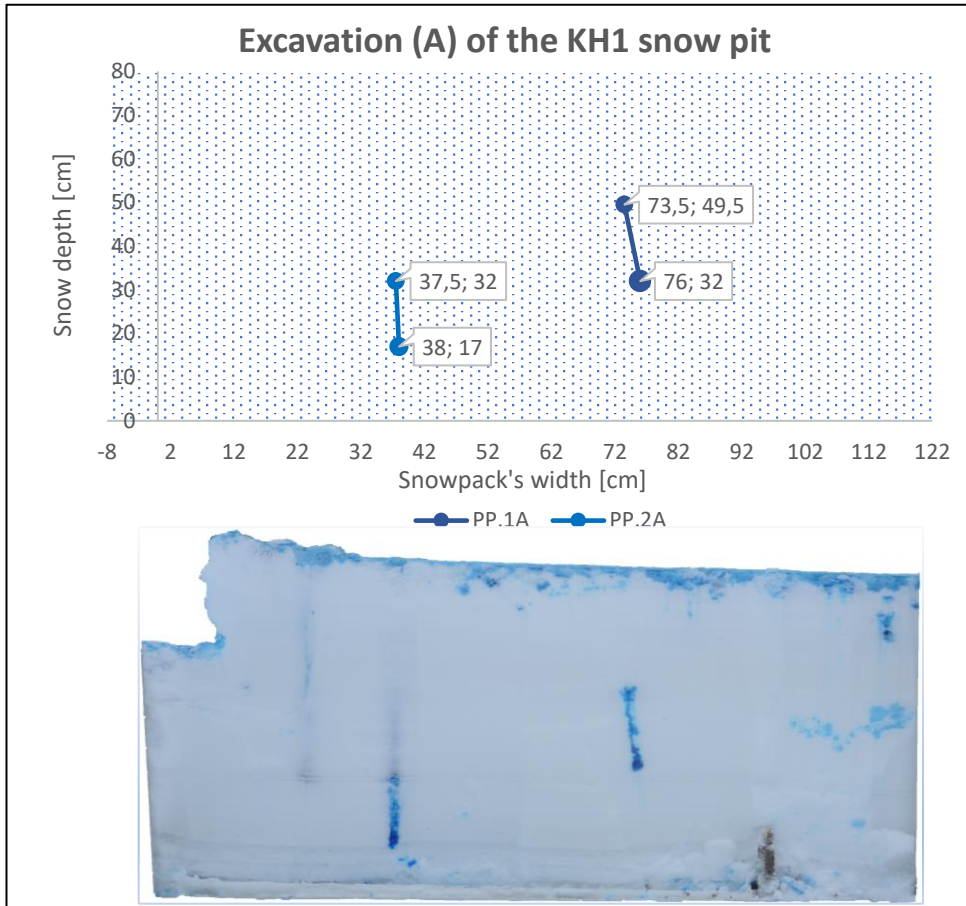
Figure 47: Graphical interpretation of water accumulation compared to the photo of the snow pit excavation (A) at the Kubova Huť 1 site.
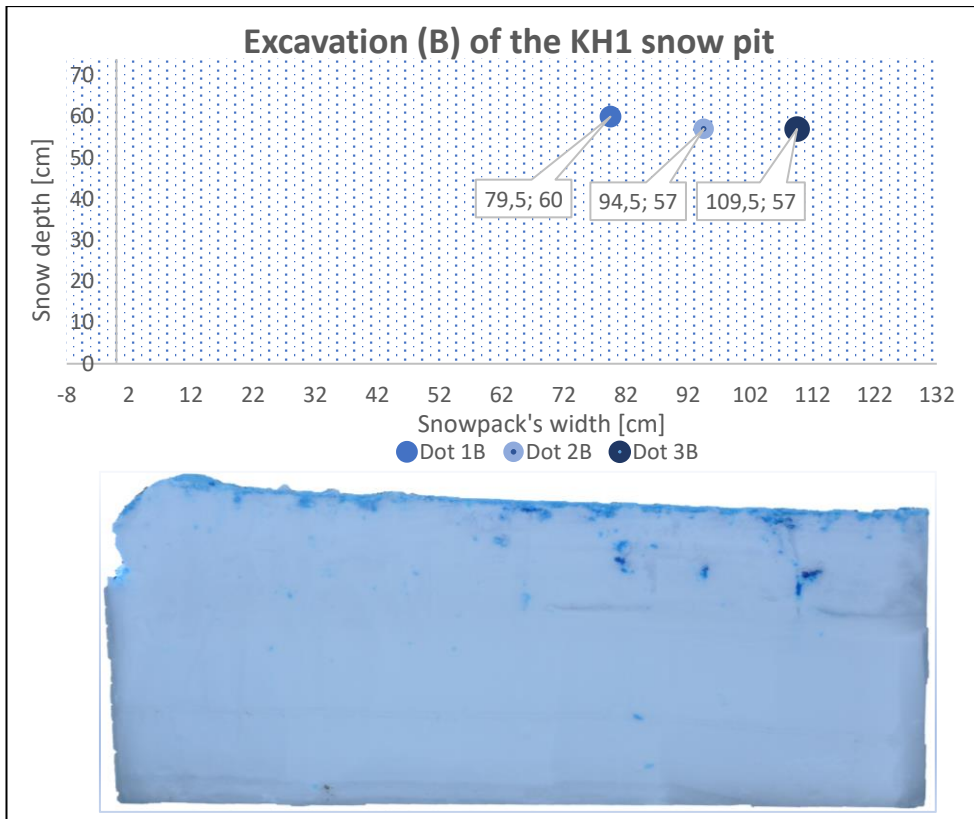
Figure 48: Graphical interpretation of water accumulation compared to the photo of the snow pit excavation (B) at the Kubova Huť 1 site.
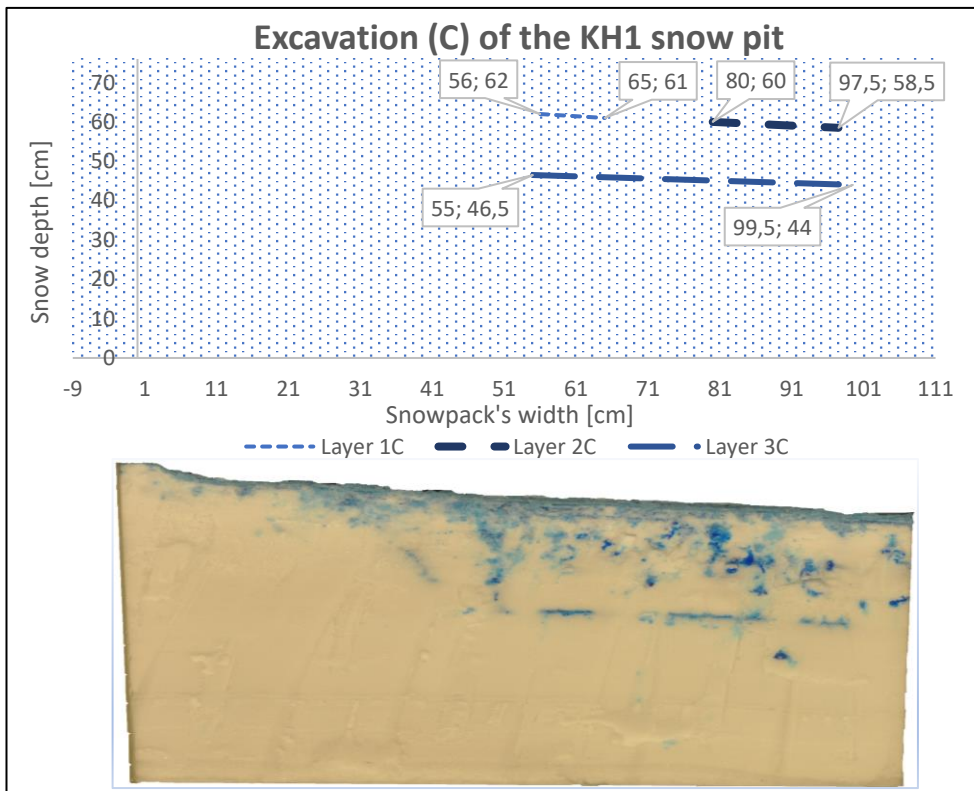
Figure 49: Graphical interpretation of water accumulation compared to the photo of the snow pit excavation (C) at the Kubova Huť 1 site.
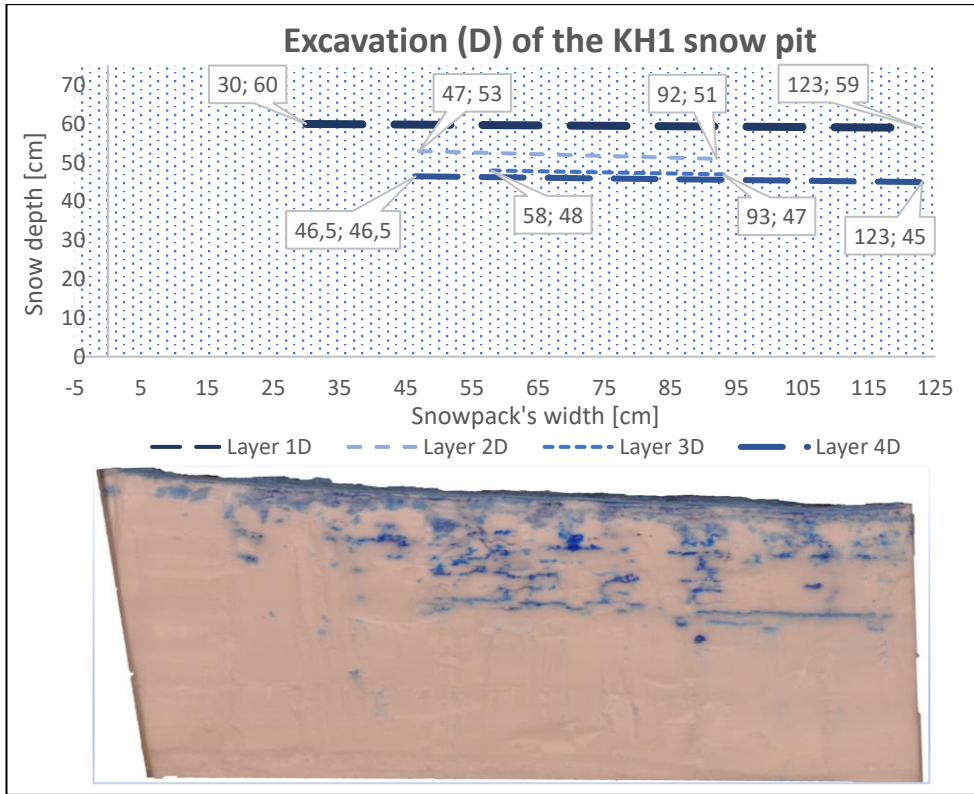
Figure 50: Graphical interpretation of water accumulation compared to the photo of the snow pit excavation (D) at the Kubova Huť 1 site.
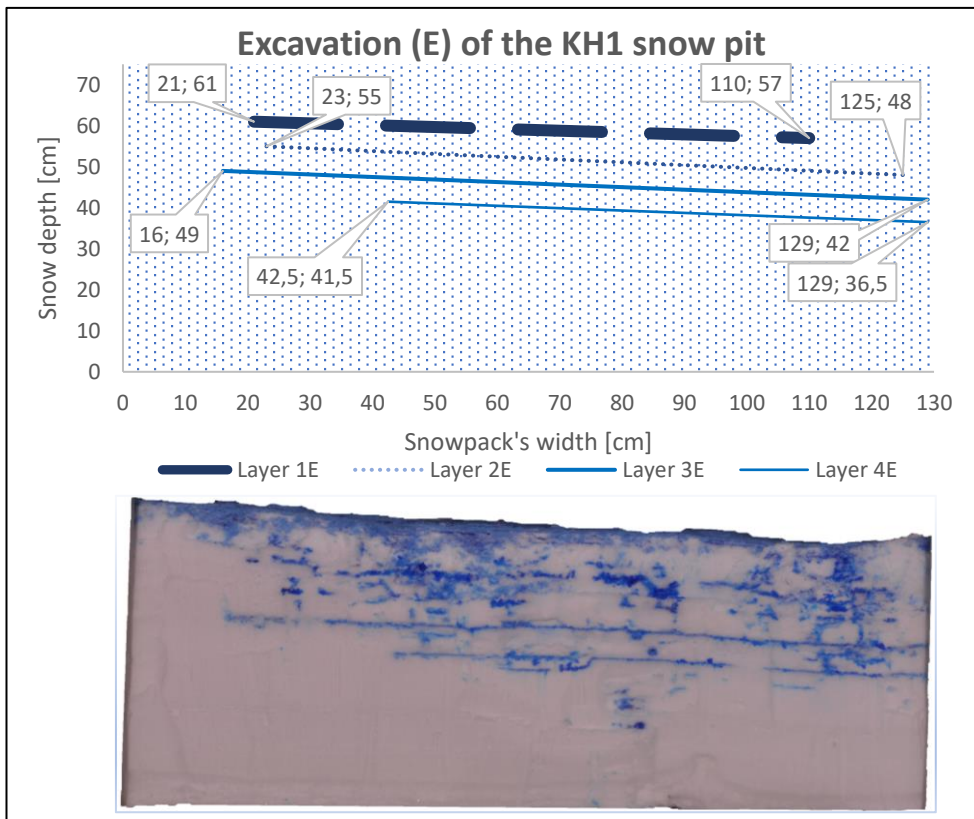
Figure 51: Graphical interpretation of water accumulation compared to the photo of the snow pit excavation (E) at the Kubova Huť 1 site.

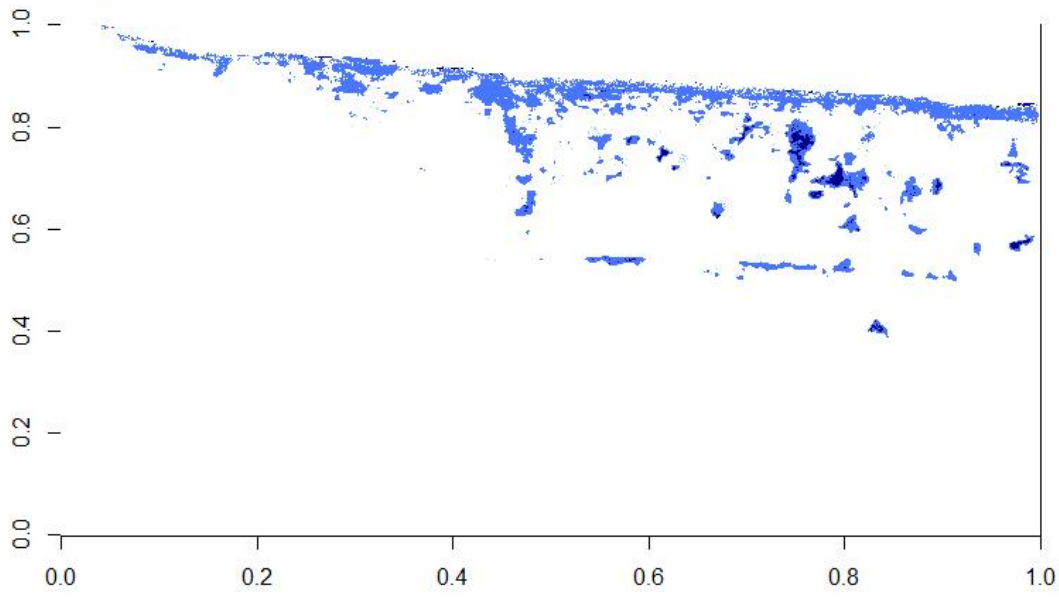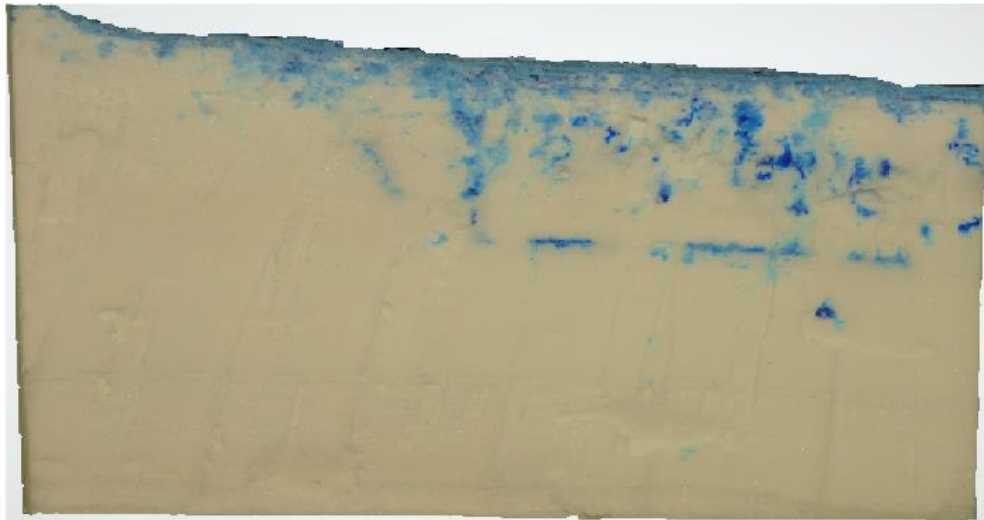## 8.4 Water behavior by the bluesnow analysis at the LU site
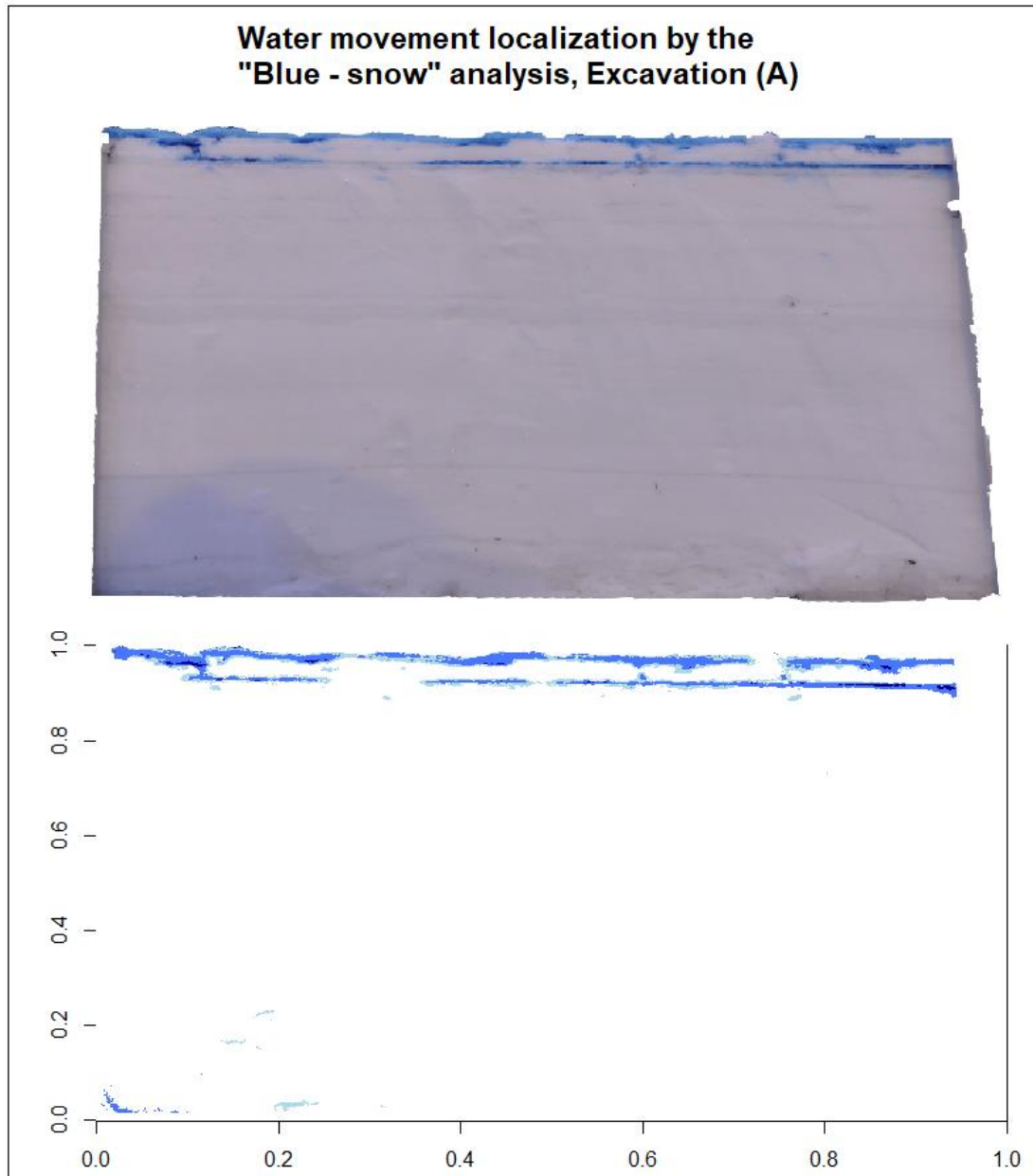
Figure 52: Photo of the excavation (A) and the bluesnow filter, which is the blue fraction distribution per pixels representing water movement induced by ROS at the Luisino Údolí site.
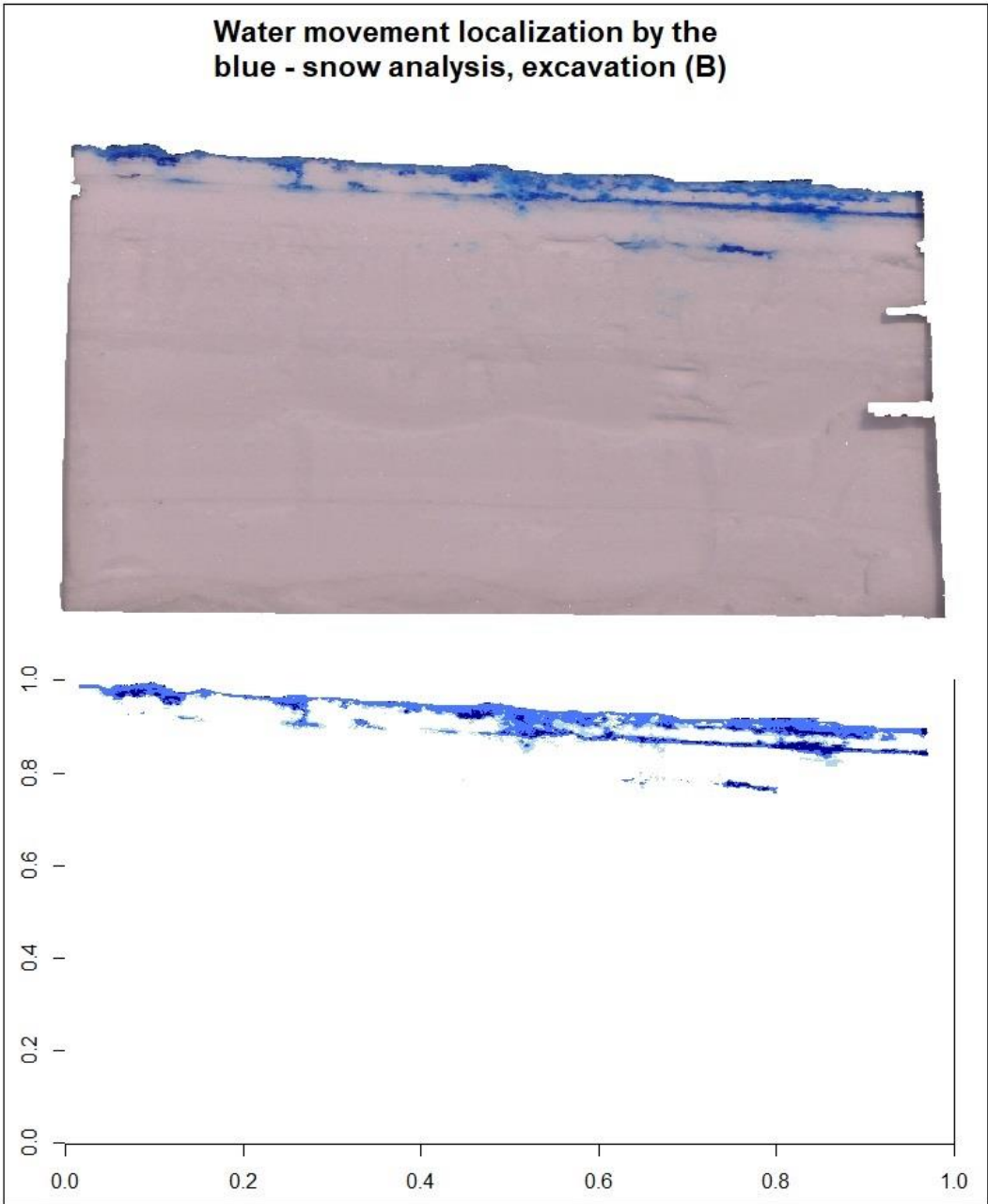
Figure 53: Photo of the excavation (B) and the bluesnow filter, which is the blue fraction distribution per pixels representing water movement induced by ROS at the Luisino Údolí site.
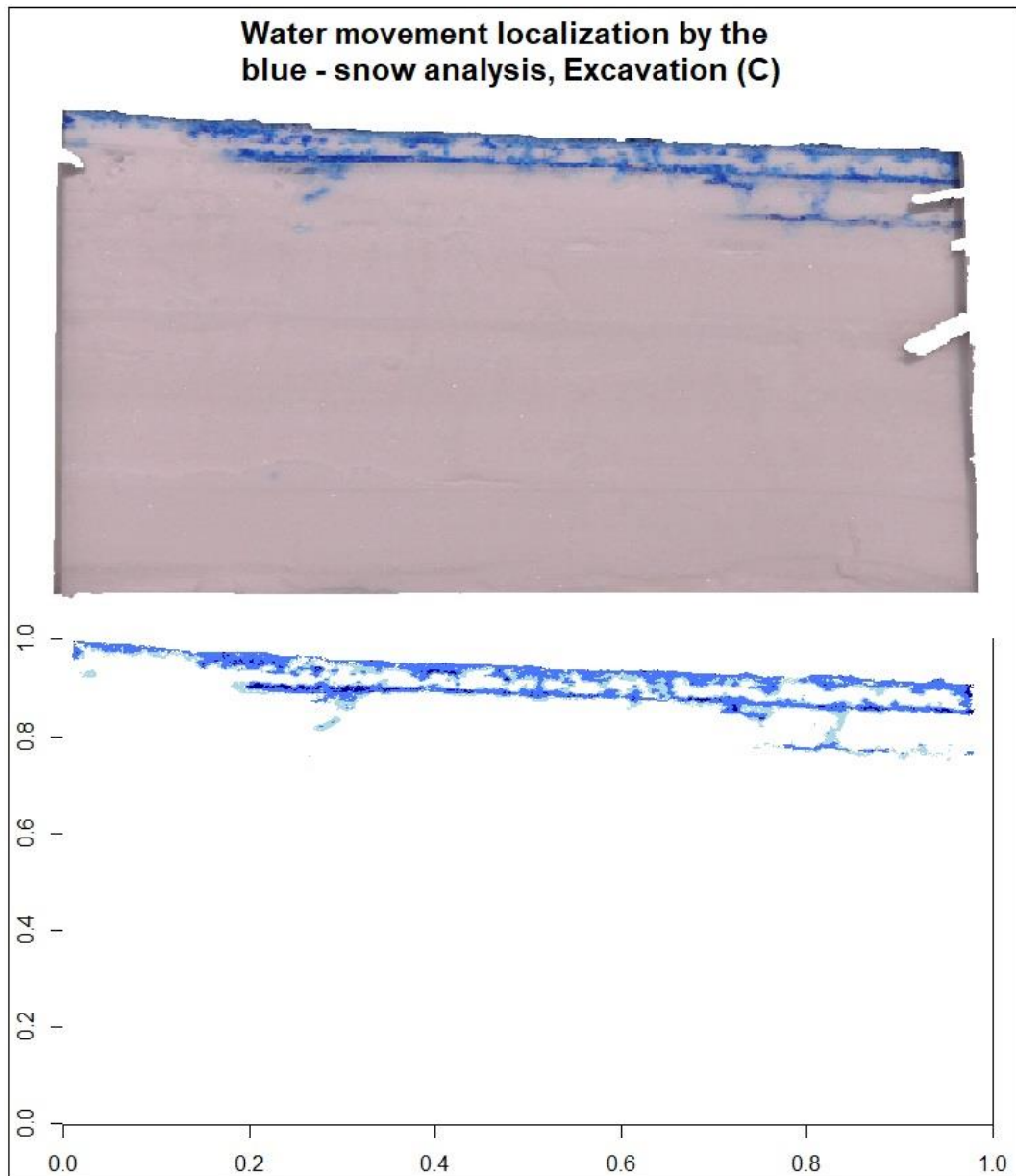
Figure 54: Photo of the excavation (C) and the bluesnow filter, which is the blue fraction distribution per pixels representing water movement induced by ROS at the Luisino Údolí site.
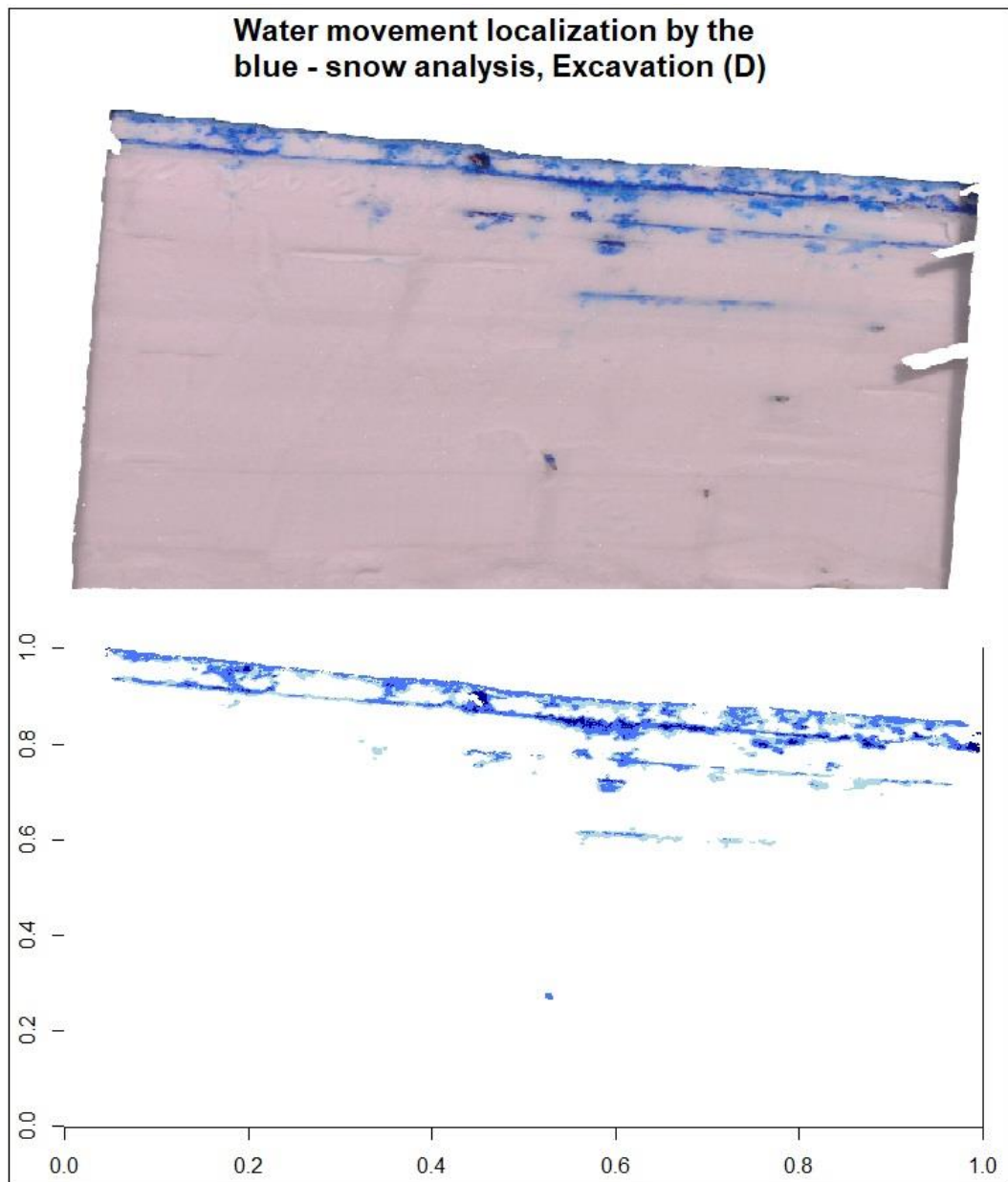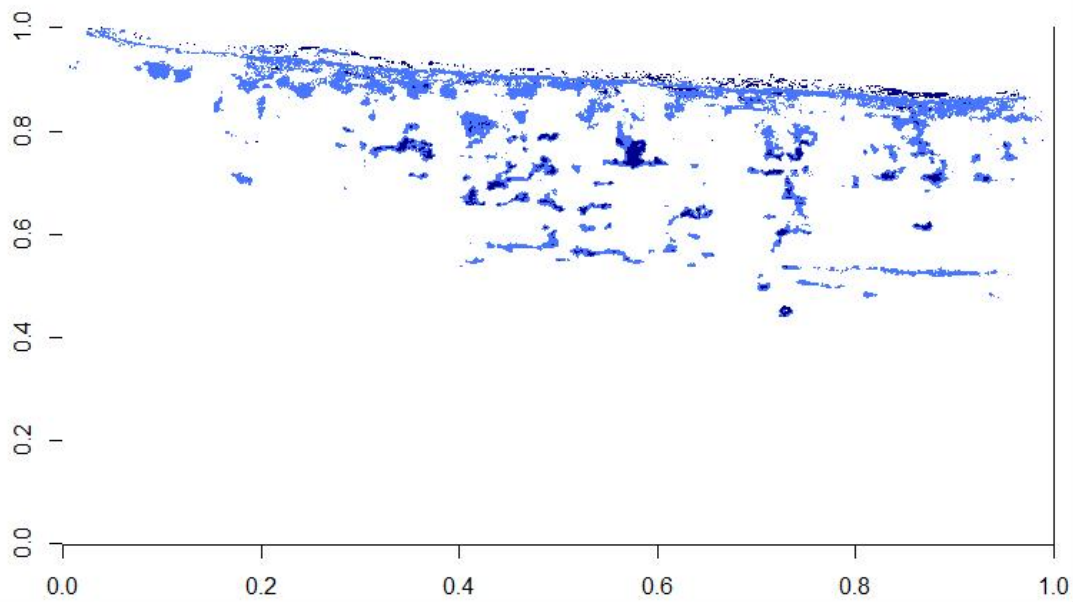
Figure 55: Photo of the excavation (D) and the bluesnow filter, which is the blue fraction distribution per pixels representing water movement induced by ROS at the Luisino Údolí site.
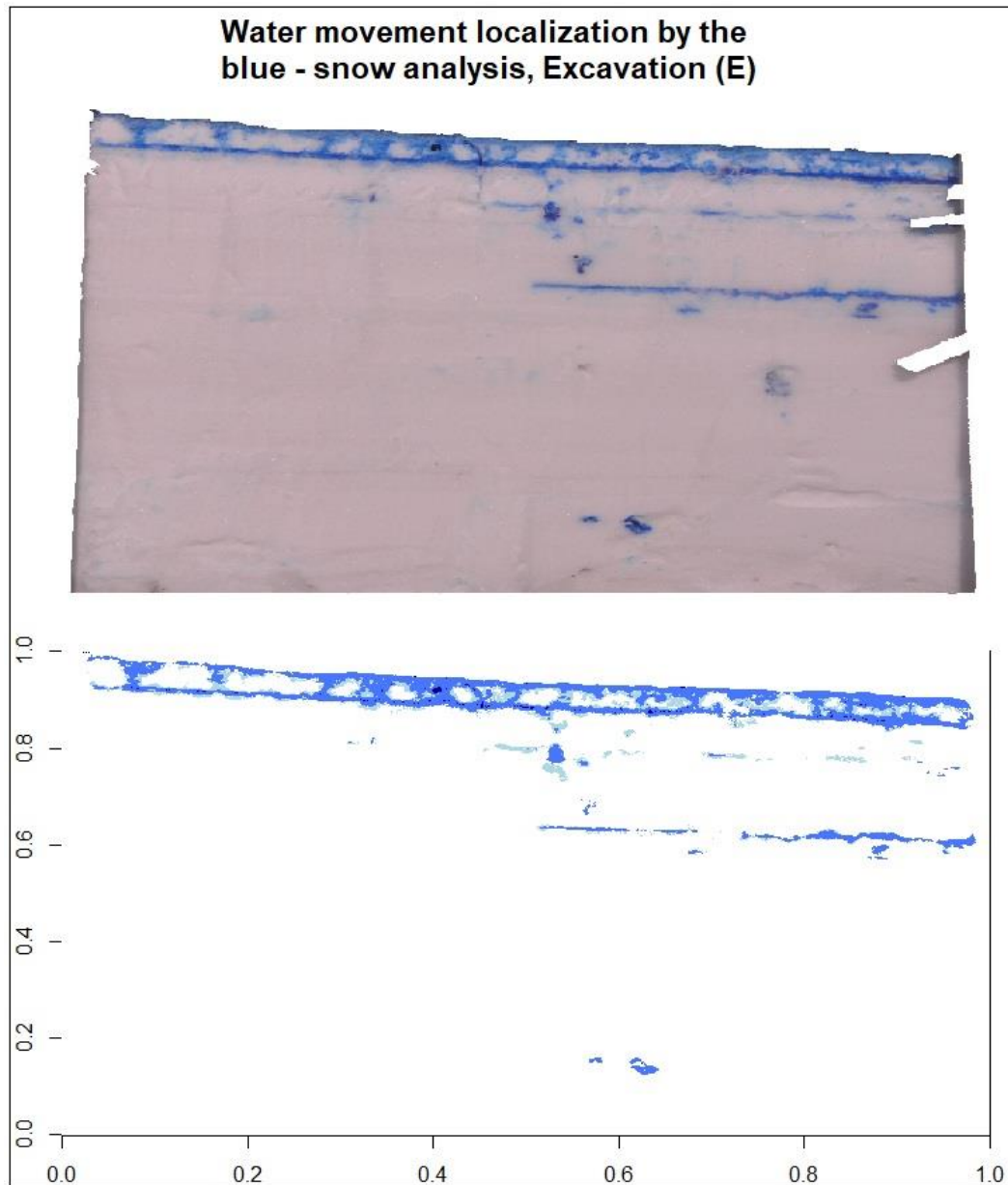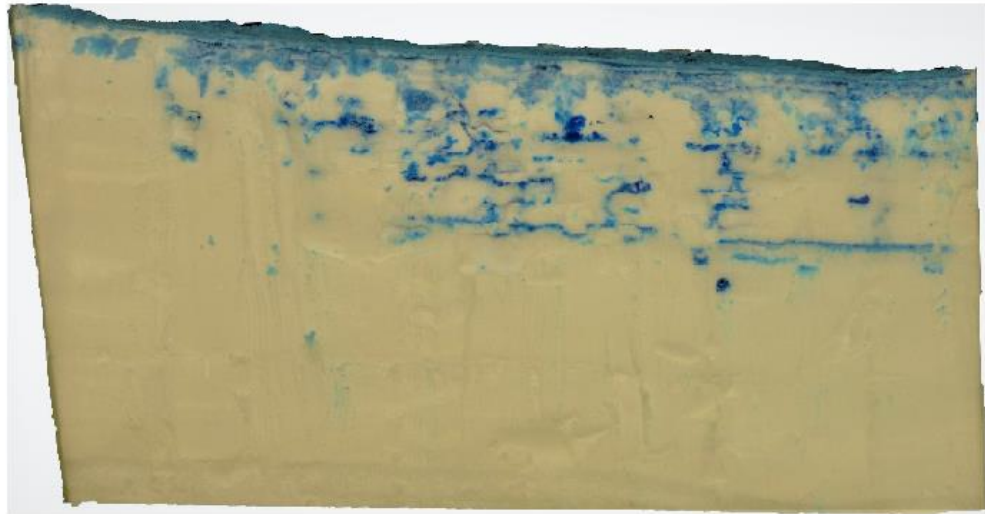
Figure 56: Photo of the excavation (e) and the bluesnow filter, which is the blue fraction distribution per pixels representing water movement induced by ROS at the Luisino Údolí site

8.5 Water behavior by the bluesnow analysis at the KH1 site
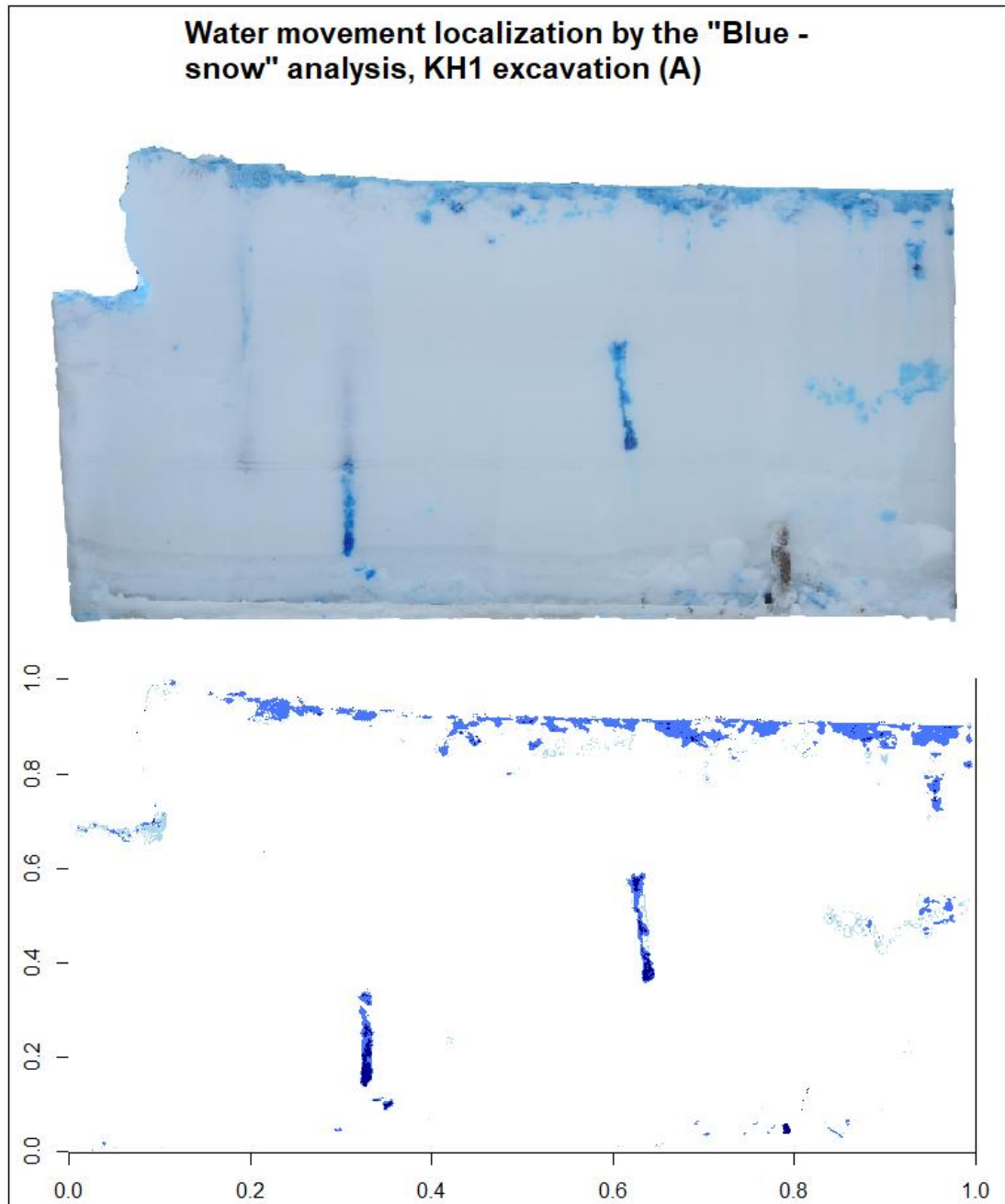
Figure 57: Photo of the excavation (A) and the bluesnow filter, which is the blue fraction distribution per pixels representing water movement induced by ROS at the Kubova Huť 1 site.
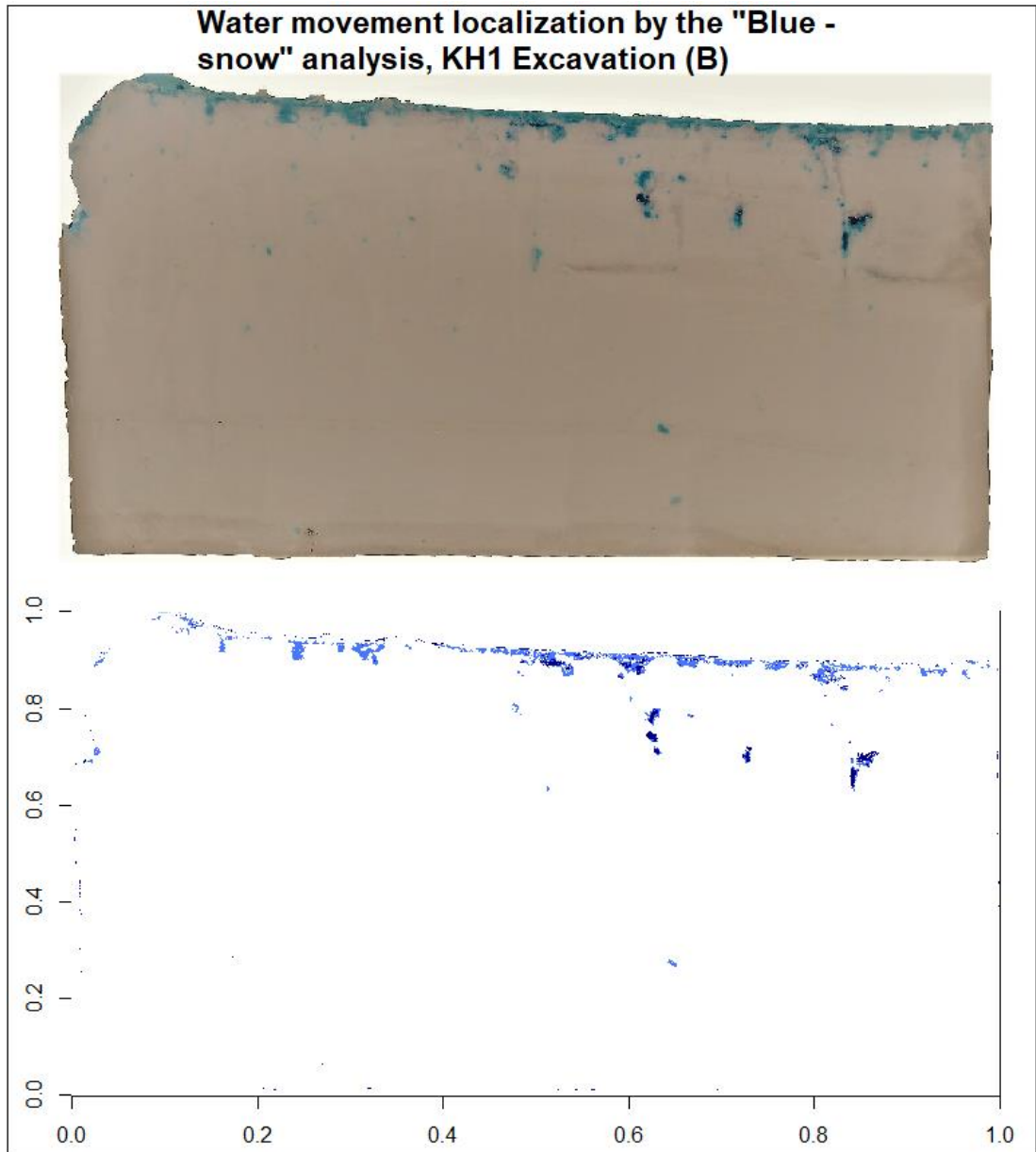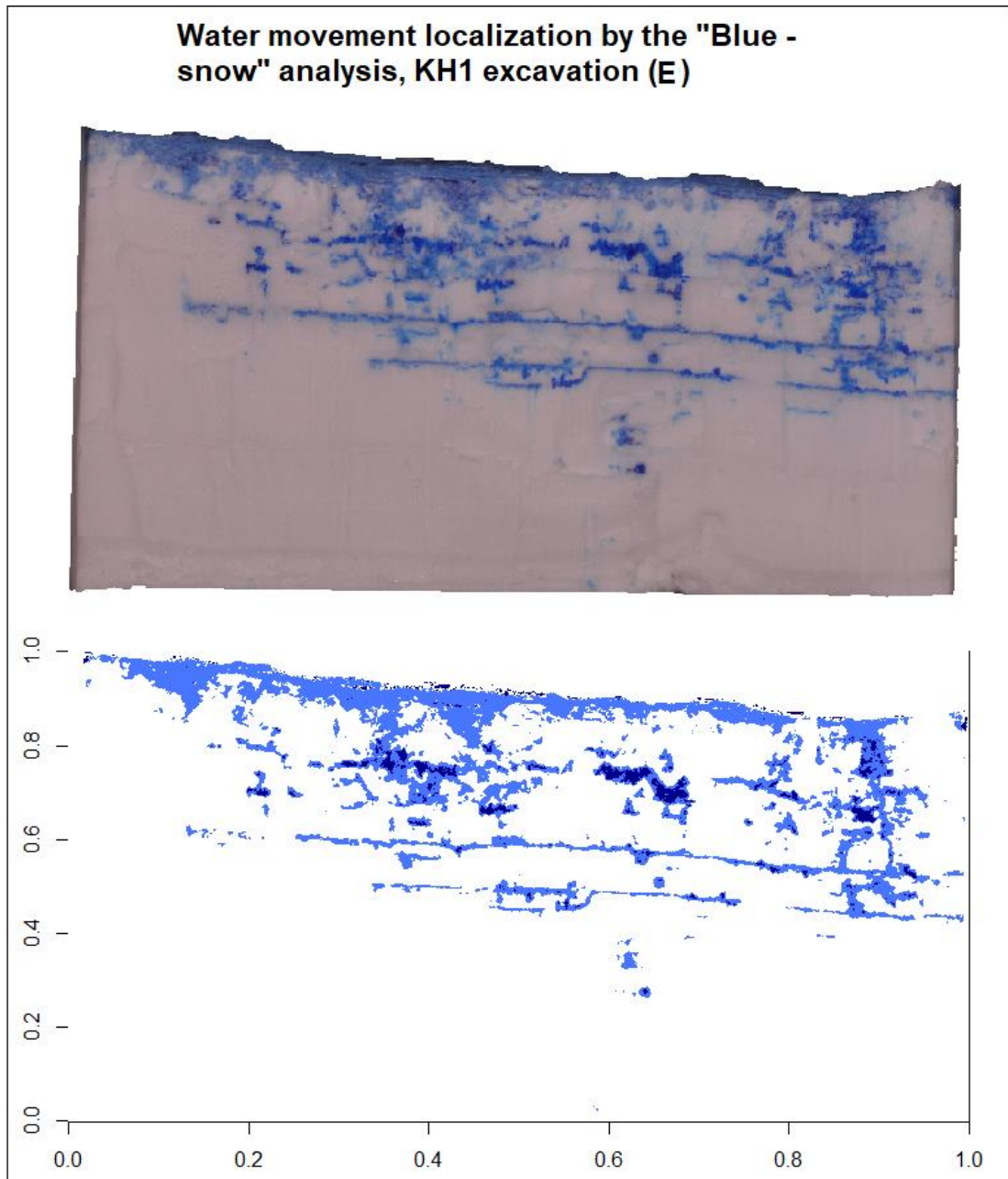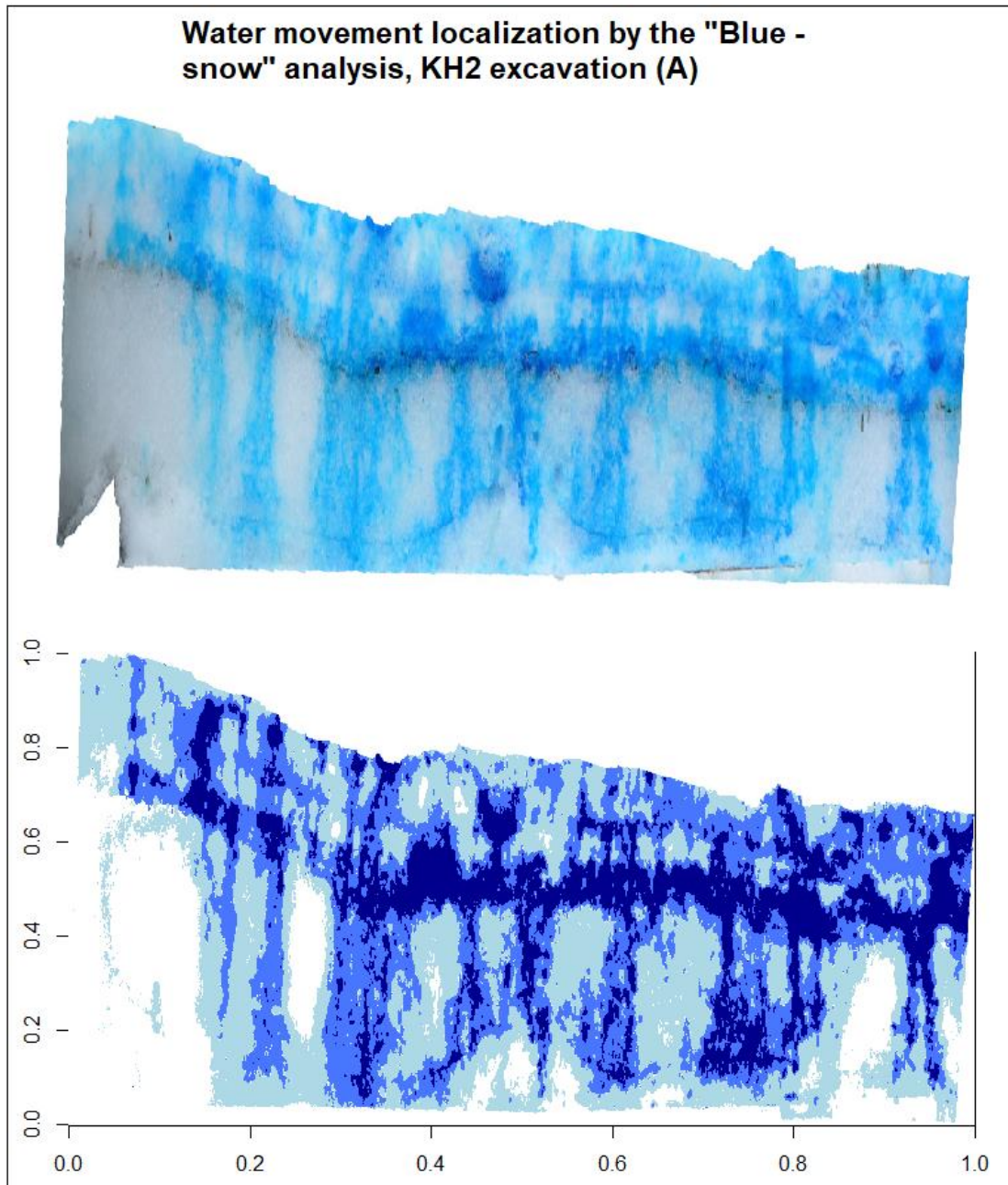
Figure 58: Photo of the excavation (B) and the bluesnow filter, which is the blue fraction distribution per pixels representing water movement induced by ROS at the Kubova Huť 1 site.

Figure 59: Photo of the excavation (C) and the bluesnow filter, which is the blue fraction distribution per pixels representing water movement induced by ROS at the Kubova Huť 1 site.

Figure 60: Photo of the excavation (D) and the bluesnow filter, which is the blue fraction distribution per pixels representing water movement induced by ROS at the Kubova Huť 1 site.
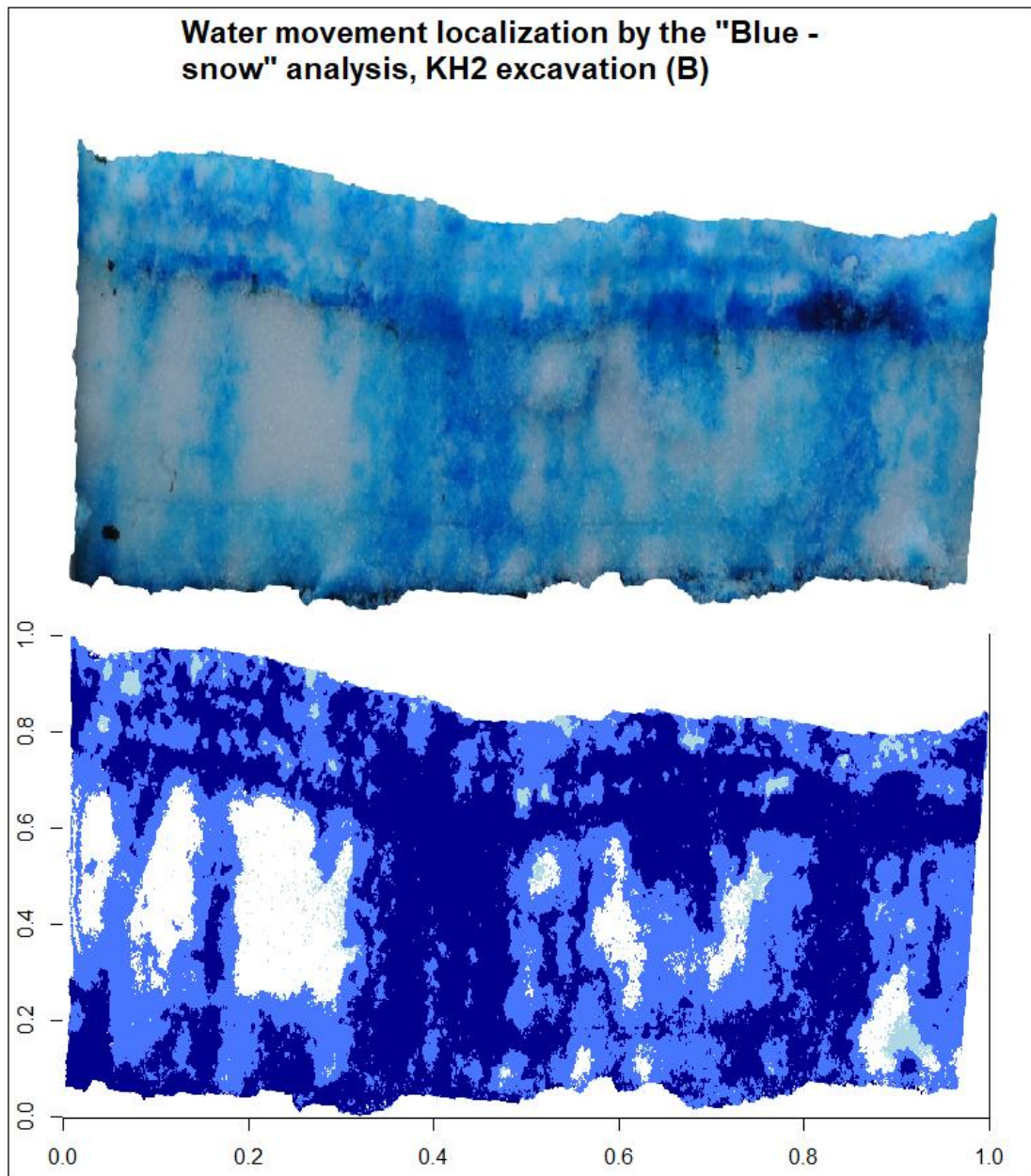
Figure 61: Photo of the excavation (E) and the bluesnow filter, which is the blue fraction distribution per pixels representing water movement induced by ROS at the Kubova Huť 1 site.

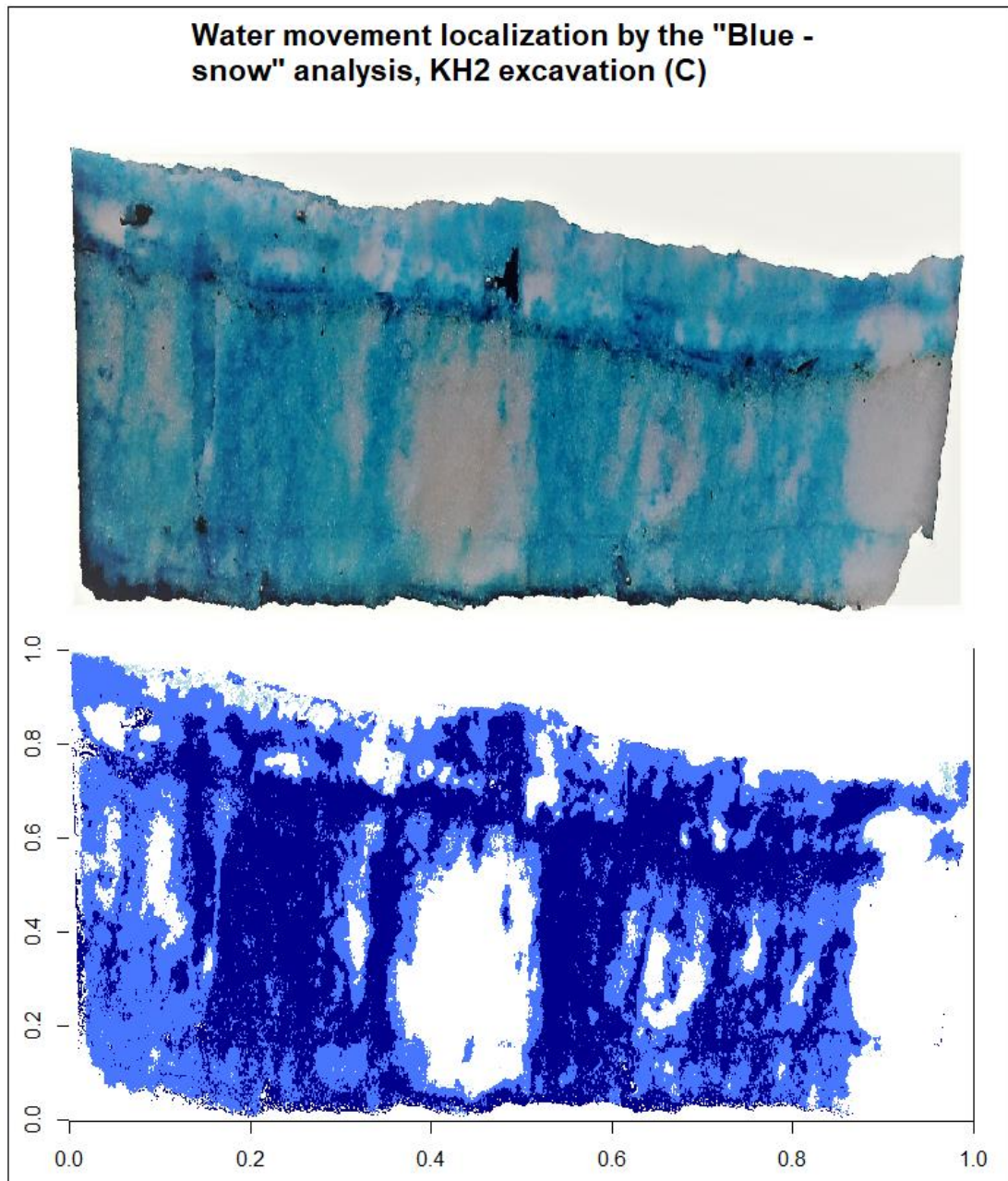## 8.6   Water behavior by the bluesnow analysis at the KH2 site

Figure 62: Photo of the excavation (A) and the bluesnow filter, which is the blue fraction distribution per pixels representing water movement induced by ROS at the Kubova Huť 2 site.
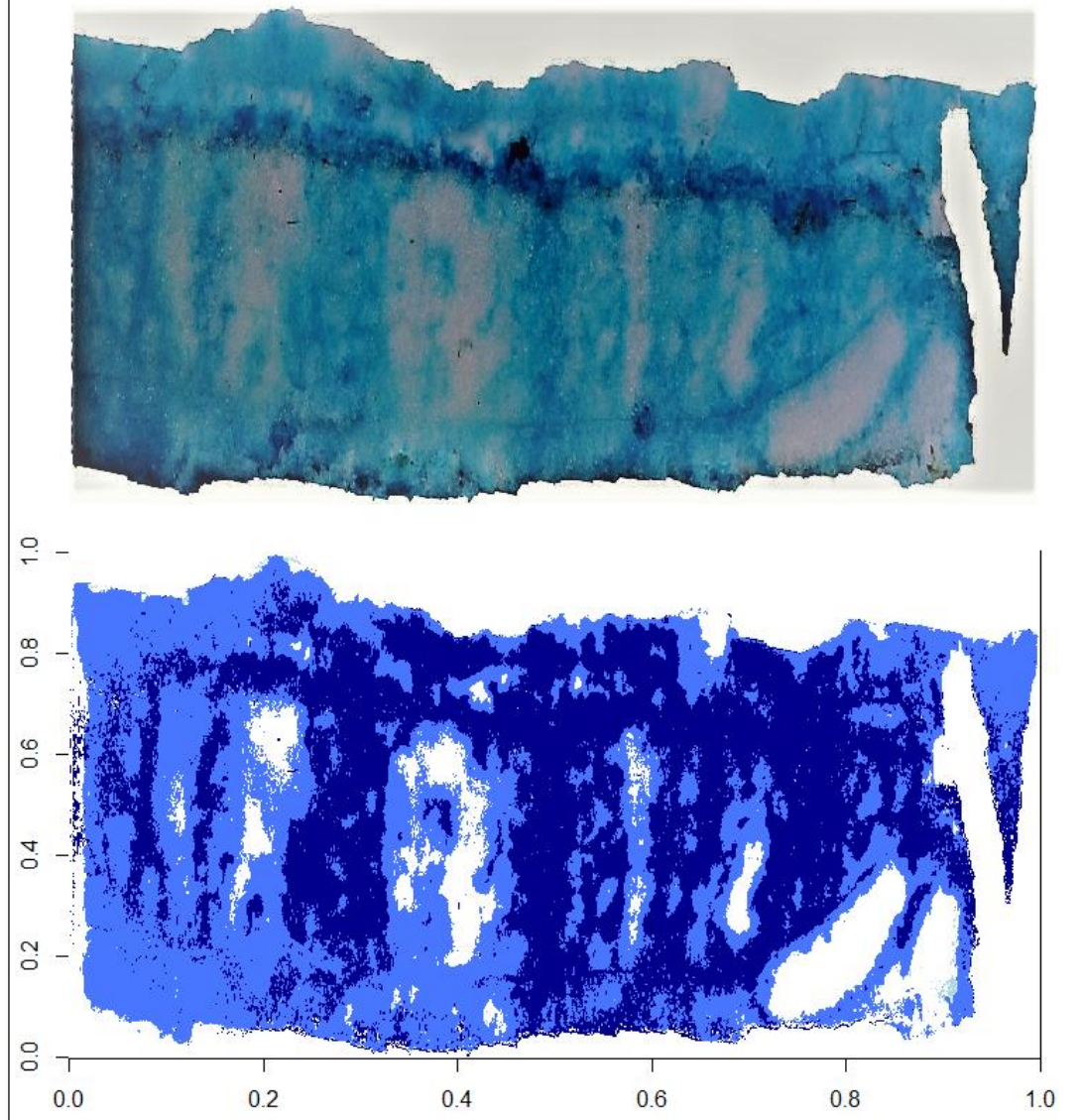
Figure 63: Photo of the excavation (B) and the bluesnow filter, which is the blue fraction distribution per pixels representing water movement induced by ROS at the Kubova Hut' 2 site.

Figure 64: Photo of the excavation (C) and the bluesnow filter, which is the blue fraction distribution per pixels representing water movement induced by ROS at the Kubova Huť 2 site.

Figure 65: Photo of the excavation (D) and the bluesnow filter, which is the blue fraction distribution per pixels representing water movement induced by ROS at the Kubova Huť 2 site.
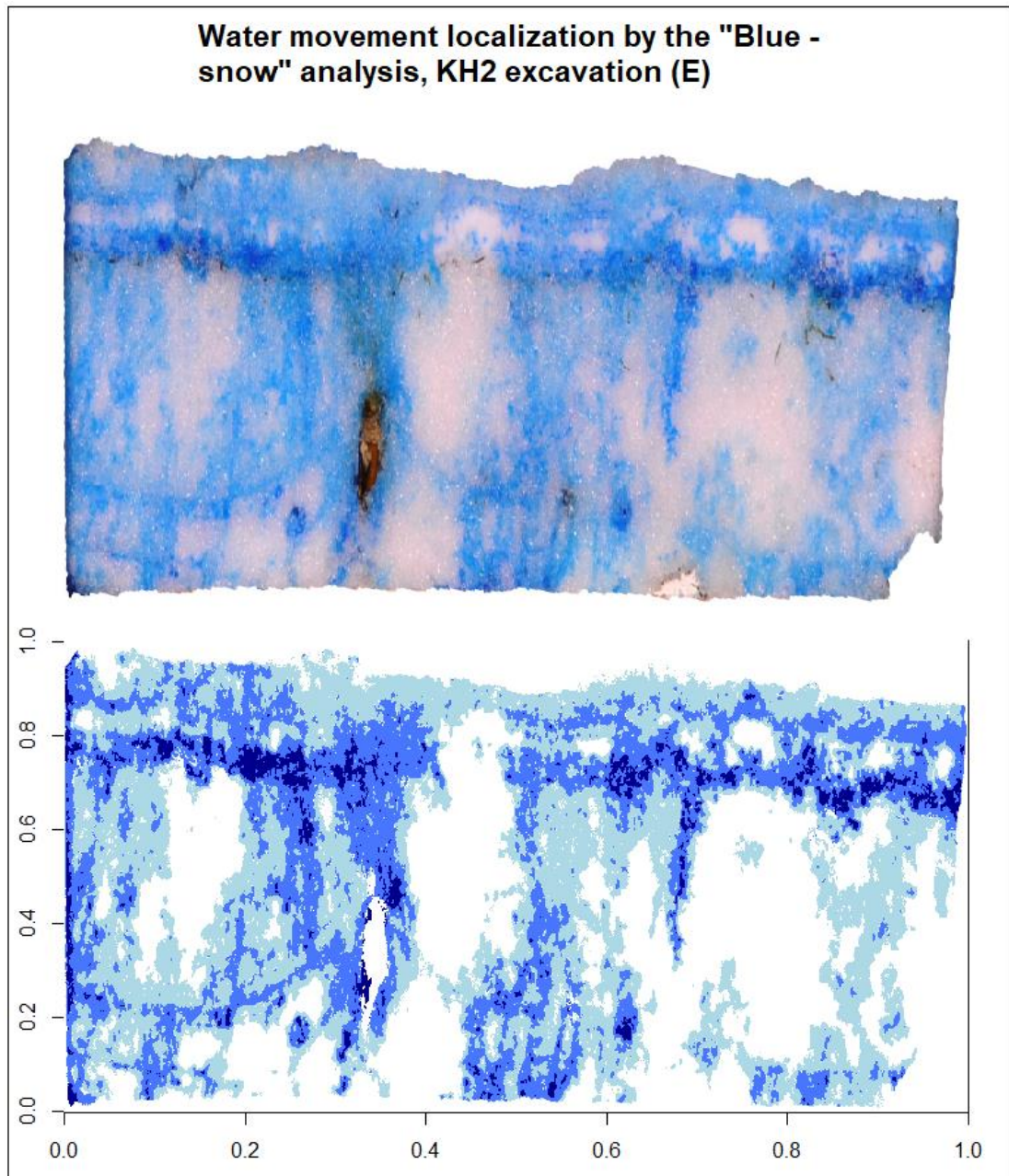
Figure 66: Photo of the excavation (E) and the bluesnow filter, which is the blue fraction distribution per pixels representing water movement induced by ROS at the Kubova Huť 2 site.